

**HARMONIC DOMAIN ANALYSIS OF POWER SYSTEM
ELEMENTS**

WITH

**NON-LINEAR OR REPETITIVE SWITCHING
COMPONENTS**

by

Robert S Burton

A thesis
submitted to the Faculty of Graduate Studies in
partial fulfilment of the requirements for the degree
of Doctor of Philosophy

at

The University of Manitoba,
Department of
Electrical and Computer Engineering

Winnipeg, Manitoba, Canada
©January, 2004

THE UNIVERSITY OF MANITOBA
FACULTY OF GRADUATE STUDIES

COPYRIGHT PERMISSION

**Harmonic Domain Analysis of Power System Elements
with Non-Linear or Repetitive Switching Components**

BY

Robert S. Burton

**A Thesis/Practicum submitted to the Faculty of Graduate Studies of The University of
Manitoba in partial fulfillment of the requirement of the degree
Of
DOCTOR OF PHILOSOPHY**

Robert S. Burton © 2004

Permission has been granted to the Library of the University of Manitoba to lend or sell copies of this thesis/practicum, to the National Library of Canada to microfilm this thesis and to lend or sell copies of the film, and to University Microfilms Inc. to publish an abstract of this thesis/practicum.

This reproduction or copy of this thesis has been made available by authority of the copyright owner solely for the purpose of private study and research, and may only be reproduced and copied as permitted by copyright laws or with express written authorization from the copyright owner.

ABSTRACT

Harmonic domain analysis (HDA) is a convenient method of analyzing power systems to determine the impact of harmonics as well as methods for their mitigation. HDA is more than a simple extension of the traditional load flow power frequency analysis tool to include analyses of the system for dc and harmonic components. Some of the most difficult aspects of HDA are the analysis of interactions that can occur between dc, power frequency and harmonic components of the power system.

The major sources of harmonics in a power system are non-linear elements such as saturation and power system electronic switching devices. HDA models of these devices have undergone significant development from fixed magnitude equivalent harmonic current sources used in early HDA models to detailed models where the magnitude and relative phase angle of the harmonics produced by the components are a function of voltage and current wave-forms at dc, power system and harmonic frequencies. Many of these mathematical models rely on information from the 'time domain' to establish driving wave-forms, degree of saturation, or 'turn-on' and 'turn-off' times for electronic switching devices.

This thesis presents a novel approach to modeling these devices entirely in the harmonic domain using a harmonic domain 'square root' function as a basic building block. The mathematics and algorithms used in the models are described and the approach is successfully demonstrated for several examples including diode applications, transformer saturation applications, and non-linear elements in power system controls.

Limitations of the mathematics and the model are described along with suggestions for future work to refine and improve the robustness of the model.

This Page is Intentionally Blank

ACKNOWLEDGEMENTS

The author wishes to thank the Faculty of Graduate studies and the Department of Electrical and Computer Engineering for their patience and guidance throughout this work. In particular the author expresses his sincere gratitude to his advisor, Dr. A.M. Gole. Dr. Gole has provided encouragement, direction and sound advice on every aspect of this project.

The author acknowledges the financial support provided by the Manitoba HVDC Research Centre during the first three years of the project and the encouragement from my employer, Teshmont Consultants LP who accommodated the “time-off” required to fulfill the classroom requirements.

I am extremely grateful to my family for their contributions, including my sons Robert, David and Andrew who would listen to my explanations and offer suggestions on improving my models. A special thanks goes to my brother Rich (Dr. R.T. Burton) who has reviewed my writings and offered suggestions on how to turn the documents into a Thesis.

I would also like to thank my mother Louisa and acknowledge my late father T.S.(Stan) Burton whose forethought, appreciation of education, and guidance 50 years ago spawned my interest in mathematics and its applications.

I would especially like to thank my wife Jean. She has made many personal sacrifices over the last nine and a half years while I was in the ‘dungeon’, working on the computer. Without her love and support, all of this would be impossible.

R.S. (Bob) Burton

Winnipeg, January 2004

This Page is Intentionally Blank

CONTENTS

Abstract	i
Acknowledgements	iii
Contents	v
List of Figures	vii
List of Tables	ix
Glossary	xi
Chapter 1 Introduction	1
1.1 Background.....	1
1.2 Objectives	6
1.3 Thesis Outline	8
Chapter 2 Summary of Harmonic Domain Mathematics	9
2.1 Introduction.....	9
2.2 Definitions.....	10
2.3 Addition and Subtractions Of Waveforms.....	11
2.4 The Product Transformation Matrix	12
2.5 The Inverse Transformation Matrix.....	15
2.6 The Square Root Function	17
2.6.1 The 'Exact' Newton-Raphson Solution	17
2.6.2 The Taylor Series Expansion	22
2.6.3 The Minimum 'Best Fit' Newton-Raphson Solution.....	24
2.6.4 Other Possible Solutions.....	31
2.7 The Absolute Function.....	31
2.8 The Sign Function.....	32
2.9 The Derivative Operator	33
2.10 Other Mathematical Functions.....	33
Chapter 3 Linear Power System Elements in the Harmonic Domain	35
3.1 Introduction.....	35
3.2 The Admittance Matrix.....	35
3.3 Resistors.....	37
3.4 Inductors	39
3.5 Capacitors	40
3.6 Other System Elements.....	41

Chapter 4	Linear Control System Functions.....	43
4.1	Introduction.....	43
4.2	First Order Lag Function	43
4.3	The Proportional Integral Derivative Function.....	44
4.4	The Compare Ramp Function.....	46
4.5	Overview.....	53
Chapter 5	Application to Power Electronics Switching Devices	55
5.1	Introduction.....	55
5.2	Application to Analysis of a Diode Circuit.....	55
5.2.1	Introduction.....	55
5.2.2	Example 1 Direct HDA Analysis of a Simple Resistor Diode Circuit	56
5.2.3	Example 2 Iterative HDA Analysis of a Simple Resistor Diode Circuit..	59
5.2.4	Example 3 Iterative HDA Analysis of a Simple Resistor Network Diode Circuit	64
5.2.5	Example 4 Iterative HDA Analysis of a Simple Resistor Inductor Diode Circuit	68
5.2.6	Independent Validation of HDA Model	71
5.2.7	Summary	75
5.3	Application to Analysis of a Thyristor Controlled Reactor	75
5.3.1	Introduction.....	75
5.3.2	Mathematical Development of Harmonic Domain Model	77
5.3.3	Sample Applications of the Harmonic Domain Model.....	83
5.3.4	Summary	92
5.4	Application to Voltage Chopping Circuit with Controls	93
5.5	Limitations of HDA	107
5.6	Overview.....	108
Chapter 6	Application to Transformer Saturation.....	111
6.1	Introduction.....	111
6.2	Harmonic Domain Model of Transformer Saturation	111
6.3	Harmonic Domain Analysis of Industrial Filter Commissioning Problems...	119
6.4	Use of HDA for Time Domain Analysis	136
Chapter 7	Concluding Remarks	141
7.1	General.....	141
7.2	Conclusions.....	142
7.3	Principal Original Contributions.....	143
7.4	Limitations of HDA and Further Work	144
REFERENCES.....		151
Appendices.....		155
	Appendix A Mathcad® Implementation of the HDA CompRamp Function	157
	Appendix B Mathcad® Data and Set-up for Sample System Described in Chapter 6	159

LIST OF FIGURES

Figure 1-1	Example of Distorted and Undistorted Waveforms.....	1
Figure 2-1	'Root' and 'Cos(x)' Solutions to $\sqrt{\cos^2(\omega t)}$	20
Figure 2-2	'Exact' Newton-Raphson Solution to $\sqrt{\text{step function}}$ after 20 Iterations.....	21
Figure 2-3	'Exact' Newton-Raphson Solution to $\sqrt{\text{step function}}$ after 10 Iterations.....	21
Figure 2-4	Taylor Series Solution to $\sqrt{\text{step function}}$ after 65 Steps	24
Figure 2-5	Variation of Error in 'Best Fit' Newton-Raphson Solution to $\sqrt{\text{step function}}$..	29
Figure 2-6	'Best Fit' Newton-Raphson Solution to $\sqrt{\text{step function}}$ after 9 Iterations ...	30
Figure 4-1	Typical Method of Determining Firing Instances (in Time Domain).....	47
Figure 4-2	Time Domain Presentation of Difference Between HDA Ramp and Reference	48
Figure 4-3	Time Domain Presentation of Difference Between HDA Ramp and Reference (Expanded View)	48
Figure 4-4	HDA Analysis of Firing Pulse Determination with HDA CompRamp Function	50
Figure 5-1	Simple Diode Resistor Test Circuit	56
Figure 5-2	Distorted Source Voltage Waveform used in Resistor-Diode Circuit.....	57
Figure 5-3	Diode Current and Voltage using Direct HDA Solution	58
Figure 5-4	Progression of Iterative Solution of Diode Resistor Circuit	63
Figure 5-5	Variation of Iterative Solution Error for Diode Resistor Circuit	64
Figure 5-6	Diode Current for Iterative Solution of Resistor Diode Circuit.....	64
Figure 5-7	Diode Resistor Circuit for Simple Network Analysis.....	65
Figure 5-8	Variation of Iterative Solution Error for Diode Resistor Network Circuit	67
Figure 5-9	Simple Diode Resistor Inductor Test Circuit.....	68
Figure 5-10	Variation of Iterative Solution Error for Diode Resistor Inductor Circuit	70
Figure 5-11	Voltage and Current Waveforms from Harmonic Content of HDA Solution to Example 4.....	71
Figure 5-12	Comparison of HDA Harmonic Content of Diode Current with Theoretical Content.....	73
Figure 5-13	Comparison of HDA Harmonic Content of Diode Voltage with Theoretical Content.....	73
Figure 5-14	Impact of Harmonic Domain and Theoretical Harmonics on Regenerated Waveforms	74
Figure 5-15	Simple Thyristor Controlled Reactor Circuit.....	76
Figure 5-16	Thyristor Controlled Reactor Conduction Interval for Switching Function Demonstration.....	77
Figure 5-17	Thyristor Controlled Reactor Circuit Current for Case 1	84
Figure 5-18	Thyristor Controller Reactor Voltage Waveforms for Case 1	85
Figure 5-19	Thyristor Controlled Reactor Circuit Current for Case 2	86

List of Figures

Figure 5-20	Thyristor Controller Reactor Voltage Waveforms for Case 2	87
Figure 5-21	Incorrect TCR Current Waveform	90
Figure 5-22	TCR Current Waveform after Adjustment to Second Firing Angle	90
Figure 5-23	TCR Voltage Waveforms after Adjustment to Second Firing Angle	91
Figure 5-24	Circuit Diagram of Test VCC and Controls	94
Figure 5-25	Data used in HDA Analysis of VCC	102
Figure 5-26	Harmonic Content of Voltages and Currents.....	103
Figure 5-27	Re-generated from Harmonic Content of HDA Results	105
Figure 5-28	PSCAD/EMTDC™ Time Domain Simulation of the VCC	106
Figure 5-29	Influence of the Presence of 3 rd Harmonic on the DC Bus.....	107
Figure 5-30	Simple Diode Resistor Capacitor Test Circuit.....	108
Figure 6-1	PSCAD/EMTDC™ Model of Transformer Saturation Characteristic	113
Figure 6-2	Transformer Magnetizing Current Waveforms for Sinusoidal Flux.....	116
Figure 6-3	Transformer Magnetizing Current Waveforms for Sinusoidal Flux with DC Offset	117
Figure 6-4	Transformer Magnetizing Current Waveforms for Flux with DC Offset and Harmonics	118
Figure 6-5	Single Line Diagram of Supply to Industrial Plant.....	120
Figure 6-6	Energization Circuit and Equivalent Circuit.....	124
Figure 6-7	Variation of AC Filter, System and Net Harmonic Impedance	125
Figure 6-8	Segment of Mathcad® Implementation of HDA Gauss-Seidel Solution	129
Figure 6-9	Convergence of HDA Solution of Transformer Filter Interaction Investigation.....	130
Figure 6-10	Harmonic Component of the Transformer Magnetizing Current	131
Figure 6-11	Harmonic Component of the Transformer Flux	131
Figure 6-12	Harmonic Component of the AC Filter 63 kV Bus Voltage.....	132
Figure 6-13	Distribution of Transformer Magnetizing Current	133
Figure 6-14	AC Filter Branch Harmonic Current.....	134
Figure 6-15	Measured Burst of Distorted Current in Rectifier 63 kV Feeder.....	138
Figure 6-16	HDA Analysis of Three Phase Transformer Saturation	138
Figure 6-17	Mathcad® Implementation of HDA of Transformer Saturation	140

LIST OF TABLES

Table 1-1	Harmonic Content of Waveforms Shown in Figure 1-1	2
Table 5-1	Harmonic Content of Voltage and Current for Diode Example Number 2 ..	62
Table 5-2	Harmonic Content of Current for Diode Example Number 3.....	67
Table 5-3	Harmonic Content of Voltage and Current in Diode Resistor-Inductor Test Circuit	70
Table 5-4	Zero Crossings of the Diode Resistor Inductor Circuit	72
Table 5-5	Harmonic Content of Waveforms for TCR Case 1.....	83
Table 5-6	Harmonic Content of Waveforms for TCR Case 2.....	86
Table 5-7	Harmonic Content of Waveforms after Adjustment to Firing Angle	92
Table 6-1	Transformer Magnetizing Harmonics for Sinusoidal Flux, Determined using Direct HDA.....	115
Table 6-2	Transformer Magnetizing Harmonics for Sinusoidal Flux with DC Offset, Determined using Direct HDA	117
Table 6-3	Transformer Magnetizing Harmonics for Flux with DC Offset and Harmonics, Determined using Direct HDA.....	118

This Page is Intentionally Blank

GLOSSARY

Fundamental Frequency. The base frequency of a repetitive wave-form expressed in Hz, equal to the inverse of the period (sec) of the wave-form. Most of the applications in this document equate fundamental frequency to the power system frequency, either 50 or 60 Hz. The methodology could apply equally to other types of analysis, (e.g. sub-synchronous analysis) in which fundamental frequency would be an integer divisor of the power system frequency (e.g., 1,2,5,10 Hz), common to both nominal system frequencies and 25 Hz (for a 50 Hz system).

Harmonic. A harmonic is an integer multiple of fundamental frequency. As used in this document, harmonic can refer either to the harmonic number (e.g., 0,1,2...50.. etc.) or it could refer indirectly to harmonic content of a wave-form, e.g., “harmonics (voltages, current, power etc.) of the power system”.

Load Flow (also Power Flow). A numerical analysis tool which solves the linear and non-linear simultaneous equations defining the fundamental frequency bus voltages and branch power flows of an electrical power system. The “Power Flow” is the most frequently used tool in the analysis, design, and operation of a power system network. Power Flow programs can solve electrical power systems with in excess of 50,000 nodes (buses).

Node. A point of connection of two or more electrical components. In the power flow, a node is the common point of connection of the positive sequence component of two or more three-phase electrical elements as represented by the positive sequence fundamental frequency impedance of each three-phase component. In HDA, a node is the point of electrical connection of each phase at each frequency.

Branch. A connection between two nodes. In the power flow, a branch is the element defining the positive sequence connection of two electrical nodes as represented by the positive sequence fundamental frequency impedance of each three-phase component. In

HDA, a branch is a connection between two physical nodes, but could represent the interaction effects between two different harmonics.

Harmonic Domain Analysis (HDA). A numerical analysis methodology similar to that used in the Power Flow, that can solve the linear and non-linear simultaneous equations defining the dc, fundamental frequency and harmonic components of bus voltages and branch power (current) flows of an electrical power system. Harmonic domain analysis tools add another two dimensions to the Power Flow. Power Flow analysis has traditionally been limited to positive sequence flows. Harmonics exhibit sequence component characteristics, but unlike the power flow which is dominated by the behaviour of the positive sequence component, magnitudes of each harmonic component are similar and must be considered, either on a phase or sequence component basis. The second dimension added to the analysis is the harmonic number. Using 50,000 nodes as an indicator of current load flow technology, HDA would be literally limited to about 300 nodes. (300 nodes times 3 phases times typically 50 harmonics). The actual limit is many times larger as the mathematical matrices involved are extremely sparse. HDA analysis of 10,000 nodes is well within the capability of current hardware/software.

Sequence Components. A numerical algorithm that resolves the electrical characteristics of the three phases of an electrical power system into a dominant component (the positive sequence component) and two secondary components (the negative sequence and the zero sequence components). For balanced operation, the latter two components are so small, they are neglected for most power systems analysis.

Time Domain Analysis. A numerical analysis methodology in which the response of a network is determined by direct simulation, i.e. determining its response as a function of time. In this thesis time domain analysis often will refer to the 'steady state' condition in which the voltage and current waveforms repeat and are essential identical from one cycle of fundamental frequency to the next. The harmonic component of a time domain waveform can be determined mathematically.

Array, Matrix and Vector. In this document the term **array** is used to describe an arrangement of elements in one or more dimensions. **Matrix** as used in this thesis refers to a two dimensional **array**. **Vector** will refer to a single dimension **array** with a single column, to be compatible with **matrix – vector** operations. When an **array** with a single row is used, it will be referenced as the transpose of a **vector**.

Identity Matrix. The identity matrix in this document is a square two dimensional array where each diagonal element has a numerical value of one and each off-diagonal element is zero.

This Page is Intentionally Blank

CHAPTER 1

INTRODUCTION

1.1 BACKGROUND

Non-linear and electronic equipment in an electrical network can distort the voltage and current waveforms throughout the system from their nominal sinusoidal waveshape. Examples of a distorted and an undistorted waveform are given in Figure 1-1. The distorted waveforms can cause unexpected overloading of system components as well as producing electrical and electromagnetic interference. If the distortion is only of a transient nature, the impacts can often be neglected. A more serious situation arises when the distortion is continuous. The problem can occur for electrical networks consisting of a few electrical components on a printed circuit board, to a power system network extending across a continent. The concepts introduced in this thesis are equally applicable to low and high power electrical networks.

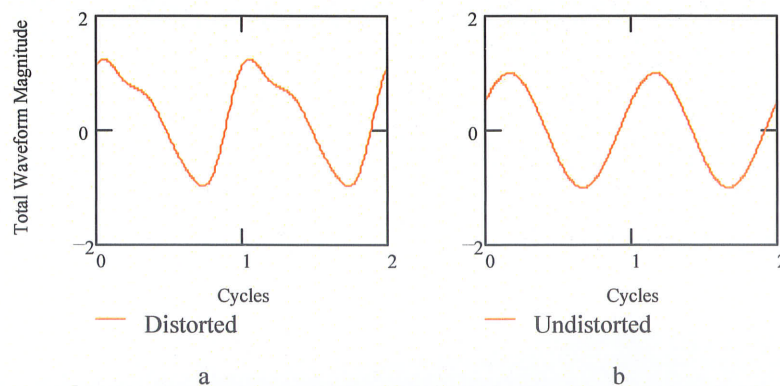


Figure 1-1 Example of Distorted and Undistorted Waveforms

A convenient method to quantify the level of distortion and its effects is to define the waveforms by a mathematical series consisting of a summation of purely sinusoidal

waveforms of different frequencies plus a dc or offset component. For electrical power systems, the major contributor to the waveform is a component at the power system frequency (50 or 60 Hz). If the distortion is repetitive every cycle, a Fourier series in which each frequency is a multiple or harmonic of the fundamental frequency component can define the waveform. Chapter 2 will describe how the magnitude of the harmonic components can be calculated from a mathematical description of the waveforms. The harmonic components of the sample waveforms shown in Figure 1-1 are given in Table 1-1.

Table 1-1 Harmonic Content of Waveforms Shown in Figure 1-1

Harmonic	Harmonic Content	
	Distorted Waveform	Undistorted Waveform
DC	0.2	0.0
Fundamental Frequency	1.0	1.0
2 nd Harmonic	0.3	0.0
3 rd Harmonic	0.1	0.0

Once the magnitude of each harmonic is known, the impact of the distortion on the network or network component is often determined by superposition of the harmonic effects [1] ... [4]. To establish heating effect, for example, the harmonics are often combined in an RMS (Root Mean Square) fashion by summing the squares of the magnitudes of each of the harmonic components, then taking the square root of the sum. If voltage rating is being considered, often the sum of the magnitude of the harmonic voltages is used. In dealing with the impact of harmonics on communications, weighed cumulation is often used, in which the magnitude of each harmonic is multiplied by a weighting factor before the summation take place.

Harmonic analysis covers the broad subject of establishing the harmonic content of a distorted waveform. In a 'traditional' harmonic analysis [5] ... [9], the waveform is first defined as a periodic function of time, either numerically (by a time series with numerical values for each time step) or mathematically (by a series of mathematical expressions). The harmonic content can be established using a numerical Fourier analysis if the function is described numerically. If the waveform can be defined by simple

mathematical relationships, the numerical Fourier analysis approach can still be used but this requires creation of a time series based on the mathematical expression before the numerical Fourier analysis can be carried out. The more common approach for mathematical expressions is to determine the harmonic content by symbolic evaluation of the relationships, followed by simple numerical evaluation of the resultant mathematical expressions to determine the harmonic content.

The 'traditional' mathematical determination of the harmonic content is limited to the analysis of relatively simple networks because of the increase in complexity of the algebraic expressions as the extent of the network is increased. For larger networks, however, a time domain simulation¹ is required of the many non-linear and discontinuous algebraic and differential equations that define the complex relationships between voltage and currents in the network. The duration of the time domain solution must be sufficient to allow all of the transients of the solution to decay. Once a repetitive time domain waveform is established, a numerical Fourier analysis can determine the harmonic content of the waveform.

Analysis of some existing or proposed electrical networks involving hundreds of thousands of differential equations would require computational capability likely in excess of even the latest and largest capacity 'super computers', waiting for the transients to die down to establish the transients-free waveforms.

A more practical approach that has been developed [10] ... [13], is harmonic domain analysis. Frequency domain analysis has been used extensively in the analysis and design of linear control systems [14], [15]. Frequency domain analysis has also been used extensively in the analysis of interactions between elements of an electrical power system at sub-synchronous and super-synchronous frequencies. Harmonic domain analysis is simply a subset of frequency domain analysis.

¹ Using time domain simulation tools such as PSCAD/EMTDC™ and EMTP® or the simulation capability of mathematical analysis tools such as Matlab®.

The load flow solution of a power system is a harmonic domain analysis carried out at the power system fundamental frequency. The linear portions of the network defined by capacitors, inductors, resistors, mutually coupled elements are solved using complex algebraic equations to define the steady state solution to the differential equations that describe their behaviour. Repetitively switched elements such as power electronics are modelled as equivalent harmonic current and voltage sources and non-linear elements are treated as Norton or Thévenin equivalents. Iterative solution algorithms such as Gauss-Seidel and/or Newton-Raphson techniques are used to solve the myriad of linear and non-linear algebraic equations. Harmonic domain analysis is simply an extension of the power flow to include the effects of dc and harmonics.

The same basic concepts used in the load flow solution can be (and have been) extended to the solution of the network at dc and harmonic frequencies [16]. The method of solution of the dc and harmonic flow on the transmission network itself is effectively the same as the method of solution at the fundamental frequency. The relationships between the currents and the voltages across the network are defined by an admittance matrix. The admittance matrix is re-defined for each harmonic frequency under consideration. While the structure of the dc admittance matrix may be different, the structure of each harmonic admittance matrix is the same as the structure at fundamental frequency.

In frequency domain application software such as NIMSCAN^{®2}, V-Harm^{®3}, CYMHARMO^{®4}, the emphasis is placed on solving for the harmonic penetration in large power systems. Each harmonic is evaluated individually, treating harmonic sources in the power system as equivalent harmonic voltage or current sources, and using direct superposition of harmonic contributions at any location in the network to establish the harmonic content of any particular waveform.

Unfortunately non-linear elements in the network introduce a dependence of the solution at one harmonic on the solutions at other harmonics. For example transformer saturation,

² Developed by Teshmont Consultants LP

³ Developed by McGraw Edison

⁴ Developed by CYME™ Power Engineering

often ignored in the fundamental frequency solution, becomes a major factor in the harmonic domain solution. The magnitude of the harmonics produced by saturation is a function of the magnitude of the fundamental frequency voltage applied to the device. In a similar vein, the magnitudes of harmonics produced by electronic switching devices are also a function of the magnitudes of the fundamental frequency voltages and currents. Not only are the magnitude of these harmonic sources dependent on the magnitude of the fundamental frequency component, they are also dependent on the magnitude of currents and voltages at other harmonic frequencies, creating in essence a three dimensional analysis problem.

Much work has been carried out by others developing the inter-harmonic spatial relationships for non-linear components such as saturation [17] ... [20] and complex electronic switching circuits such as for High Voltage DC Schemes (HVDC) [21] ... [27] and Flexible AC Transmission Systems (FACTS) devices [28] ... [32]. Much of the modelling involves transformation from frequency to time domain to solve for the non-linear effects. The time domain solution is then re-transformed back to the frequency domain for further analysis. This is the case for transformer saturation.

An extensive amount of development work has been carried out for the harmonic domain type of analysis, most recently in the application of harmonic domain switching functions [10], [33], [34] to the modelling of harmonic domain models of power electronic switching devices. However, for other than a few special conditions, a conversion from frequency domain to time domain is required to determine the instants that conduction of the devices begins and ends. The turn-on and turn-off times are then used in the harmonic domain to analyse the impact of the device harmonics on the network. A diode is a good example of this, where time domain information has been required to define the harmonic domain response. Conduction of the diode begins when the instantaneous voltage across it becomes positive and terminates when the instantaneous current through the device attempts to become negative. The turn-on and turn-off times are based on time domain information.

1.2 OBJECTIVES

Much development work has been done by others in both time domain and harmonic domain modelling. The time domain carries information about the frequency domain which can be extracted using a fast Fourier transform. The harmonic domain houses information about the steady state time domain that can be easily extracted using a Fourier series. Each of the domains should be self sufficient. Once a time domain model is built, it is self sufficient and all of its analysis can be done completely in the time domain, yet many of the harmonic domain models rely on excursions into the time domain to obtain information that intuitively should already exist in the harmonic domain.

Fundamental mathematics shows that the principle of superposition is valid for the summation and subtraction of harmonic waveforms. Multiplication of harmonic waveforms involves a shift in the harmonic spectra (i.e. in the harmonic order) but there is a rigorous mathematical relationship between the magnitude and frequency of harmonics in the product to the magnitude and frequency of the harmonics in the multiplicands, i.e. direct multiplication in the harmonic domain.

Given that three basic operators, i.e. add, subtract, and multiply can be carried out entirely in the harmonic domain, it was hypothesized that it should be possible, also, to directly divide two waveforms in the harmonic domain. With these four harmonic domain tools it should be possible, similar to the time domain, to develop more complex mathematical functions such as the square root and absolute value functions.

Several time domain programs are in existence. These programs use Dommel's Algorithm [35] to rapidly construct a set of algebraic equations from the given network parameters and interconnection data (net list). In this thesis, a new approach to solving electrical circuits with non-linear elements directly in the harmonic domain is developed. This approach is amenable to being incorporated into a general purpose 'net list' based solution package.

At first glance it appears that using the frequency domain to solve non-linear circuits should not be possible because the superposition principle only applies to linear circuits. However with the addition of iterative calculations, this approach becomes rigorously correct, as will be shown in the research chapters.

Given that the harmonic domain is also a very useful analytical tool with roots in the load flow solution, the objective of this research was to develop a Harmonic Domain Analysis (HDA) methodology given the hypothesis that the analysis can be done entirely in the harmonic domain. This would require:

- 1) development and demonstration of algorithms for the direct evaluation of advanced mathematical functions
- 2) application of the mathematical algorithms to typical source of harmonic interactions such as non-linear elements and power electronic devices
- 3) an indication of how the algorithms can be incorporated into methodologies for other types of power system analyses

The HDA would permit the utilisation of the vast data entry and analysis algorithms developed for the power flow and stability solutions and would lend itself to data mapping techniques developed for graphical simulation packages such as PSCAD/EMTDC™.

The harmonic domain approach developed in this thesis is useful to the electrical engineering community for the following reasons:

- 1) The rigorous mathematical treatment extends the art of network solution theory.
- 2) The direct calculation of harmonics is an independent check for time domain solutions followed by Fourier analysis.
- 3) Computationally, the harmonic method could be faster particularly for systems with low damping in which time domain solutions could take a very long time to converge to steady state.

- 4) Systems excited with a large range of harmonics (e.g. dc and up to 1 MHz) or systems with a large difference in their natural time constants, which could be numerically unstable in a time domain solution, can be handled.
- 5) If the development of the proposed Harmonic Domain Analysis methodologies continues, it could eventually be used to define initial conditions for time domain transients solutions.

1.3 THESIS OUTLINE

Chapter 2 of this Thesis summarises the mathematical tools that were used and developed for the proposed HDA methodology.

Chapter 3 summarises the modelling of the basic power system elements in the HDA and their compatibility with existing methodologies for power flow and time domain analysis.

Chapter 4 summarises the HDA modelling of typical functions used in the development of power system component controls.

Chapter 5 shows how the proposed HDA methodology can be applied to power electronic switching circuits, such as diodes, thyristor controlled reactors and integrated power and control systems associated with voltage sourced converter applications.

Chapter 6 shows how the proposed HDA methodology can be used for the direct harmonic domain analysis of non-linear elements such as transformer saturation characteristics.

Chapter 7 reviews the work that is presented and suggests topics for future research and development into the proposed Harmonic Domain Analysis methodology.

CHAPTER 2

SUMMARY OF HARMONIC DOMAIN MATHEMATICS

2.1 INTRODUCTION

This chapter presents the development of several of the mathematical operations and functions required to carry out the harmonic domain analysis described in other chapters. Algorithms for the direct addition, subtraction and multiplication of the harmonic component of waveforms are prerequisite for harmonic domain analyses. Algorithms for direct addition and subtraction are trivial. However, algorithms for multiplication involve a convolution of the harmonic vectors representing the waveform, and are described in many of the papers on harmonic domain analysis of power systems [10], [12]. The author was unable to locate any published reference material on the direct division of waveforms in the harmonic domain and thus developed a unique algorithm to do this task.

In this chapter, the fundamental mathematics of harmonic domain analysis are reviewed, the notational conventions used by the author are described and the algorithms for the four basic mathematical operations are presented. The procedure for the addition, subtraction and multiplication of waveforms are included for completeness. A matrix approach to multiplication of waveforms in the harmonic domain is introduced which enables the direct division of two waveforms entirely in the harmonic domain.

This is followed by several original algorithms to compute the square root of a harmonic waveform. The square root function is essential to the formation of higher order functions such as absolute value. The square root function is also critical to the harmonic domain modelling of many non-linear elements and is the fundamental building block to define

the voltage and current waveforms in electronically switched circuits. This chapter does represent one of the fundamental contributions that the author has made to this research area.

It will be shown in this chapter that the square root function can be used as a building block to define other functions such as the sign function and the comparison function.

2.2 DEFINITIONS

The Fourier series representation of a bounded periodic function is as follows⁵:

$$f(x) = \frac{a_0}{2} + \sum_{n=1}^{\infty} \left(a_n \cos \frac{n\pi x}{L} + b_n \sin \frac{n\pi x}{L} \right) \quad \{ 2-1 \}$$

where:

L is 1/2 of the period of the repetitive waveform.

$$a_n = \frac{1}{L} \int_{-L}^L f(x) \cos \frac{n\pi x}{L} dx, \quad n = 0, 1, 2, 3, \dots \quad \{ 2-2 \}$$

$$b_n = \frac{1}{L} \int_{-L}^L f(x) \sin \frac{n\pi x}{L} dx, \quad n = 1, 2, 3, \dots \quad \{ 2-3 \}$$

In this document the period is always equal to one cycle of fundamental frequency of the electrical system and the harmonic spectrum is limited to the highest harmonic under consideration in the study. I.e.:

$$F(x) = \frac{a_0}{2} + \sum_{n=1}^{n_{\max}} \left(a_n \cos \frac{n\pi x}{L} + b_n \sin \frac{n\pi x}{L} \right) \quad \{ 2-4 \}$$

where n_{\max} is the highest harmonic of interest.

For convenience, the coefficients describing the Fourier series of a given waveform are mathematically and/or numerically housed in a single dimension array for the waveform.

E.g.:

$$\bar{F} = \left[\frac{a_0}{2} \quad a_1 \quad b_1 \quad a_2 \quad b_2 \quad \dots \quad a_{n_{\max}} \quad b_{n_{\max}} \right]^T \quad \{ 2-5 \}$$

⁵ The Fourier series is defined in many documents. The specific reference used by the author is a summary provided on pages 434-435 of the CRC Standard Mathematical Tables, 16th Edition [37]

In this document, a capitalized variable name marked with an arrow header as (used above) will refer to a single dimension array of length $2n_{\max}+1$ that houses the harmonic content of a given waveform. A capitalized variable name marked with a solid bar header will refer to a transfer matrix (normally square of dimension $2n_{\max}+1$, by $2n_{\max}+1$) that houses the harmonic response of an input to output transfer characteristic. E.g., the variable \bar{Z} as used in the following equation:

$$\vec{V} = \bar{Z} \cdot \vec{I} \quad \{ 2-6 \}$$

contains the harmonic transfer characteristic from the input variable \vec{I} to the output variable \vec{V} . In many of the expressions as used in this document, the transfer matrix \bar{Z} is constant, and sparse dependent only on the physical device that it is representing.

The majority of the analysis described in this document was carried out using Mathcad[®] Version 6.0 and Excel[®] Version 7.0. One of the reasons that the Fourier series representation as described above was chosen over the more frequently used⁶ "Complex Fourier Series/Exponential Fourier Series" is that only real quantities are involved and therefore standard real vector/matrix tools (such as are available in mathematical applications such as Mathcad[®] and Excel^{®7}) can be used.

In this document, presentations of Mathcad[®] calculation sheets, functions and expressions are in line with the text or referenced as a figure or appendix, and are enclosed by a box. Unfortunately, Mathcad[®] Version 6 does not have the word processing capability to differentiate between scalar, vector and array variable names. The text preceding each presentation should clarify the nature of the variable used.

2.3 ADDITION AND SUBTRACTIONS OF WAVEFORMS

The sum (and difference) of two periodic waveforms with the same fundamental frequency is also a periodic waveform of the same fundamental frequency. The Fourier

⁶ In load flow and stability programs, the fundamental frequency component is only analyzed using complex Fourier series approach.

⁷ Mathcad[®] 6.0 can easily handle both real and complex variables, however, dealing with complex variables in Excel[®] Version 7.0 is cumbersome.

coefficients of the sum (and difference) can be determined by the direct addition (subtraction) of the two arrays housing the coefficients for the two waveforms. I.e.:

$$\bar{C} = \bar{A} + \bar{B} \quad \{ 2-7 \}$$

or:

$$\bar{C} = \bar{A} - \bar{B} \quad \{ 2-8 \}$$

For both operations the approximate time domain waveform of \bar{C} can be regenerated using Equation 2-1.

2.4 THE PRODUCT TRANSFORMATION MATRIX

The product of two periodic waveforms is also a periodic waveform where the Fourier coefficients of the product can be derived directly from the Fourier coefficients of the original waveforms. If the multiplicand and multiplier waveforms⁸ are defined to be:

$$A(\omega t) = \sum_{n=0}^{n_{\max}} [Aa_n \cos(n \cdot \omega t) + Ab_n \sin(n \cdot \omega t)] \quad \{ 2-9 \}$$

$$B(\omega t) = \sum_{n=0}^{n_{\max}} [Ba_n \cos(n \cdot \omega t) + Bb_n \sin(n \cdot \omega t)] \quad \{ 2-10 \}$$

The product can be determined from term by term multiplication of the two equations and expanding the resultant trigonometric function products into their equivalent harmonic form. I.e.:

$$C(\omega t) = A(\omega t)B(\omega t) = \left(\sum_{n=0}^{n_{\max}} [Aa_n \cos(n \cdot \omega t) + Ab_n \sin(n \cdot \omega t)] \right) \left(\sum_{n=0}^{n_{\max}} [Ba_n \cos(n \cdot \omega t) + Bb_n \sin(n \cdot \omega t)] \right) \quad \dots\{ 2-11 \}$$

or:

$$C(\omega t) = \sum_{n=0}^{2n_{\max}} [Ca_n \cos(n \cdot \omega t) + Cb_n \sin(n \cdot \omega t)] \quad \{ 2-12 \}$$

where:

⁸ In equations 2-9 and 2-10, the dc components of the cosine series are equal to ½ of the Fourier Series coefficients and the dc components of the sine series are zero.

$$\begin{aligned}
 Ca_0 &= \frac{1}{2}[2Aa_0Ba_0 + Aa_1Ba_1 + Ab_1Bb_1 + Aa_2Ba_2 + Ab_2Bb_2 + \dots] \\
 Ca_1 &= \frac{1}{2}[2Aa_1Ba_0 + (2Aa_0 + Aa_2)Ba_1 + Ab_2Bb_1 + (Aa_1 + Aa_3)Ba_2 + (Ab_1 + Ab_3)Bb_2 + \dots] \\
 Cb_1 &= \frac{1}{2}[2Ab_1Ba_0 + Ab_2 * Ba_1 + (2Aa_0 - Aa_2)Bb_1 + (-Ab_1 + Ab_3)Ba_2 + (Aa_1 - Aa_3)Bb_2 + \dots] \\
 Ca_2 &= \frac{1}{2}[2Aa_2Ba_0 + (Aa_1 + Aa_3)Ba_1 + (-Ab_1 + Ab_3)Bb_1 + (2Aa_0 + Aa_4)Ba_2 + Ab_4Bb_2 + \dots] \\
 Cb_2 &= \frac{1}{2}[2Ab_2Ba_0 + (Ab_1 + Ab_3)Ba_1 + (Aa_1 - Aa_3)Bb_1 + Ab_4 * Ba_2 + (2Aa_0 - Aa_4)Bb_2 + \dots] \\
 &: \\
 Ca_i &= \frac{1}{2} \left[\begin{aligned} &2Aa_iBa_0 + (Aa_{i-1} + Aa_{i+1})Ba_1 + (-Ab_{i-1} + Ab_{i+1})Bb_1 + (Aa_{i-2} + Aa_{i+2})Ba_2 + \\ &(-Ab_{i-2} + Ab_{i+2})Bb_2 \dots + (2Aa_0 + Aa_{2i})Ba_i + Ab_{2i}Bb_i + (Aa_1 + Aa_{2i+1})Ba_{i+1} + \\ &(Ab_1 + Ab_{2i+1})Bb_{i+1} + (Aa_2 + Aa_{2i+2})Ba_{i+2} + (Ab_2 + Ab_{2i+1})Bb_{i+2} + \dots \end{aligned} \right] \\
 Cb_i &= \frac{1}{2} \left[\begin{aligned} &2Ab_iBa_0 + (Ab_{i-1} + Ab_{i+1})Ba_1 + (Ab_{i-1} - Ab_{i+1})Bb_1 + (Ab_{i-2} + Ab_{i+2})Ba_2 + \\ &(Aa_{i-2} - Aa_{i+2})Bb_2 \dots + Ab_{2i}Ba_i + (2Aa_0 - Aa_{2i})Ba_i + (-Ab_1 + Ab_{2i+1})Ba_{i+1} + \\ &(Aa_1 - Aa_{2i+1})Bb_{i+1} + (-Ab_2 + Ab_{2i+2})Ba_{i+2} + (Aa_2 - Aa_{2i+2})Bb_{i+2} + \dots \end{aligned} \right] \\
 &:
 \end{aligned} \tag{2-13}$$

The coefficients of \bar{C} can be derived directly from the above expressions. The number of harmonics in waveform \bar{C} is twice the number in each of waveforms \bar{A} and \bar{B} as a result of the frequency doubling introduced by the products of the n^{th} terms. E.g.:

$$A_n \cos(n \cdot \omega t) \cdot B_n \sin(n \cdot \omega t) = \frac{A_n B_n}{2} (\sin 2n \cdot \omega t) \tag{2-14}$$

Most references describe the multiplication of two waveforms mathematically as:

$$\bar{C} = \bar{A} \otimes \bar{B} \tag{2-15}$$

where the symbol \otimes is a convolution operator that carries out the term by term multiplication of the waveform components. The author observed from Equation 2-13 that the “C” coefficients can also be rewritten in matrix notation as follows:

$$\bar{C} = \bar{T} \cdot \bar{B} \tag{2-16}$$

where the matrix \bar{T} is a function of only the coefficients of variable \bar{A} . I.e.:

$$\bar{T} = T_p(\bar{A}) \tag{2-17}$$

where:

$$T_p(\bar{A}) =$$

$$\frac{1}{2} \begin{bmatrix} 2a_0 & a_1 & b_1 & a_2 & b_2 & a_3 & b_3 & a_4 & b_4 \\ 2a_1 & 2a_0 + a_2 & b_2 & a_1 + a_3 & b_1 + b_3 & a_2 + a_4 & b_2 + b_4 & a_3 + a_5 & b_3 + b_5 \\ 2b_1 & b_2 & 2a_0 - a_2 & -b_1 + b_3 & a_1 - a_3 & -b_2 + b_4 & a_2 - a_4 & -b_3 + b_5 & a_3 - a_5 \\ 2a_2 & a_1 + a_3 & -b_1 + b_3 & 2a_0 + a_4 & b_4 & a_1 + a_5 & b_1 + b_5 & a_2 + a_6 & b_2 + b_6 \\ 2b_2 & b_1 + b_3 & a_1 - a_3 & b_4 & 2a_0 - a_4 & -b_1 + b_5 & a_1 - a_5 & -b_2 + b_6 & a_2 - a_6 \\ 2a_3 & a_2 + a_4 & -b_2 + b_4 & a_1 + a_5 & -b_1 + b_5 & 2a_0 + a_6 & b_6 & a_1 + a_7 & b_1 + b_7 \\ 2b_3 & b_2 + b_4 & a_2 - a_4 & b_1 + b_5 & a_1 - a_5 & b_6 & 2a_0 - a_6 & -b_1 + b_7 & a_1 - a_7 \\ 2a_4 & a_3 + a_5 & -b_3 + b_5 & a_2 + a_6 & -b_2 + b_6 & a_1 + a_7 & -b_1 + b_7 & 2a_0 + a_8 & b_8 \\ 2b_4 & b_3 + b_5 & a_3 - a_5 & b_2 + b_6 & a_2 - a_6 & b_1 + b_7 & a_1 - a_7 & b_8 & 2a_0 - a_8 \end{bmatrix}$$

.....{ 2-18 }

'a' and 'b' as referenced in the above matrix are the 'a' and 'b' coefficients of the vector 'A'. The identification 'A' has been omitted from the above description of the matrix elements as it is common to all elements of the matrix. The author has defined this matrix as a “product transformation matrix” as it transforms the single dimension array \bar{A} into a two dimensional array that can be used in the direct multiplication of the coefficients of the two single dimension arrays.

The notation:

$$\bar{C} = T_p(\bar{A})\bar{B} \quad \{ 2-19 \}$$

as used throughout the thesis, is effectively the same operation shown below:

$$\bar{C} = \bar{A} \otimes \bar{B} \quad \{ 2-20 \}$$

as used by others.

The number of columns of the product transformation matrix must match the length of the second multiplicand array. The number of rows however can be set to reflect the desired accuracy of the product. Saturation of the accuracy occurs when the number of harmonics of the product is equal to the sum of the number of harmonics of the multiplicand and the multiplier. Limiting the number of harmonics in the result effectively produces numerical filtering of the product.

Unless otherwise indicated herein, the number of harmonics in the product is set equal to

n_{max} .

2.5 THE INVERSE TRANSFORMATION MATRIX

An interesting property of a square product transformation matrix is that under certain conditions (stated later), it can be inverted. The inverse of the waveform is simply:

$$\text{Inv}\vec{A} = T_p^{-1}(A)\vec{\text{One}} \quad \{ 2-21 \}$$

where:

$$\vec{\text{One}} = [1 \ 0 \ 0 \ 0 \ \dots]^T \quad \{ 2-22 \}$$

or simply the first column of the inverse of the transformation matrix representing \vec{A} .

It is important to note that:

$$T_p(\text{Inv}\vec{A}) \neq T_p^{-1}(A) \quad \{ 2-23 \}$$

The equality is approached only if the highest harmonic order included approaches infinity.

Either method could be used to solve for the unknown vector \vec{B} in the following relationship where both \vec{C} and \vec{A} are known:

$$\vec{C} = T_p(\vec{A})\vec{B} \quad \{ 2-24 \}$$

The solutions could be:

$$\vec{B} = T_p^{-1}(\vec{A})\vec{C} \quad \{ 2-25 \}$$

or alternatively:

$$\vec{B} = T_p[T_p^{-1}(\vec{A})\vec{\text{One}}]\vec{C} \quad \{ 2-26 \}$$

The differences between the two methods have been confirmed by the author to be minimal. As the first equation results in less computation effort and fewer operations, it is used wherever possible.

If a waveform (in the time domain) has zero crossings, its inverse should have an infinite value at these zero crossings. In the proposed harmonic domain analysis, if the harmonic

array is limited to a small number of terms, its transformation matrix may appear to be non-singular and hence invertible. However, as more harmonics are added, the matrix becomes more ill-conditioned and the corresponding time domain waveform evaluated from the Fourier coefficients converges to infinite impulses at the zero crossings of the original waveform.

The power of the inverse transformation matrix can be seen for a situation where the harmonic content of the voltage ' \vec{V} ' and current ' \vec{I} ' are known at a given location in a harmonic simulation (or power network). The apparent harmonic impedance ' \bar{Z}_{app} ' of the network at the point would satisfy the expression:

$$\bar{Z}_{app} \cdot \vec{I} = \vec{V} \quad \{ 2-27 \}$$

If we consider the time varying impedance, equal to the division of the voltage waveform by the current waveform, ie

$$\bar{Z}_{tot} = T_p^{-1}(\vec{I}) \cdot \vec{V} \quad \{ 2-28 \}$$

then the product of the time-varying impedance and current vectors should, by definition, equal the voltage vector. Or,

$$T_p(\bar{Z}_{tot}) \cdot \vec{I} \equiv \vec{V} \quad \{ 2-29 \}$$

Comparing to Equation 2-27, the apparent impedance is given by:

$$\bar{Z}_{app} = T_p(T_p^{-1}(\vec{I}) \cdot \vec{V}) \quad \{ 2-30 \}$$

The same relationships can be applied if ' $\Delta\vec{V}$ ' and ' $\Delta\vec{I}$ ' are used instead of ' \vec{V} ' and ' \vec{I} ' respectively. The resultant impedance represents the harmonic Thévenin equivalent impedance ' \bar{Z}_{thev} ' at the location. This in turn can be used to predict the behaviour of the system voltage for other $\Delta\vec{I}$ situations. I.e.:

$$\Delta\vec{V}_{new} = \bar{Z}_{thev} \cdot \Delta\vec{I}_{new} \quad \{ 2-31 \}$$

2.6 THE SQUARE ROOT FUNCTION

As will be shown in Chapters 5 and 6, the harmonic domain square root function can be used for direct evaluation of saturation characteristics and is the basic building block for the direct modelling of electronic switching functions in the harmonic domain. Three algorithms have been set up and used to evaluate the square root of a waveform.

The objective of each of the algorithms is to solve (in the harmonic domain), the equivalent of the algebraic expression:

$$r^2 - x = 0 \quad \{ 2-32 \}$$

for 'r' where 'r' is the root and 'x' is the argument

2.6.1 The 'Exact' Newton-Raphson Solution

The first algorithm considered is based on a Newton-Raphson solution [36] of the algebraic equation:

$$f(r) = r^2 - x = 0 \quad \{ 2-33 \}$$

The Newton-Raphson solution is given by:

$$r_i = r_{i-1} - \left(\frac{\partial f}{\partial r} \right)^{-1} f_i \quad \{ 2-34 \}$$

since:

$$\frac{\partial f}{\partial r} = 2r \quad \{ 2-35 \}$$

$$r_i = \frac{r_{i-1} + r_{i-1}^{-1}x}{2} \quad \{ 2-36 \}$$

where i denotes the current iteration.

In the harmonic domain, Equation 2-33 becomes:

$$f(\bar{R}) = T_p(\bar{R}) \cdot \bar{R} - \bar{X} = \bar{0} \quad \{ 2-37 \}$$

It can be shown that:

$$\frac{\partial}{\partial \bar{R}} (T_p(\bar{R}) \cdot \bar{R}) = T_p(\bar{R}) \quad \{ 2-38 \}$$

and therefore, in the harmonic domain, the iterative solution becomes

$$\bar{R}_i = \frac{\bar{R}_{i-1} + T_p^{-1}(\bar{R}_{i-1})\bar{X}}{2} \quad \{ 2-39 \}$$

This is effectively the same algorithm as given by Equation 2-36⁹.

The Newton-Raphson method is known to be affected by the initial condition or “seed”. Several choices for this seed were investigated, all of which appeared to work to a limited degree as follows:

$$\text{Method 1 } \bar{R}_0 = \bar{O}ne$$

$$\text{Method 2 } \bar{R}_0 = \bar{O}ne \sqrt{\{|\bar{X}|\}}$$

$$\text{Method 3 } \bar{R}_0 = \bar{X}$$

In Method 2 above $\{|\bar{X}|\}$ is the magnitude of the harmonic domain array expressed as the root of the sum of the squared magnitudes of the elements (or Frobenius norm) in the array¹⁰. It is identical to the length of a vector equated to the single dimension array 'X'.

In order to limit the time for computations, the number of harmonics was restricted to 20, with a tolerance based on both the magnitude of the argument and the number of harmonics in the vector.

The exit criterion was based on the magnitude of the error defined as:

$$\epsilon_{rr} = \sqrt{\{|\bar{X} - T_p(\bar{R}_i)\bar{R}_i|\}} \quad \{ 2-40 \}$$

$$\left. \begin{array}{l} \epsilon_{rr} \leq \text{tol} \\ \text{tol} = \frac{10^{-10}}{n_{\max} + 1} \{|\bar{X}|\} \end{array} \right\} \quad \{ 2-41 \}$$

⁹ Information located at <http://www2.sunysuffolk.edu/wrightj/MA28/squareroots1.pdf> indicates that this algorithm has ancient Egyptian origins. The reference identifies it as 'Method of the Means' and presents several numerical examples.

¹⁰ The unusual notation used here is to avoid confusion with the absolute function denoted |X| as used elsewhere in this document

Preliminary testing of the algorithm showed that the algorithm is relatively robust with convergence to within the tolerance in about 3 to 4 iterations for positive¹¹ arguments. The algorithm could require up to 9 or 10 iterations to reach a solution for arguments where the waveform represented by the argument reaches zero a few times during the period. The number of iterations is dependant on the number of harmonics, with more iteration required for an increased number of harmonics.

The algorithm is also relatively insensitive to the choices investigated for initial values. The algorithm returns the positive root if the initial choice is positive and if the argument is positive.

The algorithm was tested for arguments that are known to have solutions where the time domain waveform could be negative. For example the time domain waveform $\cos^2(\omega t)$, which can also be expressed as its harmonic equivalent $\frac{1}{2}(1 + \cos(2\omega t))$ has a root ' $\cos(\omega t)$ ' which has negative values in the time domain for $\frac{1}{2}$ of the period. The algorithm does not return the equivalent of $\cos(\omega t)$ but returns the coefficients of only the positive root waveform as desired.

For example, in the harmonic domain the argument ' $\cos^2(\omega t)$ ' would be represented by its harmonic equivalent ' $\frac{1}{2}(1 + \cos(2\omega t))$ ' in an array¹²:

arg T =	0	1	2	3	4	5	6	7	8	9	10	11
	0.5	0	0	0.5	0	0	0	0	0	0	0	0

The coefficients of the returned solution are:

root T =	0	1	2	3	4	5	6	7	8	9	10	11	12	13	14	15	16	17	18
	0.637	0	0	0.424	0	0	0	-0.085	0	0	0	0.036	0	0	0	-0.02	0	0	0

¹¹ In this context, 'positive' means that the time domain waveform represented by the variable is greater than zero over the entire period.

¹² The arrangement of data in this array follows the convention defined by Equation 2-5.

The time domain waveform corresponding to 'root' is compared to the time domain waveform of the argument and the other possible solution 'cos(ωt)' in Figure 2-1.

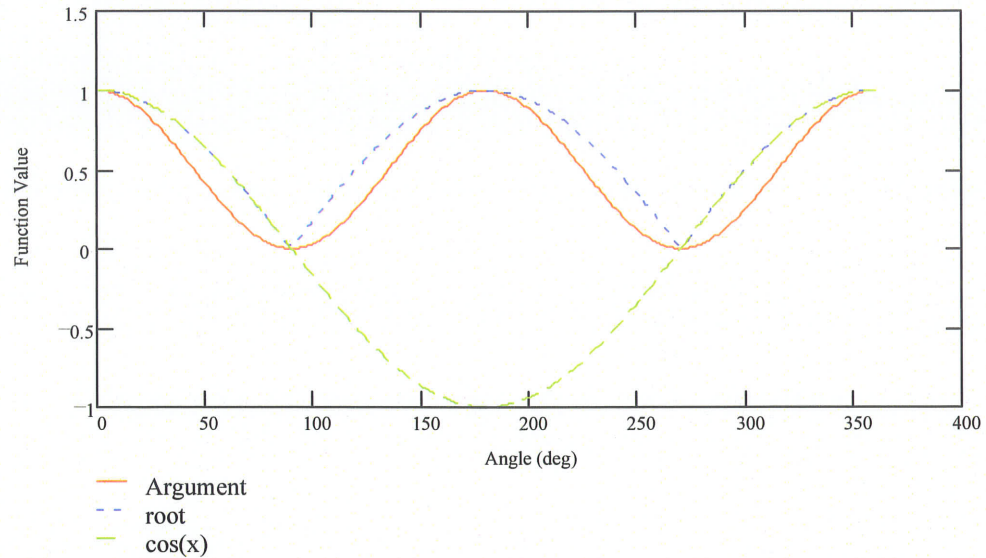


Figure 2-1 'Root' and 'Cos(x)' Solutions to $\sqrt{\cos^2(\omega t)}$

The algorithm deteriorates if the argument waveform lies at or close to zero for any extended period of the cycle. This is not surprising as the condition of the product transformation matrix becomes more ill-conditioned and eventually the algorithm fails to reach a solution within the 20 iterations, as the percentage of the time that the waveform lies at zero increases.

For a periodic step function between a value of 1.0 and 0.0, the algorithm fails to converge within 20 iterations. The time domain evaluation based on the non-converged solution is shown in Figure 2-2.

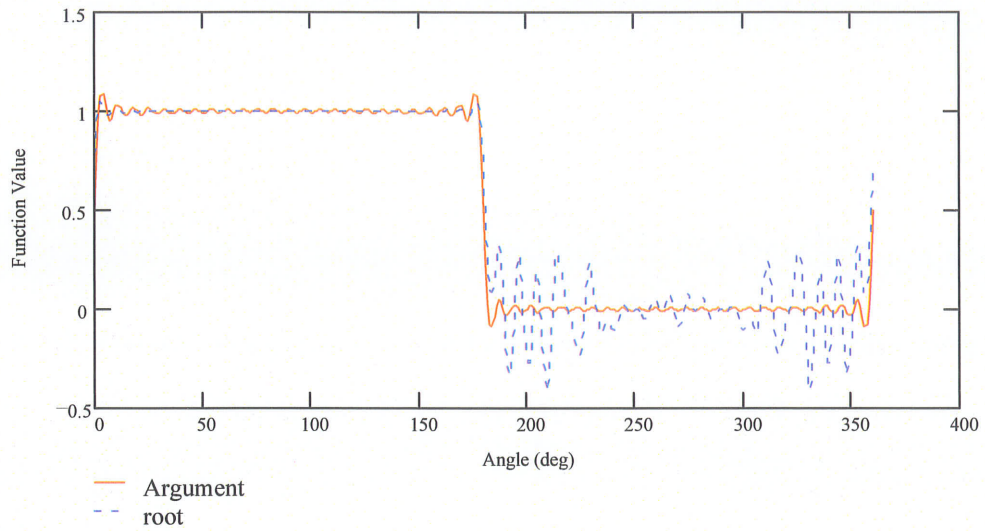


Figure 2-2 'Exact' Newton-Raphson Solution to $\sqrt{\text{step function}}$ after 20 Iterations

For this argument, the theoretical solution should be identical to the argument. Instead, the algorithm produces an unsatisfactory solution.

The solution does not improve with increased iterations. In fact, the solution has less visual error after the 10th iteration as depicted in the regenerated waveform of Figure 2-3.

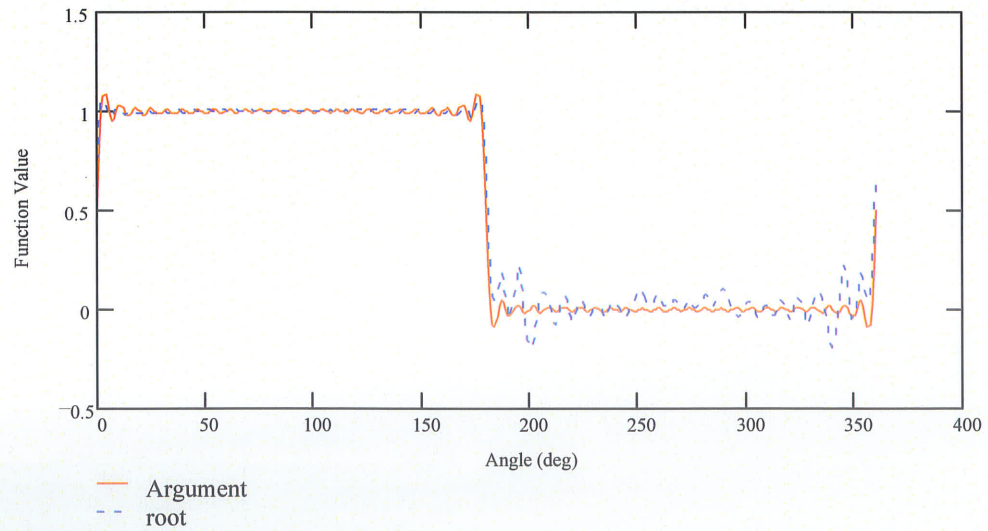


Figure 2-3 'Exact' Newton-Raphson Solution to $\sqrt{\text{step function}}$ after 10 Iterations

As many applications using power switching devices result in voltage or current waveforms similar to the step function above, the above algorithm is considered to have only limited applications.

2.6.2 The Taylor Series Expansion

A second solution algorithm was developed based on the Taylor series expansion:

$$f(a+y) = \sum_{n=0}^N \frac{y^n}{n!} f^{(n)}(a) + R_N \quad \{ 2-42 \}$$

around a value of $a=1$.

The operating point of 1 was selected to be consistent with the Taylor series expansion of the square root function given in [37]¹³.

The Taylor series approximation of the square root function is:

$$f(1+y) = \sqrt{1+y} = \sqrt{x} \quad \{ 2-43 \}$$

where:

$$\begin{aligned} y &= x - 1 \\ f'(a) &= \frac{1}{2} a^{-\frac{1}{2}} \\ f''(a) &= -\frac{1}{4} a^{-\frac{3}{2}} = -\frac{1}{2} f'(a) a^{-1} \\ f^{(3)}(a) &= -\frac{3}{2} \left(-\frac{1}{4}\right) a^{-\frac{5}{2}} = -\frac{3}{2} f''(a) \end{aligned} \quad \{ 2-44 \}$$

Since, $n! = n(n-1)!$ and since $a=1$, the change in the coefficient from the $(n-1)^{\text{th}}$ derivative to the n^{th} derivative is the multiplying factor:

$$c_n = \frac{\frac{3}{2} - n}{n} \text{ where } c_0 = 1 \quad \{ 2-45 \}$$

Thus, the change in the Taylor series term is:

$$\text{corr}_n = c_n y^{n-1} \quad \{ 2-46 \}$$

¹³ The series given in [37] only provides the first few coefficients of the expansion. The rest can be derived using Equation 2-45

With a sufficient number of terms in the series, the remainder term R_N can be neglected.

Applying the same algorithm to the harmonic domain analysis, the change in the Taylor series term becomes:

$$\bar{C}orr_n = c_n T_p(\bar{Y}) \bar{Y}^{n-1} \quad \{ 2-47 \}$$

where:

$$\bar{Y}^{n-1} = T_p(\bar{Y}) \bar{Y}^{n-2} \text{ etc.} \quad \{ 2-48 \}$$

As the algebraic algorithm converges only for values of y between +1.0 and -1.0, the argument is first divided by a scalar constant:

$$\text{factor} = \{ \{ \bar{X} \} \} \quad \{ 2-49 \}$$

where $\{ \{ \bar{X} \} \}$ again denotes the magnitude of the vector equivalent to \bar{X} .

The result is multiplied by $\sqrt{\text{factor}}$.

The exit criteria selected is based on a pre-selected maximum value of 'N' or if:

$$\{ \{ \bar{C}orr_n \} \} < \text{tol} \quad \{ 2-50 \}$$

or:

$$\{ \{ \bar{C}orr_n \} \} > \{ \{ \bar{C}orr_{n-1} \} \} \quad \{ 2-51 \}$$

The algorithm is efficient in terms of computing requirements in that the product transposition matrix is created once and only matrix multiplication is involved.

An arbitrary limit of 500 corrections was used in the test algorithm. An exit tolerance of $10^{-5}|x|$ was chosen.

The algorithm again works well for waveforms which do not cross or touch zero. Test systems not shown here with a maximum harmonic of 50 and with a waveform minimum of about 50% of its maximum satisfies the exit criteria in about 10 steps. The 'cos²' test

again solves to the positive root but over 360 corrections are required. The periodic step function test exits prematurely after about 65 steps after which the magnitude of the correction term starts to increase.

The evaluated waveform based on the Fourier coefficients on exit is compared to the waveform of the argument in Figure 2-4:

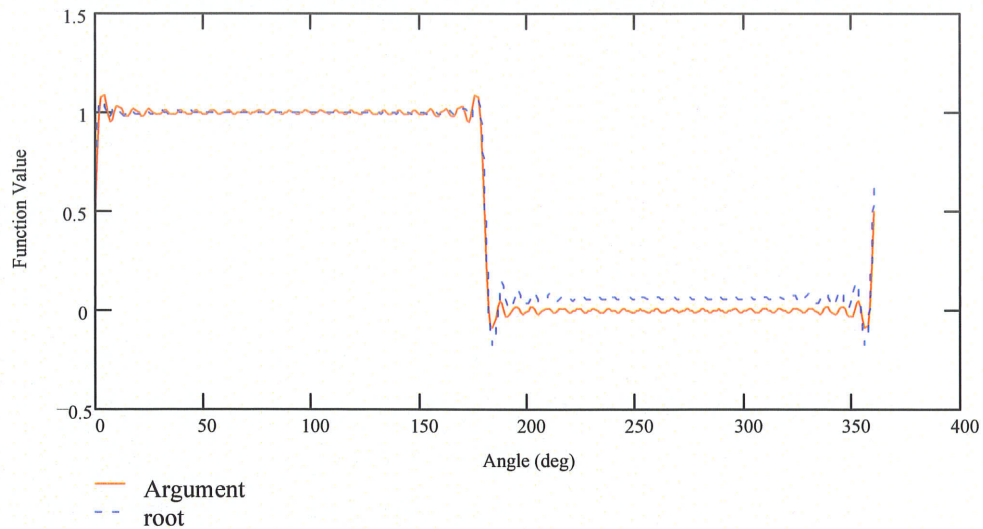


Figure 2-4 Taylor Series Solution to $\sqrt{\text{step function}}$ after 65 Steps

The solution reproduces a satisfactory waveform for the positive portion of the cycle but introduces a 'dc' offset error for the 'zero' portion of the waveform.

Similar to the Newton-Raphson solution, the above algorithm is considered to have only limited applications.

2.6.3 The Minimum 'Best Fit' Newton-Raphson Solution

In the 'exact' Newton-Raphson solution, the algorithm sometimes diverges after a 'close' solution is reached. It was believed that truncation of the harmonic series during harmonic multiplication was creating a situation where a solution to the basic equation:

$$\bar{X} - T_p(\bar{R}_i)\bar{R}_i = \bar{0} \quad \{ 2-52 \}$$

was not possible.

A 'best fit' Newton-Raphson algorithm was proposed and developed. The algorithm is an improvement over the 'exact' solutions in that it is more 'robust' and as will be demonstrated does not diverge for tested arguments including the step function. In this 'best fit' Newton-Raphson algorithm, the error defined by the scalar 'ε' is minimized in the 'least squared' sense where:

$$\varepsilon = \bar{F}^T \bar{F} \quad \{ 2-53 \}$$

where:

$$\bar{F} = \bar{X} - T_p(\bar{R})\bar{R} \quad \{ 2-54 \}$$

At the minimum value of ε:

$$\frac{\partial \varepsilon}{\partial \bar{R}} = \bar{0} \quad \{ 2-55 \}$$

where $\frac{\partial \varepsilon}{\partial \bar{R}}$ is defined to be:

$$\frac{\partial \varepsilon}{\partial \bar{R}} = \left[\frac{\partial \varepsilon}{\partial Ra_0} \quad \frac{\partial \varepsilon}{\partial Ra_1} \quad \frac{\partial \varepsilon}{\partial Rb_1} \quad \dots \quad \frac{\partial \varepsilon}{\partial Ra_{n \max}} \quad \frac{\partial \varepsilon}{\partial Rb_{n \max}} \right]^T \quad \{ 2-56 \}$$

$$\frac{\partial \varepsilon}{\partial Ra_0} = \frac{\partial (\bar{F}^T \bar{F})}{\partial Ra_0} = 2 \frac{\partial \bar{F}^T}{\partial Ra_0} \bar{F} \quad \{ 2-57 \}$$

or:

$$\frac{\partial \varepsilon}{\partial \bar{R}} = 2 \frac{\partial \bar{F}^T}{\partial \bar{R}} \bar{F} \quad \{ 2-58 \}$$

$$\begin{aligned} \frac{\partial \bar{F}}{\partial Ra_0} &= -T_p(\bar{R}) [1 \ 0 \ 0 \ \dots]^T - \frac{1}{2} \begin{bmatrix} 2 & 0 & \dots \\ 0 & 2 & \dots \\ \vdots & \vdots & \ddots \end{bmatrix} \bar{R} \\ &= -\bar{R} - [\bar{1}] \bar{R} = -2\bar{R} \text{ or } -2T_p(\bar{R}) \begin{bmatrix} 1 \\ 0 \\ \vdots \end{bmatrix} \end{aligned} \quad \{ 2-59 \}$$

Similarly:

$$\frac{\partial F}{\partial \bar{R} a_1} = -2T_P(\bar{R}) \begin{bmatrix} 0 \\ 1 \\ 0 \\ \vdots \end{bmatrix} \quad \{ 2-60 \}$$

Therefore:

$$\frac{\partial F^T}{\partial \bar{R}} = -2T_P^T(\bar{R}) \quad \{ 2-61 \}$$

or:

$$\frac{\partial F}{\partial \bar{R}} = -2T_P^T(\bar{R}) \quad \{ 2-62 \}$$

Since:

$$\frac{\partial \varepsilon}{\partial \bar{R}} = 2 \frac{\partial \bar{F}^T}{\partial \bar{R}} \bar{F} \quad \{ 2-63 \}$$

then:

$$\frac{\partial \varepsilon}{\partial \bar{R}} = -4T_P^T(\bar{R}) \bar{F} \quad \{ 2-64 \}$$

For minimum error, the algorithm must find \bar{R} such that:

$$T_P^T(\bar{R}) \bar{F} = \bar{0} \quad \{ 2-65 \}$$

Using Newton-Raphson solution

$$\bar{Q} = T_P^T(\bar{R}) \bar{F} = T_P^T(\bar{R}) \bar{X} - T_P^T(\bar{R}) T_P(\bar{R}) \bar{R} \quad \left| \right. \\ \frac{\partial \bar{Q}}{\partial \bar{R}} = \frac{\partial [T_P^T(\bar{R}) \bar{X}]}{\partial \bar{R}} - \frac{\partial [T_P^T(\bar{R}) T_P(\bar{R}) \bar{R}]}{\partial \bar{R}} \quad \{ 2-66 \}$$

$$\begin{aligned}
 & T_P^T(\bar{R})\bar{X} \\
 &= \frac{1}{2} \begin{bmatrix} 2Ra_0Xa_0 + 2Ra_1Xa_1 + 2Rb_1Xb_1 + 2Ra_2Xa_2 + 2Rb_2Xb_2 + \dots \\ Ra_1Xa_0 + (2Ra_0 + Ra_2)Xa_1 + 2Rb_2 * Xb_2 + (Ra_1 + Ra_3)Xa_2 + (Rb_1 + Rb_3)Xb_2 + \dots \\ \vdots \end{bmatrix} \\
 &= \frac{1}{2} \begin{bmatrix} 2Xa_0 & 2Xa_1 & 2Xb_1 & 2Xa_2 & 2Xb_2 & 2Xa_3 & 2Xb_3 & \dots \\ 2Xa_1 & Xa_0 + Xa_2 & 2Xb_2 & Xa_1 + Xa_3 & Xb_1 + Xb_3 & Xa_2 + Xa_4 & Xb_2 + Xb_4 & \dots \\ 2Xb_1 & 2Xb_2 & Xa_0 - Xa_2 & -Xb_1 + Xb_3 & Xa_1 - Xa_3 & -Xb_2 + Xb_4 & Xa_2 - Xa_4 & \dots \\ 2Xa_2 & Xa_1 + Xa_3 & -Xb_1 + Xb_3 & Xa_0 + Xa_4 & 2Xb_4 & Xa_1 + Xa_5 & Xb_1 + Xb_5 & \dots \\ 2Xb_2 & Xb_1 + Xb_3 & Xa_1 - Xa_3 & 2Xb_4 & Xa_0 - Xa_4 & -Xb_1 + Xb_5 & Xa_1 - Xa_5 & \dots \\ 2Xa_3 & Xa_2 + Xa_4 & -Xb_2 + Xb_4 & Xa_1 + Xa_5 & -Xb_1 + Xb_5 & Xa_0 + Xa_6 & 2Xb_6 & \dots \\ 2Xb_3 & Xb_2 + Xb_4 & Xa_2 - Xa_4 & Xb_1 + Xb_5 & Xa_1 - Xa_5 & 2Xb_6 & Xa_0 - Xa_6 & \dots \\ \vdots & \vdots & \vdots & \vdots & \vdots & \vdots & \vdots & \ddots \end{bmatrix} \begin{bmatrix} Ra_0 \\ Ra_1 \\ Rb_1 \\ Ra_2 \\ Rb_2 \\ Ra_3 \\ Rb_3 \\ \vdots \end{bmatrix}
 \end{aligned}$$

.....{ 2-67 }

If we define:

$$T_2(\bar{X}) = \begin{bmatrix} 2Xa_0 & 2Xa_1 & 2Xb_1 & 2Xa_2 & 2Xb_2 & 2Xa_3 & 2Xb_3 & \dots \\ 2Xa_1 & Xa_0 + Xa_2 & 2Xb_2 & Xa_1 + Xa_3 & Xb_1 + Xb_3 & Xa_2 + Xa_4 & Xb_2 + Xb_4 & \dots \\ 2Xb_1 & 2Xb_2 & Xa_0 - Xa_2 & -Xb_1 + Xb_3 & Xa_1 - Xa_3 & -Xb_2 + Xb_4 & Xa_2 - Xa_4 & \dots \\ 2Xa_2 & Xa_1 + Xa_3 & -Xb_1 + Xb_3 & Xa_0 + Xa_4 & 2Xb_4 & Xa_1 + Xa_5 & Xb_1 + Xb_5 & \dots \\ 2Xb_2 & Xb_1 + Xb_3 & Xa_1 - Xa_3 & 2Xb_4 & Xa_0 - Xa_4 & -Xb_1 + Xb_5 & Xa_1 - Xa_5 & \dots \\ 2Xa_3 & Xa_2 + Xa_4 & -Xb_2 + Xb_4 & Xa_1 + Xa_5 & -Xb_1 + Xb_5 & Xa_0 + Xa_6 & 2Xb_6 & \dots \\ 2Xb_3 & Xb_2 + Xb_4 & Xa_2 - Xa_4 & Xb_1 + Xb_5 & Xa_1 - Xa_5 & 2Xb_6 & Xa_0 - Xa_6 & \dots \\ \vdots & \vdots & \vdots & \vdots & \vdots & \vdots & \vdots & \ddots \end{bmatrix}$$

.....{ 2-68 }

then:

$$T_P^T(\bar{R})\bar{X} = T_2(\bar{X})\bar{R} \quad \{ 2-69 \}$$

and:

$$\begin{aligned}
 \frac{\partial(T_P^T(\bar{R})\bar{X})}{\partial Ra_0} &= \frac{\partial(T_2(\bar{X})\bar{R})}{\partial Ra_0} = \text{col}_1(T_2(\bar{X}))^T \\
 \frac{\partial(T_P^T(\bar{R})\bar{X})}{\partial Ra_1} &= \frac{\partial(T_2(\bar{X})\bar{R})}{\partial Ra_1} = \text{col}_2(T_2(\bar{X}))^T \\
 &\vdots
 \end{aligned} \quad \{ 2-70 \}$$

or:

$$\frac{\partial(T_P^T(\bar{R})\bar{X})}{\partial \bar{R}} = (T_2(\bar{X}))^T = T_2(\bar{X}) \quad \{ 2-71 \}$$

since $T_2(\bar{X})$ is symmetrical.

It can be shown that:

$$\frac{\partial [T_P^T(\bar{R}) T_P(\bar{R}) \bar{R}]}{\partial \bar{R}} = \frac{\partial [T_P^T(\bar{R}) \bar{K}_1]}{\partial \bar{R}} + \frac{\partial [\bar{A}_1 T_P(\bar{R}) \bar{K}_2]}{\partial \bar{R}} + \frac{\partial [\bar{A}_2 \bar{R}]}{\partial \bar{R}} \quad \{ 2-72 \}$$

and if we make the following substitutions:

$$\left. \begin{aligned} \bar{K}_1 &= T_P(\bar{R}) \bar{R} \\ \bar{A}_1 &= T_P^T(\bar{R}) \\ \bar{K}_2 &= \bar{R} \\ \bar{A}_2 &= T_P^T(\bar{R}) T_P(\bar{R}) \end{aligned} \right\} \quad \{ 2-73 \}$$

then:

$$\left. \begin{aligned} \frac{\partial [T_P^T(\bar{R}) \bar{K}_1]}{\partial \bar{R}} &= T_2(\bar{K}_1) = T_2(T_P(\bar{R}) \bar{R}) \\ \frac{\partial [\bar{A}_1 T_P(\bar{R}) \bar{K}_2]}{\partial \bar{R}} &= \frac{\partial [\bar{A}_1 T_P(\bar{R}) \bar{K}_2]}{\partial \bar{R}} = \frac{\partial [\bar{A}_1 T_P(\bar{K}_2) \bar{R}]}{\partial \bar{R}} = T_P^T(\bar{R}) T_P(\bar{R}) [\bar{I}] \\ \frac{\partial [\bar{A}_2 \bar{R}]}{\partial \bar{R}} &= T_P^T(\bar{R}) T_P(\bar{R}) [\bar{I}] \end{aligned} \right\} \quad \{ 2-74 \}$$

Therefore:

$$\frac{\partial [T_P(\bar{R})^T T_P(\bar{R}) \bar{R}]}{\partial \bar{R}} = T_2(T_P(\bar{R}) \bar{R}) + 2T_P^T(\bar{R}) T_P(\bar{R}) \quad \{ 2-75 \}$$

The Jacobian is given by:

$$\bar{J} = \left(\frac{\partial \bar{Q}}{\partial \bar{R}} \right)^T = \frac{\partial \bar{Q}}{\partial \bar{R}} = T_2(\bar{X}) - T_2(T_P(\bar{R}) \bar{R}) - 2T_P^T(\bar{R}) T_P(\bar{R}) \quad \{ 2-76 \}$$

and the iterative solution becomes:

$$\left. \begin{aligned} \bar{\Delta} &= -\bar{J}^{-1} \bar{Q}_{i-1} \\ \bar{R}_i &= \bar{R}_{i-1} + \bar{\Delta} \end{aligned} \right\} \quad \{ 2-77 \}$$

The initial values for the solution and the exit tolerance were chosen to be the same as the 'exact' Newton-Raphson solution on the assumption that the algorithm would always converge to a minimum error solution.

Initial trials with the algorithm indicated some problems. The algorithm worked well for positive waveforms and for waveforms that just 'touched' zero. For the step waveform argument, however, the error ' ϵ ' would reduce logarithmically for initial iterations but eventually the rate of reduction would decrease, the error would approach a minimum value, and at a critical iteration the error would increase dramatically. The value of the error ' ϵ ' at each iteration is shown in Figure 2-5. The error reaches a minimum at the 9th iteration, after which, numerical 'hunting' begins.

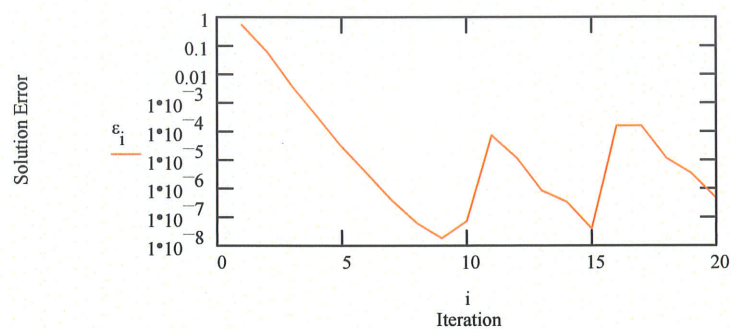


Figure 2-5 Variation of Error in 'Best Fit' Newton-Raphson Solution to $\sqrt{\text{step function}}$

The solution at the iteration with minimum error (iteration 9) is closer to the actual solution as shown in Figure 2-6. There is still a slight dc offset in the 'zero' portion of the time domain waveform. This can be explained by closer examination of the time domain waveform of the argument to the square root function. High frequency Gibb's-like oscillations are evident in the equivalent time domain representation of the original step function¹⁴. The consequence of the oscillations is that the argument to the square root function is actually negative over some portions of the time domain. In the time domain the solution at these locations would be imaginary, implying that in the frequency domain, there should be a corresponding complex harmonic content in the solution.

¹⁴This is a well known and documented phenomena, arising at discontinuities as a result of truncation of the number of harmonics in the series representing the function.

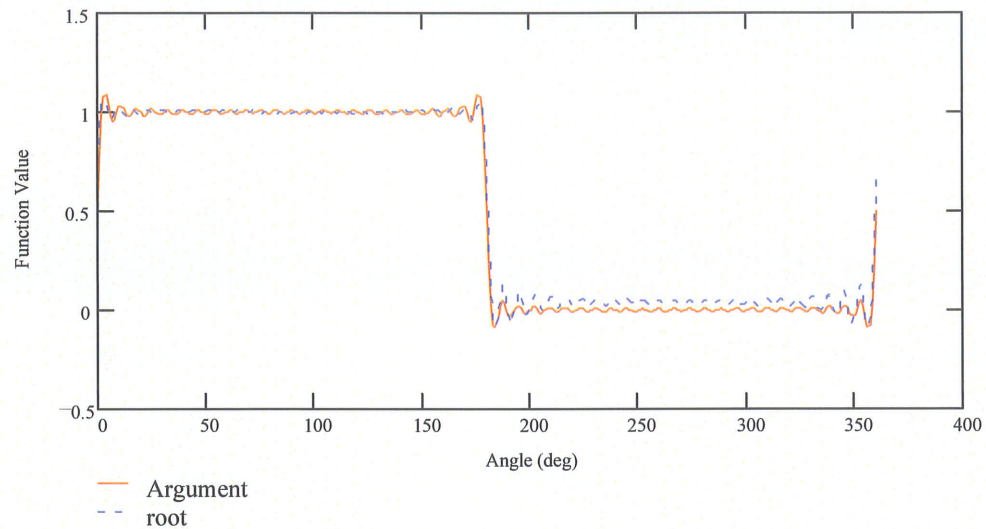


Figure 2-6 'Best Fit' Newton-Raphson Solution to $\sqrt{\text{step function}}$ after 9 Iterations

The whole basis of the author's approach to harmonic domain analysis is the use of 'real' variables. The minimum error solution of the 'best fit' algorithm is most likely the closest solution that can be achieved within the 'real' variable constraint for the given step waveform.

The failure to converge to a minimum is likely due to numerical issues. The Jacobian of the algorithm involves transformation matrices that are a function of both the harmonic content of the argument and the latest estimate of the root. The transformation matrices for the argument are poorly conditioned due to the proportion of the time domain that the step waveform is at zero. As the estimate of the root gets closer to the actual solution, the condition of the root matrix will also reduce. At the minimum solution the condition of the resultant Jacobian likely deteriorates to a situation where it is almost singular and although the error is small, the product of the inverse of the Jacobian and the error array is numerically incorrect, resulting in over-correction of the root. Once the latest estimate of the root is sufficiently separated from the actual solution, the conditions of its matrices improve and hunting in the solution occurs.

The convergence/numerical issue was overcome by exiting the algorithm when the absolute value of the error 'ε' increased over the previous iteration. The modified algorithm, 'robust' in its solutions for the step wave as well as for non-zero positive waveforms is likely the 'best' that can be achieved within the constraint of real harmonic domain coefficients. The resultant solution, though not precisely accurate, is acceptable for the analysis of most situations covered in this thesis.

2.6.4 Other Possible Solutions.

Although an 'acceptable' solution is obtained with the 'best fit' algorithm discussed in the above section, the author believes there may be other solutions that would improve the accuracy of the square root evaluation for the step function, but he leaves this problem for future investigators. These ideas are discussed in Chapter 7.

While other solutions may be available, the 'best fit' algorithm does provide good results when applied to direct evaluation of saturation effects as described in Chapter 6 and for basic diode switching operations as described in Chapter 5.

2.7 THE ABSOLUTE FUNCTION

In many control and measuring circuits, the absolute function '|x|' where x is a time varying quantity, is frequently used to simulate the behaviour of a full wave rectifier circuit. It can also be used to obtain an estimate of the state of a sinusoidal waveform. If the input waveform is dominated by a single frequency, the peak and RMS quantities can be determined to a very good approximation by appropriate scalar multiplication of the average of the absolute or fully rectified signal. The accuracy of the approximation reduces in the presence of harmonics in the signal.

With a robust harmonic domain square root function, a very good approximation of the 'absolute' function can be developed based on the algorithm:

$$\text{Abs}(\vec{X}) = \text{Sqrt}(T_P(\vec{X})\vec{X}) \quad \{ 2-78 \}$$

This harmonic domain algorithm was tested on many different waveforms as part of this work. Provided that the corresponding time domain waveform to the argument has only transitions through zero, not sustained operation at close to zero, all three square root algorithms described in Section 2.6 of this chapter perform well as part of the harmonic domain absolute function. The harmonic domain absolute function, of course, suffers from the same limitations as each of the square root functions.

As the algebraic function can be used to simulate fully rectified control signals, it was believed that the corresponding harmonic domain function could be used to simulate the behaviour of power system rectifier circuits. The use of the harmonic domain application of the absolute function to the harmonic analysis of power systems is given in Chapter 5.

2.8 THE SIGN FUNCTION

The time domain sign function [$f(x) = 1$ for positive x , 0 for $x=0$ and -1 for negative x] is useful in the analysis of many power electronic circuits, for example in a comparator which compares a ramp with a level for issuing firing pulses. As it is also the derivative of the absolute value function it (in harmonic domain form) could prove useful in developing Newton-Raphson algorithms for the solution of systems using the absolute function.

The sign function can be generated from the absolute function in one of several ways:

$$\begin{aligned} \text{Sign}(\vec{X}) &= (T_p(\vec{X}))^{-1} \vec{A} \text{Abs}(\vec{X}) \\ \text{Sign}(\vec{X}) &= (T_p(\vec{A} \text{Abs}(\vec{X})))^{-1}(\vec{X}) \end{aligned} \quad \{ 2-79 \}$$

Both functions are subject to the limitations of the underlying square root function.

The sign function is used in the Newton-Raphson solution of the test circuit described in Section 5.4 of Chapter 5.

2.9 THE DERIVATIVE OPERATOR

Development of harmonic domain models of inductors of the electrical system and many of the transfer function block diagrams of control systems require the ability to differentiate a waveform with respect to time. In this section a sparse harmonic domain transformation matrix is developed that provides the harmonic content of the time derivative of the original waveform. Since some form of this technique is used in almost all harmonic domain analysis tools methods, it is presented here to contribute to the documentation of the author's harmonic domain analysis methodology.

Given the function:

$$f(\omega t) = \frac{fa_0}{2} + \sum_{n=1}^{\infty} [fa_n \cos(n \cdot \omega t) + fb_n \sin(n \cdot \omega t)] \quad \{ 2-80 \}$$

$$\frac{d}{dt} f(\omega t) = \sum_{n=1}^{\infty} [-n\omega \cdot fa_n \sin(n \cdot \omega t) + n\omega \cdot fb_n \cdot \cos(n \cdot \omega t)] \quad \{ 2-81 \}$$

In the harmonic domain:

$$\frac{d}{d\omega t} \bar{F} = \bar{D} \cdot \bar{F} \quad \{ 2-82 \}$$

where \bar{D} is a matrix representing a derivative operator:

$$\bar{D} = \begin{vmatrix} 0 & 0 & 0 & \dots & 0 & 0 \\ 0 & 0 & 1 & & 0 & 0 \\ 0 & -1 & 0 & & 0 & 0 \\ \vdots & & & \ddots & & \\ 0 & 0 & 0 & 0 & 0 & n \\ 0 & 0 & 0 & 0 & -n & 0 \end{vmatrix} \quad \{ 2-83 \}$$

Use of the derivative function to set up the characteristic of an electrical network is described in Chapter 4. Use of the derivative function to model several control function block diagrams is described in Chapter 3.

2.10 OTHER MATHEMATICAL FUNCTIONS

This chapter has described the development of what the author believes are the fundamental mathematical harmonic domain models that are essential to the development

of a direct harmonic domain analysis tool. The operations and functions can be used to develop more complete models by the users of the HDA methodology proposed by the author.

CHAPTER 3

LINEAR POWER SYSTEM ELEMENTS IN THE HARMONIC DOMAIN

3.1 INTRODUCTION

This chapter describes how power system passive electrical elements are modelled in the proposed HDA model. The same principles have been used in almost all HDA models considered in this thesis. They are presented here, however, to complete the description of the propose HDA methodology and to highlight some of the limitations.

3.2 THE ADMITTANCE MATRIX

One of the most common equations used to model electrical elements in the power system is the admittance matrix equation, i.e.:

$$\begin{bmatrix} i_1 \\ \vdots \\ i_k \end{bmatrix} = \begin{bmatrix} y_{11} & \cdots & y_{1k} \\ \vdots & \ddots & \vdots \\ y_{k1} & \cdots & y_{kk} \end{bmatrix} \cdot \begin{bmatrix} v_1 \\ \vdots \\ v_k \end{bmatrix} \quad \{ 3-1 \}$$

where:

v_k corresponds to the voltage at node 'k' in the network

i_k corresponds to the current injections into the network at node 'k'

$y_{*,*}$ corresponds to the elements of the admittance matrix

The off-diagonal elements of the matrix correspond to the negative of the admittance of the branch interconnecting the two nodes. The diagonal of the matrix (e.g. y_{kk}) corresponds to the sum of the admittances of all branches connected to node 'k' including admittance of all shunt connected devices.

One of the advantages of the admittance matrix is that the mathematical model of the network can be built up component by component. As each new branch is encountered in the data, its corresponding locations in the admittance matrix are identified, creating a new node if the node does not exist. A new node is often added at the end of the array for convenience along (with its corresponding row and column in the matrix).

In a similar fashion, the location for information associated with any shunt connected element is determined directly from its node number.

The admittance matrix itself is created from an initially empty matrix by sequentially adding the admittance (or negative admittance for off-diagonal elements) of each branch or shunt to the admittance(s) already present in the matrix at the appropriate locations.

In a power system network, there are generally only a few branches emanating from any given node, possibly only 3 to 4 times as many branches as there are nodes for the network. Hence, the admittance matrix above is very sparse. In addition, for most conditions the admittance matrix is symmetrical (i.e. y_{ij} is equal to y_{ji}). Most applications take advantage of the matrix sparsity and symmetry in the storage of the definition of the network structure and admittances.

In power system load flow and stability analysis tools, the voltage v_k and the current i_k are complex variables (real and imaginary components), representing the fundamental frequency component of the power system voltage waveform by its positive sequence equivalent voltage. The magnitude of the voltage is equal to the magnitude of its complex variable. The phase displacement of the voltage relative to other buses in the system is contained in the angle of the polar presentation of the complex variable. Therefore, in the load flow and stability tools, the admittance matrix houses the admittances expressed in complex form.

Most time domain solution algorithms of a network use Dommel's approach [35] in which inductive and capacitive elements are treated as a Norton equivalent with only real time-independent admittances (i.e. conductances) and real time-dependent current

injections at the node. Therefore, the admittance matrix as used in the time domain house only real variables.

Most harmonic domain algorithms known to the author use a formulation of an admittance matrix with a similar structure to Equation 3-1, except that in the harmonic domain each element in the admittance matrix of Equation 3-1 represents a complete matrix defining the harmonic relationships of the branch and each element in the voltage and current vectors is an array housing all of the harmonic content of the current and voltage.

In the methodology proposed by the author, each element of the current and voltage arrays of Equation 3-1 consists of a real array of dimension $(2n_{\max}+1, \text{ by } 1)$ containing the harmonic content of the current or voltage waveform for its corresponding node in accordance with the layout described in Section 2.2 of Chapter 2.

In some other HDA schemes [10], the complex Fourier series has been adopted¹⁵, and as a result, the equivalent arrays (now of dimension only $n_{\max}+1$) would house complex variables. Other HDA schemes [29] could have slightly different structures for the arrays, but in general, the basic form of Equation 3-1 will likely be used.

The remaining sections in this chapter document the treatment of the main power system passive elements in the authors HDA model.

3.3 RESISTORS

A resistor whose resistance is independent of frequency is very simply modelled in the harmonic domain by the array ' \bar{R} ' where ' \bar{R} ' satisfies the ohmic equation:

$$\bar{V}_R = \bar{R} \cdot \bar{I}_R \quad \{ 3-2 \}$$

¹⁵ as opposed to the cosine, sine series expansion used by the author

' \bar{V}_R ' and ' \bar{I}_R ' are arrays housing the harmonic component of the voltage across the resistor and the current through the resistor. The resistance is given by:

$$\bar{R} = r \cdot \bar{I} \quad \{ 3-3 \}$$

Here 'r' is a scalar variable and is equal to the resistance of the resistor and ' \bar{I} ' is the identity matrix.

Resistance of a transmission element can be a function of frequency. This is common in a power system where skin effect plays an important role at higher order harmonics. The resistance of transmission lines and other inductive devices such as transformers and reactors is known to increase with frequency.

Although frequency dependent resistance models have not been specifically addressed elsewhere in this thesis, they can be incorporated very easily into the proposed HDA model. A frequency dependent resistor can be modelled by the diagonal array:

$$\bar{R}(n) = \begin{bmatrix} r(0) & & & & \\ & r(1) & & & 0 \\ & & r(1) & & \\ & & & \ddots & \\ & 0 & & & r(n) \\ & & & & & r(n) \end{bmatrix} \quad \{ 3-4 \}$$

In this matrix, the resistance is assumed to vary according to harmonic in accordance to the function 'r(n)'. The dual entries for the harmonic components are used on the assumption that resistance is independent of the phase relationship at each harmonic between voltage across the resistor and the current through the resistor.

If the resistance is non-zero at every frequency, the matrix ' \bar{R} ' can be inverted into its 'admittance' (in this case conductance) matrix form, i.e.:

$$\bar{G} = \bar{R}^{-1} \quad \{ 3-5 \}$$

As the resistance matrix is diagonal, its inverse is also diagonal.

3.4 INDUCTORS

In the time domain the relationship between the voltage 'v' across an inductor 'L' and the current 'i' through the inductor is given by:

$$\begin{aligned} v(\omega t) &= L \frac{d}{dt} i(\omega t) \\ &= 2\pi f_0 L \frac{d}{d\omega t} i(\omega t) \end{aligned} \quad \{ 3-6 \}$$

The equivalent harmonic domain expression is given by:

$$\bar{V} = \bar{Z}_L \cdot \bar{I} \quad \{ 3-7 \}$$

where:

$$\bar{Z}_L = 2\pi f_0 \cdot L \cdot \bar{D} \quad \{ 3-8 \}$$

and:

\bar{D} is the derivative matrix described in Section 2.9

\bar{V} is the harmonic domain voltage array

\bar{I} is the harmonic domain current array

The zero impedance of the inductor at a frequency of zero creates a singularity in the harmonic impedance matrix. All elements of the first row and first column of the impedance matrix are zero. As a result it cannot be included directly into the complete harmonic domain matrix of the system.

The problem disappears if there is resistance in series with the inductor. In a typical power system application, this is almost always the case. The resultant impedance of the inductor would be:

$$\begin{aligned} \bar{Z}_L &= 2\pi f_0 \cdot L \cdot \bar{D} + r \cdot \bar{I} \\ \text{or:} \\ \bar{Z}_L &= 2\pi f_0 \cdot L \cdot \bar{D} + \bar{R}(n) \end{aligned} \quad \{ 3-9 \}$$

The latter equation would be used if the resistance is dependent on frequency as described in Section 3.3 of this chapter.

With resistance and inductance based on typical power system elements, the matrix ' \bar{Z}_L ' is well conditioned and bounded¹⁶

The admittance matrix formed by the inverse of the impedance matrix, i.e.:

$$\bar{Y}_L = \bar{Z}_L^{-1} \quad \{ 3-10 \}$$

is also bounded and hence sparse.

An alternative way to handle an ideal inductor (i.e. no resistance) would be to treat the dc and harmonic components differently. This is discussed in Chapter 7 along with other ideas for future research in this area.

3.5 CAPACITORS

The harmonic admittance (mhos) of a capacitor can be calculated directly and incorporated into the admittance matrix of:

$$\bar{Y}_C = 2\pi f_0 \cdot C \cdot \bar{D} \quad \{ 3-11 \}$$

where Y is the capacitance (F).

While the admittance can be readily calculated, the singularity in the derivative matrix precludes the creation of an impedance matrix. Similar to the treatment of the inductor (as described in the previous section), if a resistance (or in this case conductance) is included in parallel with the capacitor, the resultant matrix can be inverted.

Unfortunately, capacitors themselves are low loss devices and inclusion of a parallel resistor may not be appropriate. Use of a resistance, consistent with a typical capacitor, would not significantly improve the condition of the resultant admittance matrix. Fortunately, only the admittance matrix, and not its inverse, is required to represent the capacitor using the admittance matrix formulation. The overall admittance matrix can be inverted, provided that there are resistance elements elsewhere in the network,

¹⁶ The matrix is diagonal with a single adjacent element

In Chapter 5, it is suggested that a capacitor could be treated as an impedance to assist in the solution of numerical interaction between capacitor and switching devices. If so, the capacitor impedance issues will have to be addressed at that time.

3.6 OTHER SYSTEM ELEMENTS

The above approach of including Rs and Ls into a Harmonic Domain admittance matrix can be readily extended to other passive elements, although this analysis is not explicitly included in the thesis, for brevity. Step-up and step-down transformers can be incorporated using treatment similar to the model of an off-nominal tap transformer in the load flow and stability model. While directly equating transformer voltage ratios to the tap position(s) of the Edith Clark equations [38] is mathematically exact, large differences in voltage ratios may introduce numerical issues, and in a fashion similar to the power flow, voltage scaling of the system model will likely be required to avoid these problems.

This Page is Intentionally Blank

CHAPTER 4

LINEAR CONTROL SYSTEM FUNCTIONS

4.1 INTRODUCTION

Frequency domain analysis has long been one of the favoured tools in the analysis and design of linear control systems [14], [15]. The proposed Harmonic Domain Analysis of control system functions turns out to be a subset of frequency domain analysis. Control systems are comprised of individual control functions, where the dependence of the output response on the characteristics of the input is defined by a frequency dependent transfer function, often expressed in a Laplace transform form [39].

This chapter describes how simple control functions such as first order lag and proportional-integral-derivative type controllers can be transcribed into the non-linear HDA model proposed. It proceeds to describe the development of a harmonic domain model of a time domain function that compares a repetitive ramp signal with another time varying (but also repetitive) input signal. This time domain function is fundamental to most phase-locked loop controls used to derive firing pulses for thyristors or other gate driven electronic switching devices.

4.2 FIRST ORDER LAG FUNCTION

The first order lag function can be described by the Laplace transform form:

$$\frac{O(s)}{I(s)} = \frac{1}{1 + \tau \cdot s} \quad \{ 4-1 \}$$

where:

$O(s)$ is the Laplace transform of the output response

$I(s)$ is the Laplace transform of the input response

s is the Laplace operator

τ is the time constant of the response.

In the proposed harmonic domain model, the relationship between the harmonic content of the output waveform \bar{O} and the input waveform \bar{I} can be defined by:

$$\bar{O} = \bar{K} \cdot \bar{I} \quad \{ 4-2 \}$$

where:

\bar{O} is a an array housing the harmonics of $O(\omega t)$

\bar{I} is a an array housing the harmonics of $I(\omega t)$

\bar{K} is matrix defining the harmonic relationship between \bar{I} and \bar{O}

The Laplace Transform domain response can be re-written in the form:

$$(1 + \tau \cdot s) \cdot O(s) = I(s) \quad \{ 4-3 \}$$

In the harmonic domain model, the equation becomes:

$$(\bar{I} + \tau \cdot \bar{D}) \cdot \bar{O} = \bar{I} \quad \{ 4-4 \}$$

where:

\bar{I} is the identify matrix

\bar{D} is the derivative operator described in Chapter 3

from which:

$$\bar{K} = (\bar{I} + \tau \cdot \bar{D})^{-1} \quad \{ 4-5 \}$$

It can be shown that the matrix \bar{K} is very sparse and can be developed directly without having to carry out the inversion.

4.3 THE PROPORTIONAL INTEGRAL DERIVATIVE FUNCTION

The Proportion Integral Derivative (PID) controller and the Proportional Integral (PI) controller are used in many control system functions. The PI controller (i.e. the PID controller without the derivative term), is simply a subset of the PID controller.

The Laplace Transform of the PID controller is:

$$\frac{O(s)}{I(s)} = g_p + \frac{1}{\tau_i s} + \tau_d s \quad \{ 4-6 \}$$

where:

g_p is the controller gain

τ_i is the integrator time constant

τ_d is the derivative time constant

Again in the harmonic domain the input to output response can be given in the form:

$$\bar{O} = \bar{K}_{PID} \cdot \bar{I} \quad \{ 4-7 \}$$

where:

\bar{O} is the HDA equivalent of the output

\bar{I} is the HDA equivalent of the input

\bar{K}_{PID} is a transfer matrix defining the harmonic relationship between \bar{I} and \bar{O}

The transfer matrix is constrained however due to the presence of the integrator. Each component of the Laplace Transform form the PID controller has its corresponding component in the harmonic domain. I.e.:

$$\bar{K}_{PID} = \bar{K}_P + \bar{K}_I + \bar{K}_D \quad \{ 4-8 \}$$

The gain component as it applies equally to all frequencies (hence harmonics) is simply:

$$\bar{K}_P = g_p \cdot \bar{I} \quad \{ 4-9 \}$$

where ' \bar{I} ' is the identity matrix.

The derivative component contains a frequency dependent component based on the derivative of the input. I.e.:

$$\bar{K}_D = \tau_d \cdot \bar{D} \quad \{ 4-10 \}$$

Similar to a treatment of a capacitor in the electrical network (as discussed in Chapter 3), the dc input to the integrator by definition is zero, which in turn means that the input to the whole PID controller must also be zero. The harmonic domain implies no change in

time domain waveform from one period to the next. As the output of the integrator in the time domain would continue to build-up for a constant 'dc' input, the average input in the time domain must be zero, implying a zero value of dc input in the harmonic domain.

The harmonic component of the integral term can be expressed as:

$$\bar{K}_{i_h} = \frac{1}{\tau_i} \bar{D}_h^{-1} \quad \{ 4-11 \}$$

In the proposed harmonic domain methodology, the dc component of the matrix is arbitrarily set to zero and the resultant total harmonic domain gain is given by:

$$\bar{K}_i \equiv \begin{bmatrix} 0 & \bar{0}^T \\ \bar{0} & \bar{K}_{i_h} \end{bmatrix} \quad \{ 4-12 \}$$

When combined with the proportional and derivative component, the total harmonic domain representation of the PID Controller is given by:

$$\begin{aligned} \bar{K}_{PID} &= \bar{K}_p + \bar{K}_i + \bar{K}_d \\ &= g_p \cdot \bar{1} + \tau_d \cdot \bar{D} + \frac{1}{\tau_i} \cdot \begin{bmatrix} 0 & \bar{0}^T \\ \bar{0} & \bar{D}_h^{-1} \end{bmatrix} \end{aligned} \quad \{ 4-13 \}$$

with the added constraint that the dc component of the input to the PID controller ' \bar{I} ' must be set elsewhere in the model to zero, i.e.:

$$\bar{I}_0 = 0 \quad \{ 4-14 \}$$

From the equation it can be seen that if the proportional and derivative components are not present, the respective scalars g_p and τ_d can be set to zero, leaving just the integrator term.

Use of the PID Controller is described in Section 5.4 of Chapter 5.

4.4 THE COMPARE RAMP FUNCTION

The firing pulses for controlled power electronic switching devices are often derived by control circuits that compare a periodic ramp function with a reference signal [40] as

shown in Figure 4-1. The controller generates a pulse signal that has a value of zero for the interval when the value of the ramp is less than the reference value and a value of one if the value of the ramp exceeds the reference. The reference signal would normally consist of a constant 'dc' value, but harmonics could be present in the control system giving the reference signal a periodic time dependent characteristic.

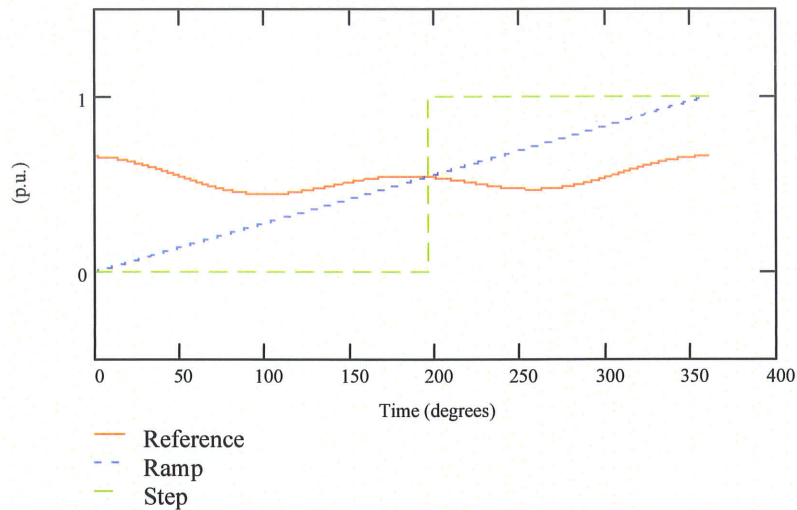


Figure 4-1 Typical Method of Determining Firing Instances (in Time Domain)

The intersection of a ramp signal and a reference signal can be directly handled in the frequency domain by subtracting the harmonic content of the reference signal from the harmonic content of the ramp. The HDA sign function applied to the difference will generate the harmonic content of a waveform that has a value of 1 if the difference is positive and a value of -1 if the value is negative.

Unfortunately, this method is somewhat flawed. Truncation of the harmonic series representing the ramp function introduces Gibb's-like oscillations that could result in multiple crossings of the difference waveform.

This effect is illustrated in the following example where a ramp function is compared to a 'dc' reference signal. The harmonic content of a periodic ramp that varies between the values of 0 and 1 is given by:

$$\bar{R}^T = \left[.5 \quad 0 \quad \frac{-1}{\pi} \quad 0 \quad \frac{-1}{2\pi} \quad \dots \right]$$

With a reference value of 80 degrees ($\frac{80}{360}$ of the ramp), the difference waveform would have the harmonic content:

$$\vec{\theta}_{\text{diff}}^T = \left[.2778 \quad 0 \quad \frac{-1}{\pi} \quad 0 \quad \frac{-1}{2\pi} \quad \dots \right]$$

In the time domain, the difference waveform is shown in Figure 4-2. An expanded view at the zero crossing is shown in Figure 4-3.

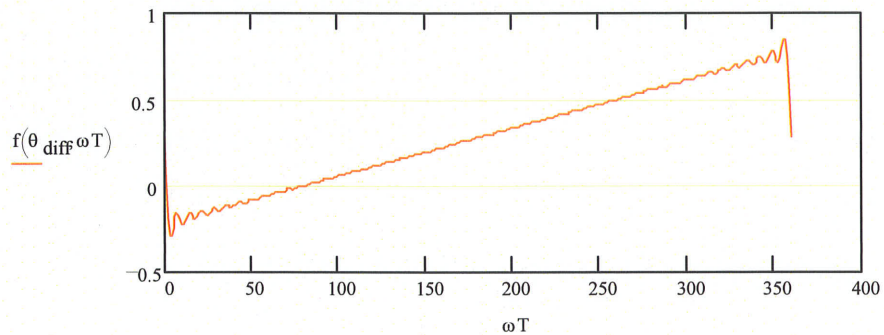


Figure 4-2 Time Domain Presentation of Difference Between HDA Ramp and Reference

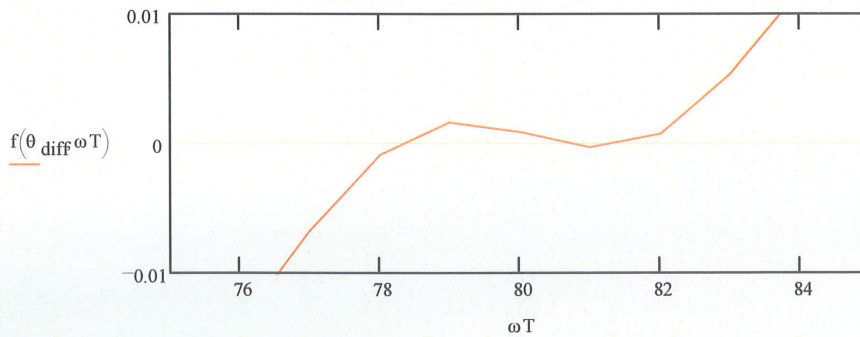


Figure 4-3 Time Domain Presentation of Difference Between HDA Ramp and Reference (Expanded View)

In the above example, there are three zero crossings at the reference angle of 80 degrees, within a range of about 78.5 to 81 degrees.

If the reference signal were closer to zero or closer to 360 degrees (a signal of 1.0) the Gibb's-like effect is larger possibly creating additional zero crossings over a larger time interval. With a truncation to 50 harmonics, the range of 'error' in the representation of the crossover could be as high as 15 degrees.

An error of 15 degrees in the calculated firing circuit of a valve would have a significant impact on its estimated behaviour. A Lanczos filter could be applied to the difference waveform eliminating the multiple crossovers at reference signals in the middle of the range; however, reference signals close to zero or 360 degrees could still cause difficulties.

An alternative solution is to numerically solve for the intersection of the reference waveform with a ramp, and generate the harmonic response of the output based on the calculated point of intersection. Using a Newton-Raphson algorithm, the equation to be solved is:

$$f = \omega t - \beta_{a0} - \sum_{n=1}^{n_{\max}} (\beta_{an} \cdot \cos(n\omega t) + \beta_{bn} \cdot \sin(n\omega t)) = 0 \quad \{ 4-15 \}$$

The variable β in the above represents the harmonic coefficients of the reference signal.

The derivative of the equation is given by:

$$\frac{df}{d\omega t} = 1 - n - \sum_{n=1}^{n_{\max}} (\beta_{an} \cdot \sin(n\omega t) + \beta_{bn} \cdot \cos(n\omega t)) \quad \{ 4-16 \}$$

As the reference signal will typically be dominated by the 'dc' component, a reasonable initial guess for the solution ' α ' is:

$$\alpha_{\text{iter}=0} = \omega t = \beta_{a0} \quad \{ 4-17 \}$$

and successive correction terms are given by:

$$\Delta\alpha_{iter} = -\frac{f_{iter-1}}{\left(\frac{df}{d\alpha}\right)_{iter-1}} \quad \{ 4-18 \}$$

The solution ' α ' is subsequently used to define the harmonic coefficients of the resultant pulse signal. I.e.:

$$P^T(\alpha) = \left[\left(1 - \frac{\alpha}{2\pi}\right) \left(\frac{-\sin(\alpha)}{\pi}\right) \left(\frac{\cos(\alpha)-1}{\pi}\right) \left(\frac{-\sin(2\alpha)}{2\pi}\right) \left(\frac{\cos(2\alpha)-1}{2\pi}\right) \dots \right] \quad \{ 4-19 \}$$

A numerical HDA function named 'CompRamp' was developed based on the preceding equations. The Mathcad[®] implementation of the algorithm is shown in Appendix A. It is demonstrated for a reference signal with a significant harmonic component in the following example:

The components of the sample reference signal and resultant pulse are:

$$\bar{\beta}^T = \frac{[192 \ 20 \ -5 \ 25 \ 0 \ \dots]}{360}$$

$$\text{CompRamp}(\bar{\beta})^T = [0.457 \ 0.085 \ -0.625 \ -0.082 \ -0.023 \ 0.077 \ -0.179 \ \dots]$$

The reference signal β and resultant pulse P are shown along with the intermediate ramp in the time domain representation shown in Figure 4-4.

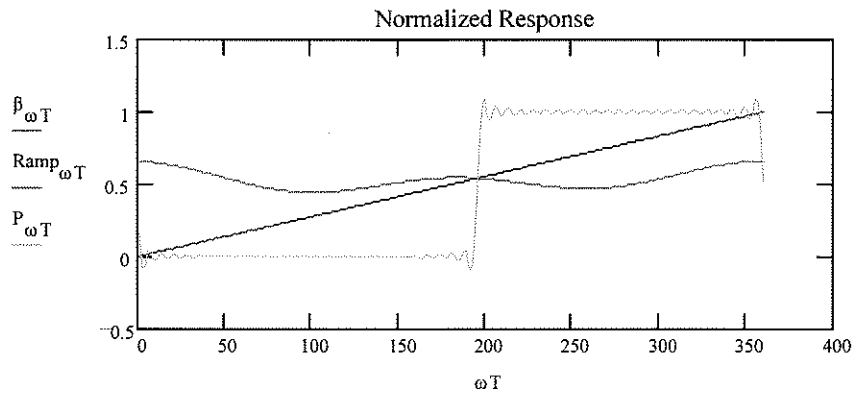


Figure 4-4 HDA Analysis of Firing Pulse Determination with HDA CompRamp Function

The solution is relatively robust and rapidly converges if the reference signal is dominated by a dc component.

The Partial derivatives of the 'CompRamp' function with respect to each of the harmonic components in the reference signal can be used in the analysis of non-linear systems that incorporate the 'CompRamp' function.

The derivative is determined by evaluating the influence of the components of the reference signal on the intersection point. The impact of variations in intersection point on the harmonic content of the resultant pulse is calculated and combined with the first set of derivatives to obtain the overall derivative.

The derivative of the intersection point with respect to each harmonic component in the reference signal is as follows:

Since at the intersection point α ,

$$\alpha = \beta a_0 + \sum_{n=1}^{n_{\max}} (\beta a_n \cdot \cos(n\alpha) + \beta b_n \cdot \sin(n\alpha)) \quad \{ 4-20 \}$$

then differentiating both sides of the equation with respect to βa_0 gives:

$$\frac{d\alpha}{d\beta a_0} = 1 + n \sum_{n=1}^{n_{\max}} (-\beta a_n \cdot \sin(n\alpha) + \beta b_n \cdot \cos(n\alpha)) \frac{d\alpha}{d\beta a_0}$$

or:

$$\frac{d\alpha}{d\beta a_0} = \frac{1}{1 + n \sum_{n=1}^{n_{\max}} (\beta a_n \cdot \sin(n\alpha) - \beta b_n \cdot \cos(n\alpha))} \quad \{ 4-21 \}$$

Similarly:

$$\begin{aligned} \frac{d\alpha}{d\beta a_1} &= \frac{\cos(\alpha) + n \sum_{n=1}^{n_{\max}} (-\beta a_n \cdot \sin(n\alpha) + \beta b_n \cdot \cos(n\alpha))}{1 + n \sum_{n=1}^{n_{\max}} (\beta a_n \cdot \sin(n\alpha) - \beta b_n \cdot \cos(n\alpha))} \frac{d\alpha}{d\beta a_1} \\ \frac{d\alpha}{d\beta a_1} &= \frac{\cos(\alpha)}{1 + n \sum_{n=1}^{n_{\max}} (\beta a_n \cdot \sin(n\alpha) - \beta b_n \cdot \cos(n\alpha))} \\ \frac{d\alpha}{d\beta b_1} &= \frac{\sin(\alpha)}{1 + n \sum_{n=1}^{n_{\max}} (\beta a_n \cdot \sin(n\alpha) - \beta b_n \cdot \cos(n\alpha))} \\ \frac{d\alpha}{d\beta a_2} &= \frac{\cos(2\alpha)}{1 + n \sum_{n=1}^{n_{\max}} (\beta a_n \cdot \sin(n\alpha) - \beta b_n \cdot \cos(n\alpha))} \\ \frac{d\alpha}{d\beta b_2} &= \frac{\sin(2\alpha)}{1 + n \sum_{n=1}^{n_{\max}} (\beta a_n \cdot \sin(n\alpha) - \beta b_n \cdot \cos(n\alpha))} \\ &\vdots \end{aligned}$$

or:

$$\frac{d\alpha}{d\beta} = \frac{[1 \quad \cos(\alpha) \quad \sin(\alpha) \quad \cos(2\alpha) \quad \sin(2\alpha) \quad \dots]}{1 + n \sum_{n=1}^{n_{\max}} (\beta a_n \cdot \sin(n\alpha) - \beta b_n \cdot \cos(n\alpha))} \quad \{ 4-22 \}$$

The derivative of each of the harmonic components of the pulse waveform \bar{P} as defined above (Equation 4-22) with respect to the intercept angle α are as follows:

$$\left(\frac{d\bar{P}}{d\alpha} \right)^T = \frac{-\left[\frac{1}{2} \quad \cos(\alpha) \quad \sin(\alpha) \quad \cos(2\alpha) \quad \sin(2\alpha) \quad \dots \right]}{\pi} \quad \{ 4-23 \}$$

The derivative of the pulse waveform \bar{P} with respect to each harmonic component of the reference signal by chain rule is the product of the two derivatives:

$$\frac{d\bar{P}}{d\beta} = \frac{-\left[\frac{1}{2} \quad \cos(\alpha) \quad \sin(\alpha) \quad \cos(2\alpha) \quad \sin(2\alpha) \quad \dots \right]^T}{\pi} \frac{[1 \quad \cos(\alpha) \quad \sin(\alpha) \quad \cos(2\alpha) \quad \sin(2\alpha) \quad \dots]}{1 + n \sum_{n=1}^{n_{\max}} (\beta a_n \cdot \sin(n\alpha) - \beta b_n \cdot \cos(n\alpha))} \quad \dots\{ 4-24 \}$$

The derivative is a matrix but it can be easily constructed from two almost identical vectors. It was used in the development of the Jacobian for the iterative solution of the voltage chopping circuit described in Section 5.4 of Chapter 5.

4.5 OVERVIEW

This chapter has shown the development of three typical control system models as required for the proposed HDA model. The use of these functions is demonstrated in Chapter 5.

The modelling of the first order lag and PID controller characteristics would be similar in most HDA models. Modelling of the valve firing pulse system by a conventional algebraic sign function (or its logical equivalent) is likely to be common in most time domain implementations. Its implementation in the harmonic domain as an HDA sign function appears to be novel.

This Page is Intentionally Blank

CHAPTER 5

APPLICATION TO POWER ELECTRONICS SWITCHING DEVICES

5.1 INTRODUCTION

In this chapter, application of the author's proposed HDA methodology to power electronic switching devices and circuits is investigated. Section 5.2 discusses and demonstrates the application to diodes and how the simple harmonic domain model can be incorporated into a typical admittance model of an electrical network. Section 5.3 discusses and demonstrates the compatibility of harmonic domain switching functions with the proposed HDA methodology with a demonstration using a thyristor controlled reactor circuit. Section 5.4 presents an example of the application to models comprising both electrical circuits as well as non-linear control systems, where the electrical circuit consists of basic network components along with a voltage chopping circuit.

5.2 APPLICATION TO ANALYSIS OF A DIODE CIRCUIT

5.2.1 Introduction

The harmonic domain methodology can be applied to either direct or iterative analysis of simple diode circuits. It is the objective of this chapter to illustrate how the harmonic domain methodology developed in Chapters 3 and 4 can be applied to a practical example. The analysis presented is carried out entirely in the harmonic domain and is based entirely on a solution of simultaneous equations. Turn-on and turn-off times of the diode are not required.

Consider the simple diode resistor circuit shown in Figure 5-1. The voltage ' v_s ' is the input to the device. In this example the voltage waveform is repetitive and therefore can be considered in both the time domain and the harmonic domain. Its waveform can take on any shape as long as it is repetitive and does not contain more than a few discontinuities¹⁷. The objective is to determine the output diode current ' i_d ' for a specified input waveform. The voltage across the diode and resistor can be determined given ' v_s ' and ' i_d '.

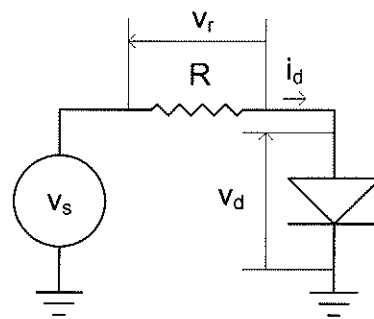


Figure 5-1 Simple Diode Resistor Test Circuit

This chapter presents several harmonic domain analysis examples starting with a direct approach to solving for the output current in the above example, and progresses to show how the direct approach can be extended to an iterative analysis of more complex circuits.

5.2.2 Example 1 Direct HDA Analysis of a Simple Resistor Diode Circuit

The relationship between the applied voltage in this circuit ' v_s ' and the current through the diode ' i_d ' can be described in the time domain by the following equation:

$$i_d(\omega t) = \frac{1}{2 \cdot R} \cdot (v_s(\omega t) + |v_s(\omega t)|) \quad \{ 5-1 \}$$

and the voltage across the diode by the equation:

$$v_d(\omega t) = v_s(\omega t) - R \cdot i_d(\omega t) \quad \{ 5-2 \}$$

¹⁷ Satisfying the Fourier series requirement.

The above equations have direct one-to-one equivalents in the harmonic domain including the absolute function developed by the author and described in Chapter 2. In the proposed harmonic domain, the equations would be:

$$\vec{I}_d = \frac{1}{2 \cdot R} \cdot (|\vec{V}_s| + \vec{V}_s) \quad \{ 5-3 \}$$

$$\vec{V}_d = \vec{V}_s - R \cdot \vec{I}_d \quad \{ 5-4 \}$$

Consider a severely distorted source voltage with a Harmonic Domain content¹⁸ of:

$V_s^T =$	0	1	2	3	4	5	6	7
	0	0.4	1	-0.3	1.5	0.2	0	0

and a circuit resistance of 0.01Ω .

The time domain waveform corresponding to this content is shown in Figure 5-2.

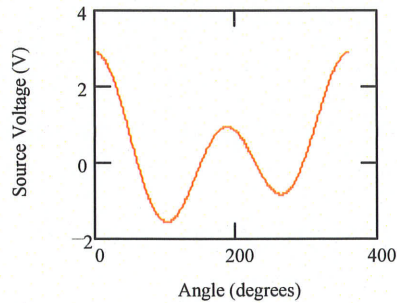


Figure 5-2 Distorted Source Voltage Waveform used in Resistor-Diode Circuit

Equations 5-3 and 5-4 can be solved directly in the harmonic domain for this condition. The lower order harmonic content of the diode current and voltage arrays calculated directly in the harmonic domain are:

$I_d^T =$	0	1	2	3	4	5	6	7	8
	0	74.75	86.06	-4.353	98.873	6.033	24.129	-7.066	19.461

$V_d^T =$	0	1	2	3	4	5	6	7	8
	0	-0.348	0.139	-0.256	0.511	0.14	-0.241	0.071	-0.195

¹⁸ The array houses the Fourier series representing the waveform. The contents of the array are described in Section 2.2 of Chapter 2.

To demonstrate that the harmonic content is actually correct, the corresponding time domain waveforms, as generated from the harmonic content, are shown in Figure 5-3.

By inspection of the simple circuit:

1. The time domain waveform of diode current should be proportional to the source voltage when the source voltage is positive.
2. It should be zero when the source voltage is negative.
3. The peak of the diode current should have a magnitude equal to the peak of the source voltage divided by the resistance of the resistor.
4. The diode voltage should match the source voltage when the diode is not conducting

Points 1, 2 and 4 above can be confirmed to demonstrate accuracy by inspection of the waveforms.

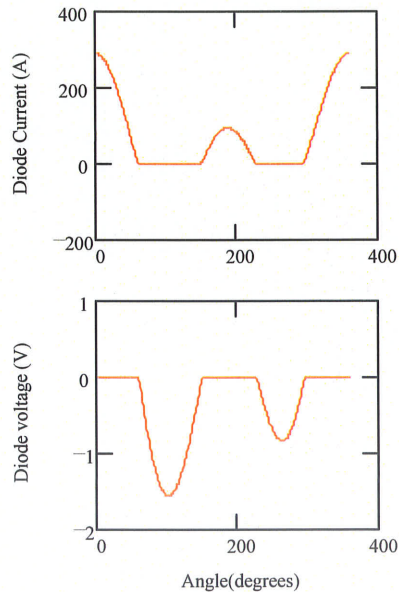


Figure 5-3 Diode Current and Voltage using Direct HDA Solution

To confirm point 3, the peak source voltage occurs at the start of the cycle so the equivalent time domain magnitude is equal to the sum of the 'a' coefficients¹⁹ of the

¹⁹ as defined in Section 2.2 of Chapter 2.

harmonic domain, i.e., 2.9 V. With a resistance of 0.01Ω the peak current should therefore be 290 A. The sum of the 'a' coefficients of the current array is 289.999 A. In this example a maximum of 50 harmonics was considered.

A direct solution of diode current is a convenient mechanism to demonstrate that harmonic domain analysis can be carried out without excursions into the time domain to determine turn-on and turn-off times of the diode. As Equations 5.1 and 5.3 are only valid for a resistor located between the voltage source and the diode, an alternative approach was developed (described next), that could be expanded into a resistive network approach (described in Section 5.2.3 of this chapter) and eventually into an impedance network approach (described in Section 5.2.4 of this chapter).

5.2.3 Example 2 Iterative HDA Analysis of a Simple Resistor Diode Circuit

While the first example shows that the harmonic content of the diode can be computed effectively in a single step, this approach is generally not possible when the diode forms part of a larger network. It may be more efficient to incorporate the iterations associated with the computation of the absolute function into the iteration process of the whole scheme, i.e. putting the diode as part of the overall Jacobian for the network.

In this example, the equations leading to the absolute value of the applied voltage in the first example are restructured into a format that lends itself to inclusion in the Jacobian. The test circuit of Figure 5-1 will be used again in the validation of the revised algorithm.

Here, we will define the variable ' \vec{V}_{squared} ' to be the product of the source voltage by itself using the harmonic domain product transformation matrix described in Section 2.4 of Chapter 2, i.e.:

$$\vec{V}_{\text{squared}} = T(\vec{V}_s) \cdot \vec{V}_s \quad \{ 5-5 \}$$

The product is then used again to solve for the absolute value of ' \vec{V}_s ' herein denoted ' \vec{V}_{abs} ' i.e.:

$$T(\vec{V}_{abs}) \cdot \vec{V}_{abs} = \vec{V}_{ssquared} \quad \{ 5-6 \}$$

An initial guess at the vector ' \vec{V}_{abs} ' is to set the 'dc' component of ' \vec{V}_{abs} ' equal to the square root of the dc component of ' $\vec{V}_{ssquared}$ ' and all of the harmonic components to zero.

Correction terms at each iteration are selected based on the Newton-Raphson iterative solution, i.e.:

$$\Delta \vec{V}_{abs} = - \left[\frac{d}{d\vec{V}_{abs}} \left(T(\vec{V}_{abs}) \cdot \vec{V}_{abs} - \vec{V}_{ssquared} \right) \right]^{-1} \cdot \left(T(\vec{V}_{abs}) \cdot \vec{V}_{abs} - \vec{V}_{ssquared} \right) \quad \{ 5-7 \}$$

It can be shown that:

$$\frac{d}{d\vec{V}_{abs}} \left(T(\vec{V}_{abs}) \cdot \vec{V}_{abs} - \vec{V}_{ssquared} \right) = 2 \cdot T(\vec{V}_{abs}) \quad \{ 5-8 \}$$

Therefore, the value of ' \vec{V}_{abs} ' at the ' n^{th} ' iteration is given by:

$$\vec{V}_{abs_n} = \vec{V}_{abs_{n-1}} - \left(2T(\vec{V}_{abs_{n-1}}) \right)^{-1} \cdot \left(T(\vec{V}_{abs_{n-1}}) \cdot \vec{V}_{abs_{n-1}} - \vec{V}_{ssquared} \right) \quad \{ 5-9 \}$$

which simplifies to:

$$\vec{V}_{abs_n} = \frac{1}{2} \left(\vec{V}_{abs_{n-1}} + T^{-1}(\vec{V}_{abs_{n-1}}) \cdot \vec{V}_{ssquared} \right) \quad \{ 5-10 \}$$

If ' \vec{V}_{abs} ' at the ' n^{th} ' iteration is considered to be close enough to the final solution, then:

$$\begin{array}{l} \vec{V}_{abs_n} = \vec{V}_{abs_{n-1}} = \vec{V}_{abs} \\ \text{or:} \\ \vec{V}_{abs} = T^{-1}(\vec{V}_{abs}) \cdot \vec{V}_{ssquared} \\ \text{or:} \\ \vec{V}_{abs} = T^{-1}(\vec{V}_{abs}) \cdot T(\vec{V}_s) \cdot \vec{V}_s \end{array} \quad \{ 5-11 \}$$

Substituting for ' \bar{V}_{abs} ' into the equation for current,

$$\bar{I}_d = \frac{1}{2 \cdot R} \cdot \left(T^{-1}(\bar{V}_{abs}) \cdot T(\bar{V}_s) \cdot \bar{V}_s + \bar{V}_s \right)$$

or collecting terms:

$$\bar{I}_d = \frac{1}{2 \cdot R} \cdot \left(T^{-1}(\bar{V}_{abs}) \cdot T(\bar{V}_s) + \bar{I} \right) \cdot \bar{V}_s$$

$$\bar{I}_d = \bar{Y} \cdot \bar{V}_s$$

where:

$$\bar{Y} = \frac{1}{2 \cdot R} \cdot \left[\bar{I} + T^{-1}(\bar{V}_{abs}) \cdot T(\bar{V}_s) \right] \quad \{ 5-12 \}$$

where ' \bar{I} ' is the identity matrix. This result is significant as ' \bar{Y} ' is in the form of an admittance matrix. This is conducive to including the model of the diode directly into a full network admittance array.

The voltage across the resistor can be determined from the product of the current array ' \bar{I}_d ' and the value of the circuit resistance 'R'. i.e.:

$$\bar{V}_r = R \cdot \bar{I}_d \quad \{ 5-13 \}$$

The exit criteria selected for the algorithm is based on the cumulative solution error:

$$Error_n = \sqrt{\sum_{k=0}^{k_{max}} \left(\left(\bar{V}_{s_{squared}} \right)_k - \left(\bar{V}_{abs_k} \right)^2 \right)^2} \leq tolerance \quad \{ 5-14 \}$$

where 'k' denotes the harmonic number.

The algorithm is demonstrated for a test case where the source voltage contains a dc offset, a fundamental frequency and a second harmonic component. The circuit resistance is assumed to be .01 Ω . The largest harmonic of interest ' k_{max} ' is 50. The voltage source in this example is the same as used in the first example with the time domain response shown in Figure 5-2.

After five steps (iteration 6) of the above algorithm, the calculated values for the harmonic component²⁰ of the absolute value of diode voltage and circuit²¹ current are given in Table 5-1.

Table 5-1 Harmonic Content of Voltage and Current for Diode Example Number 2

Harmonic Content of Waveforms					
Vd (V)			Ir (A)		
n	series	vd	n	series	Ir
0	a	1.095	0	a	74.7
1	a	0.721	1	a	86.1
1	b	0.213	1	b	-4.3
2	a	0.477	2	a	98.9
2	b	-0.079	2	b	6.0
3	a	0.483	3	a	24.1
3	b	-0.141	3	b	-7.1
4	a	0.389	4	a	19.5
4	b	0.161	4	b	8.1
5	a	-0.208	5	a	-10.4
5	b	-0.062	5	b	-3.2
6	a	-0.089	6	a	-4.5
6	b	0.055	6	b	2.8
7	a	-0.036	7	a	-1.8
7	b	-0.002	7	b	-0.1

The progression of the algorithm at each iteration is demonstrated pictorially with the reconstruction of the absolute value of the diode voltage waveform from the harmonic content. The waveform is compared to the source voltage (solid curve), which is constant for this example, in Figure 5-4.

²⁰'a' and 'b' correspond to the cosine and sin coefficients of the Fourier series as described in Section 2.2 of Chapter 2

²¹In this case, the circuit current 'i_r' is identical to the diode current 'i_d'

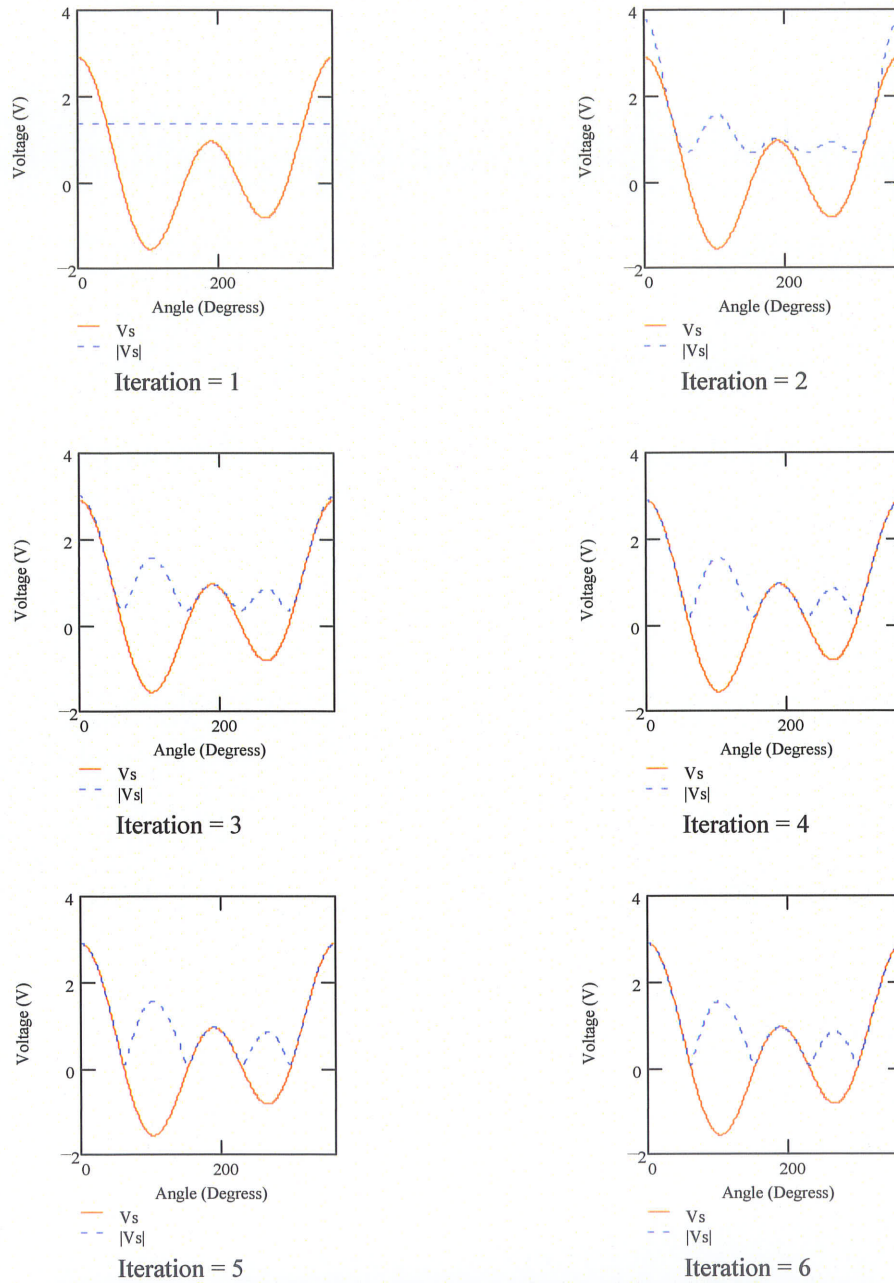


Figure 5-4 Progression of Iterative Solution of Diode Resistor Circuit

The variation in solution error with iteration is shown in Figure 5-5.

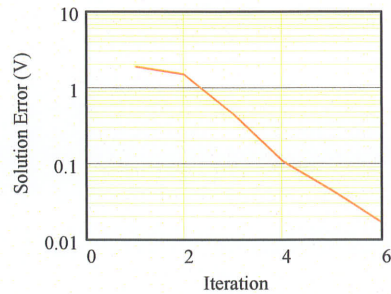


Figure 5-5 Variation of Iterative Solution Error for Diode Resistor Circuit

The current waveform on termination is shown in Figure 5-6.

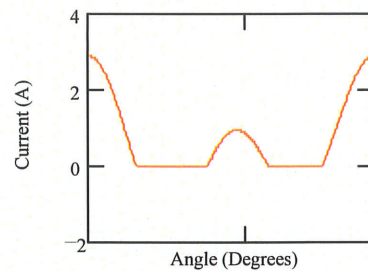


Figure 5-6 Diode Current for Iterative Solution of Resistor Diode Circuit

5.2.4 Example 3 Iterative HDA Analysis of a Simple Resistor Network Diode Circuit

A third example is now considered in which an intermediate bus has been introduced into the circuit of Example 2, to allow admittance matrix equations to be formulated for the circuit introduced. The modified circuit is shown in Figure 5-7. For this example the series resistor diode (R_d) combination is taken to be a base element of the HDA methodology.

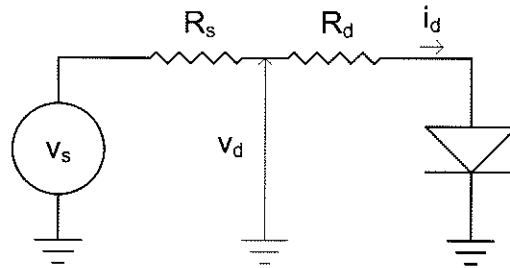


Figure 5-7 Diode Resistor Circuit for Simple Network Analysis

At the midpoint bus, the current into the diode is calculated in the same manner as the first example. I.e.:

$$\bar{I}_d = \bar{Y}_d \cdot (|\bar{V}_d| + \bar{V}_d) \quad \{ 5-15 \}$$

The current error equation (to be solved using Newton-Raphson solution techniques) at the midpoint bus becomes:

$$f_1(\bar{V}_d, \bar{E}_d) = -\bar{Y}_s \cdot \bar{V}_s + (\bar{Y}_s + \bar{Y}_d) \cdot \bar{V}_d + \bar{Y}_d \cdot \bar{E}_d = \bar{0} \quad \{ 5-16 \}$$

where:

$$\left. \begin{aligned} \bar{Y}_s &= \frac{1}{R_s} \cdot \bar{I} \\ \bar{Y}_d &= \frac{1}{2 \cdot R_d} \cdot \bar{I} \end{aligned} \right\} \quad \{ 5-17 \}$$

and by definition:

$$\bar{E}_d = |\bar{V}_d| \quad \{ 5-18 \}$$

which can be also be defined by the Newton-Raphson form of the harmonic domain equation:

$$f_2(\bar{V}_d, \bar{E}_d) = T(\bar{V}_d) \cdot \bar{V}_d - T(\bar{E}_d) \cdot \bar{E}_d = \bar{0} \quad \{ 5-19 \}$$

The Jacobian for the Newton-Raphson solution of the two sets of simultaneous equations can be expressed by the following partitioned matrix:

$$\text{Jac}(\bar{V}_d, \bar{E}_d) = \begin{bmatrix} \frac{\partial f_1}{\partial \bar{V}_d} & \frac{\partial f_1}{\partial \bar{E}_d} \\ \frac{\partial f_2}{\partial \bar{V}_d} & \frac{\partial f_2}{\partial \bar{E}_d} \end{bmatrix} \quad \{ 5-20 \}$$

or:

$$\text{Jac}(\bar{V}_d, \bar{E}_d) = \begin{bmatrix} \bar{Y}_s + \bar{Y}_d & \bar{Y}_d \\ 2 \cdot T(\bar{V}_d) & -2 \cdot T(\bar{E}_d) \end{bmatrix} \quad \{ 5-21 \}$$

The correction term at each iteration is given by:

$$\begin{bmatrix} \Delta \bar{V}_d \\ \Delta \bar{E}_d \end{bmatrix} = - \begin{bmatrix} \bar{Y}_s + \bar{Y}_d & \bar{Y}_d \\ 2 \cdot T(\bar{V}_d) & -2 \cdot T(\bar{E}_d) \end{bmatrix}^{-1} \cdot \begin{bmatrix} -\bar{Y}_s \cdot \bar{V}_s + (\bar{Y}_s + \bar{Y}_d) \cdot \bar{V}_d + \bar{Y}_d \cdot \bar{E}_d \\ T(\bar{V}_d) \cdot \bar{V}_d - T(\bar{E}_d) \cdot \bar{E}_d \end{bmatrix} \quad \{ 5-22 \}$$

For this example, 18 iterations were carried out. The error measured in terms of the sum of the norms of the vector equivalent of the arrays representing two error functions f_1 and f_2 is shown in Figure 5-8. The solution is within acceptable tolerance after five or six iterations, similar to the second example. The number of iterations was increased to examine numerical issues. The error reduces rapidly but after the 10th iteration the magnitude of the error is essentially unchanged. There is some hunting of the solution but the numerical error remains extremely small, and is well within acceptable tolerances.

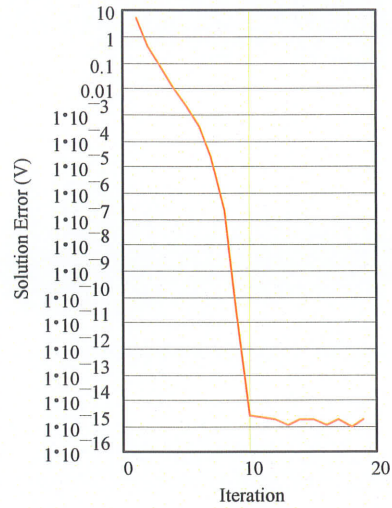


Figure 5-8 Variation of Iterative Solution Error for Diode Resistor Network Circuit

The solution obtained for diode current is almost identical to the current calculated in Example 1. The diode current is shown in Table 5-2.

Table 5-2 Harmonic Content of Current for Diode Example Number 3

Harmonic Content Current Waveform (A)		
n	series	I _r
1	a	74.8
1	b	86.1
2	a	-4.4
2	b	98.9
3	a	6.0
3	b	24.1
4	a	-7.1
4	b	19.5
5	a	8.1
5	b	-10.4
6	a	-3.1
6	b	-4.5
7	a	2.8
7	b	-1.8

This calculation method involves more computation than the first method. However, it does lend itself to inclusion of a more extensive ac system as demonstrated in Example 4.

5.2.5 Example 4 Iterative HDA Analysis of a Simple Resistor Inductor Diode Circuit

The fourth example is based on the simple diode resistor-inductor test circuit shown in Figure 5-9. The objective here is to show that the basic network solution algorithm for a diode circuit, as developed through the first three examples, can be extended to include frequency dependent components in the transmission network²².

The inclusion of the inductance in the network will introduce discontinuities in the diode voltage. The current through an inductor cannot be suddenly interrupted. It must be forced to zero by a reverse voltage. While the source voltage may become negative while the diode is conducting the diode will continue to conduct maintaining zero voltage until the inductor current is extinguished.

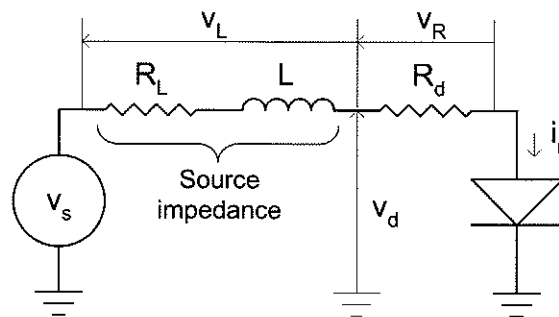


Figure 5-9 Simple Diode Resistor Inductor Test Circuit

The presence of discontinuities increases the magnitude of the higher order harmonics, and therefore provides a less favourable environment for numerical solution involving iterative techniques.

The basic algorithm presented in Example 3 can also be used to solve for the harmonic content the resistor-inductor circuit shown in Figure 5-9. To use the algorithm, the source admittance must be modified to include the frequency dependent characteristic

²²The series R_L and L_L components of the circuit represent transmission from the source to the diode.

introduced by the additional inductor. In the harmonic domain, the source impedance as discussed in Chapter 3 is given by:

$$\bar{Z}_s = R_L \cdot \bar{I} + \bar{D} \cdot L_L \quad \{ 5-23 \}$$

The matrix \bar{Z} is sparse and bounded. Its inverse \bar{Y} is also sparse and is given by:

$$\bar{Y}_s = \bar{Z}_s^{-1} \quad \{ 5-24 \}$$

It can be readily shown through theoretical analysis using elementary circuit theory that inclusion of an inductor with an impedance of 0.1Ω at its fundamental frequency when inserted in series with the source and resistor of Figure 5-7 results in a solution where the diode is continuously turned on. The algorithm converged to a solution where the diode voltage was zero at all harmonics. When the dc component of the source voltage was reduced to -0.3 V (originally $+0.4 \text{ V}$), the diode cycled through blocking and conducting states in agreement with the analytical solution.

The step changes in diode voltage resulting from turn-off of the diode and their associated high frequency in the waveform are accompanied by Gibb's-like oscillations creating a situation where potentially many solutions may exist to the set of harmonic simultaneous equations. With careful selection of initial conditions for the voltage across the diode, the algorithm does converge to a solution.

For this example, the norm of the voltage correction vector is used as an indicator of proximity to a solution. The convergence rate as shown in Figure 5-10 is initially slow but after about 16 iterations, the algorithm rapidly converges to a solution.

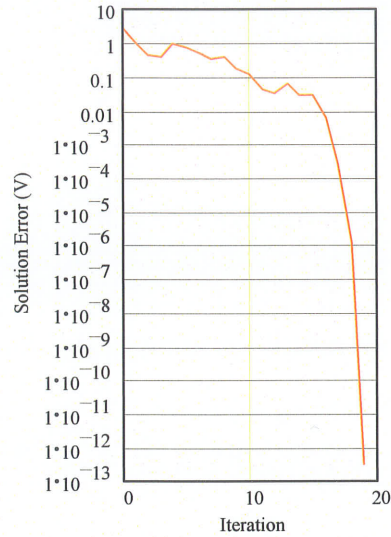


Figure 5-10 Variation of Iterative Solution Error for Diode Resistor Inductor Circuit

The resultant harmonic content of the diode voltage and current is given in Table 5-3.

Table 5-3 Harmonic Content of Voltage and Current in Diode Resistor-Inductor Test Circuit

Harmonic Content of Waveforms					
vd (V)			Id (A)		
n	series	vd	n	series	Ir
0	a	-0.409	0	a	5.467
1	a	0.267	1	a	6.612
1	b	0.241	1	b	6.006
2	a	0.397	2	a	0.558
2	b	0.202	2	b	5.457
3	a	-0.293	3	a	-1.343
3	b	-0.424	3	b	1.067
4	a	0.066	4	a	0.081
4	b	0.036	4	b	-0.169
5	a	-0.039	5	a	0.405
5	b	0.201	5	b	0.061
6	a	-0.076	6	a	-0.192
6	b	-0.118	6	b	0.133
7	a	0.132	7	a	0.042
7	b	0.033	7	b	-0.190

Harmonic Content of Source Voltage (V)		
n	series	Vs
0	a	-0.300
1	a	1.000
1	b	-0.300
2	a	1.500
2	b	0.200

Waveforms generated from the harmonic content are shown in Figure 5-11.

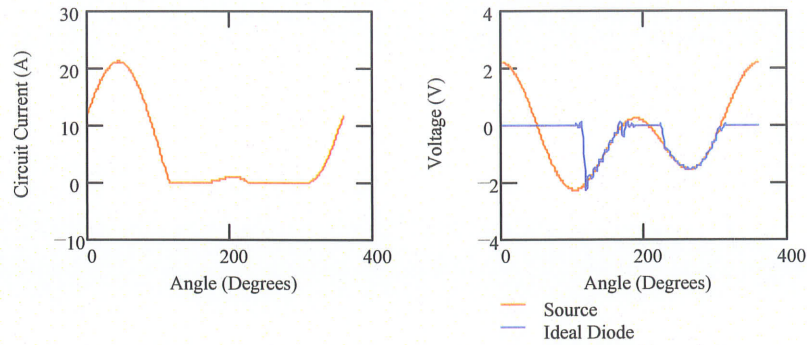


Figure 5-11 Voltage and Current Waveforms from Harmonic Content of HDA Solution to Example 4

5.2.6 Independent Validation of HDA Model

In order to validate the proposed method of harmonic domain analysis as in Example 4 above, a completely independent time domain solution as well its Fourier series representation was carried out analytically as discussed below. The result, as will be shown agrees well with the proposed approach.

For example, the current in the diode at the start of its conduction at about an angle of 170° can be defined in Laplace Transform notation as:

$$I_d(s) = \frac{1}{R + s \cdot L} \cdot V_s(s) \quad \{ 5-25 \}$$

where R is the total circuit resistance.

The Laplace Transform of the source voltage is given by the Laplace Transform of its individual harmonic components, i.e.:

$$V_s(s) = \mathcal{L}(v_s(\omega t)) \quad \{ 5-26 \}$$

$$\mathcal{L}(v_s(\omega t)) = \mathcal{L}(v_{s0}) + \sum_n \mathcal{L}((v_{s2n-1} \cdot \cos(n \cdot \omega t + \gamma)) + \mathcal{L}(v_{s2n} \cdot \sin(n \cdot \omega t + \gamma))) \quad \{ 5-27 \}$$

where 'γ' is the angle where conduction starts.

The Laplace Transform of the source voltage becomes:

$$V_s(s) = \frac{V_{s0}}{s} + \sum_n \left(\frac{s \cdot \cos(\gamma) - n \cdot \omega \cdot \sin(\gamma)}{s^2 + n^2 \cdot \omega^2} \cdot V_{s(2-n-1)} + \frac{s \cdot \sin(\gamma) + n \cdot \omega \cdot \cos(\gamma)}{s^2 + n^2 \cdot \omega^2} \cdot V_{s(2-n-1)} \right) \dots\{ 5-28 \}$$

The equation representing the time response of the current for the conduction interval is the inverse Laplace Transform of Equation 5-25 with V(s) defined by Equation 5-28. The time domain expression for the current was derived from the two equations using the symbolic functions in Mathcad^{®23}. Both Equation 5-28 and its Inverse Laplace Transform can be applied to both conduction intervals with suitable selection of 'γ'. For the interval when the diode is not conducting, the diode voltage is zero in the time domain.

The turn on times of the diode can be determined by solving the time domain equations for the zero crossovers at the angles corresponding to the start and end of diode conduction. The start of each conduction period can be determined from the positive transition, zero crossing of source voltage. The end of conduction can be determined from the negative transition, zero crossing of the current waveform. The Mathcad[®] symbolic equations were incorporated into time domain functions and iterated to establish the solutions for the zero crossings for the test circuit. The resultant zero crossings are shown in Table 5-4:

Table 5-4 Zero Crossings of the Diode Resistor Inductor Circuit

Condition	Angle (Degrees)
Current Crossing	115.8
Voltage Crossing	169.8
Current Crossing	225.4
Voltage Crossing	308.1

A symbolic Fourier analysis of the contribution of each of the continuous components of the diode voltage and current waveforms was determined in accordance with the definitions given in Section 2.2 of Chapter 2. The resultant harmonic spectra is compared

²³ The equations are not included here because of their complexity and since they are only being used to validate the answers from the Harmonic Domain Analysis.

to the spectra calculated using the Harmonic Domain Analysis in Figure 5-12 and Figure 5-13. Figure 5-12 (the comparison of the harmonic content of the current) shows good agreement between the Harmonic Domain Analysis and the theoretical harmonic component. The error, expressed as a percentage of the fundamental frequency component is less than 0.3% for all 50 harmonics.

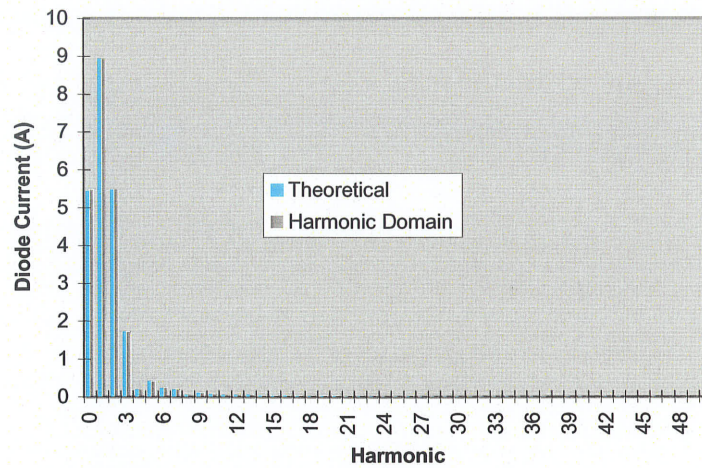


Figure 5-12 Comparison of HDA Harmonic Content of Diode Current with Theoretical Content

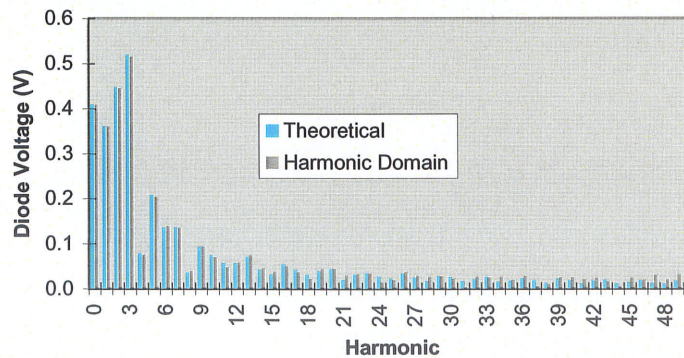


Figure 5-13 Comparison of HDA Harmonic Content of Diode Voltage with Theoretical Content

The comparison of the harmonic content of the diode voltage (Figure 5-13) above about the 25th harmonic deteriorates. The percent error in the magnitude of the harmonic

voltage across the diode again expressed as a percentage of the fundamental frequency component is as high as 4% at the high order harmonics.

This is also evident in the reconstruction of the voltage waveforms over one cycle. The waveform recreated from the reconstruction using the first 50 harmonics of the theoretical harmonic content is compared to the actual waveform in the upper graph of Figure 5-14. The waveform created from the reconstruction using the harmonics from the harmonic domain analysis are compared to the actual voltage waveform in the lower graph.

From the figures, it is evident that the impact of the Gibb's-like oscillations that occur at the discontinuity of the waveform is less in the Harmonic domain analysis method. However, additional oscillations are introduced into the harmonic domain analysis results at the start of the diode conduction. It can be concluded that the harmonic domain algorithm has converged to a solution that is slightly different from the theoretical solution. These differences are attributed to truncation of the harmonic series while equating the square of the absolute value of bus voltage to the square of the bus voltage.

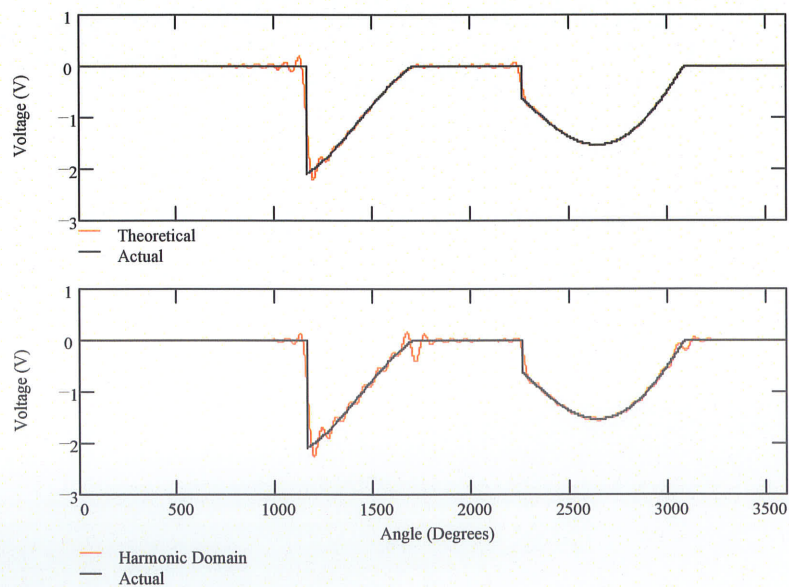


Figure 5-14 Impact of Harmonic Domain and Theoretical Harmonics on Regenerated Waveforms

5.2.7 Summary

The examples with the diode-resistor and diode inductor networks demonstrate that the proposed Harmonic Domain Analysis model of the Diode can be incorporated into a typical Newton-Raphson Jacobian. This will facilitate a sequential build-up of the proposed Harmonic Domain Model that includes a diode, which is analysed entirely in the harmonic domain.

The accuracy of the harmonic content in the current is well within the accuracy that can be expected for an electrical power system. While there are some numerical differences in the harmonic content of the diode voltage waveform, their effects would be limited to the diode itself. At locations more remote from the diode, the impact of any errors in the harmonic content of the diode voltage itself will be attenuated by system inductance.

5.3 APPLICATION TO ANALYSIS OF A THYRISTOR CONTROLLED REACTOR

5.3.1 Introduction

In this chapter, the use of harmonic domain switching functions [33], [34], [13] and their compatibility with the proposed HDA methodology will be examined. A thyristor controlled reactor will be used in the examples presented herein, but the switching function approach can be applied to the harmonic domain analysis of almost all 'controlled' power electronic devices. It is well adapted for circuits where the start of conduction and end of conduction is defined by controls such as in the voltage chopping circuit example in Section 5.4.

This section identifies some of its limitations, particularly where end of conduction is determined by the system to which the power electronic device is connected. An example is power electronic circuits where end of conduction is established by end of the commutation process from one power electronic device to another²⁴.

²⁴ This is the case with the TCR circuit analysed in this chapter.

In the set of examples to follow, the harmonic domain and switching function methodology is applied to a simple thyristor controlled reactor circuit such as shown in Figure 5-15. The circuit consists of a voltage source ' v_s ' applied across a series arrangement of an ideal reactor ' L ', resistor ' R ' and a parallel thyristor switch. For this example, it is assumed that the thyristor firing angles ' α_1 ' and ' α_2 ' are controlled to achieve a reference conduction angle ' σ '. The set point may be varying over a cycle in response to ac system requirements and as a result, conduction angles for the positive and negative current cycles could be different. Voltages and currents are as defined in the figure.

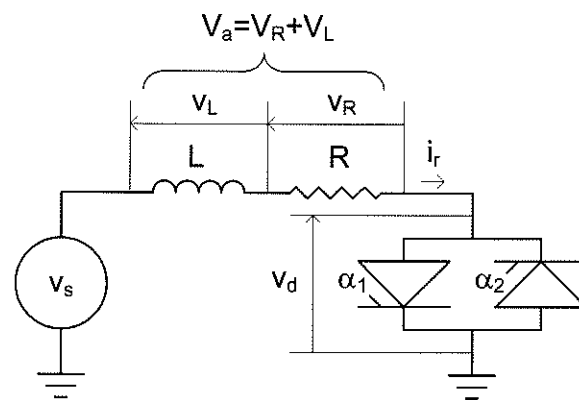


Figure 5-15 Simple Thyristor Controlled Reactor Circuit

The conduction intervals, angles, ' σ_1 ' and ' σ_2 ' respectively, for each thyristor switch define a cyclic time dependent switching function, which is dependent on the characteristics of the applied voltage. Rico et al [13] suggested a 'simple' harmonic domain switching function based only on the conduction intervals could be used to describe the behaviour of the TCR. They consider only the TCR inductor (i.e. no resistance) and determine a voltage ' V_a ' which is calculated based on the harmonic convolution (harmonic multiplication) of the switching function ' S ' and the source voltage ' V_s '. The voltage ' V_a ' is applied to the inductor to determine the circuit current ' I_r '. As will be shown in the following section, their method when used in conjunction with heavily distorted source voltage will give erroneous results. The proposed HDA methodology as presented in this section overcomes the limitations in their method.

5.3.2 Mathematical Development of Harmonic Domain Model

In the following mathematical development, the concepts presented by Rico et al are transformed into a form that is compatible and consistent with the direct harmonic domain model that is being proposed.

With reference to an applied fundamental frequency voltage waveform consisting of only a cosine component, the midpoint of the first conduction interval is assumed to occur at a phase delay of 90 degrees from the peak of the applied voltage. The midpoint of the second conduction interval is assumed to occur after a further 180 degree phase displacement. Figure 5-16 shows the relationship of the assumed switching function to the applied voltage. Relatively large unbalanced conduction intervals have been assumed to demonstrate the application, i.e.:

$$\sigma_1 = 60 \text{ deg}$$

$$\sigma_2 = 30 \text{ deg}$$

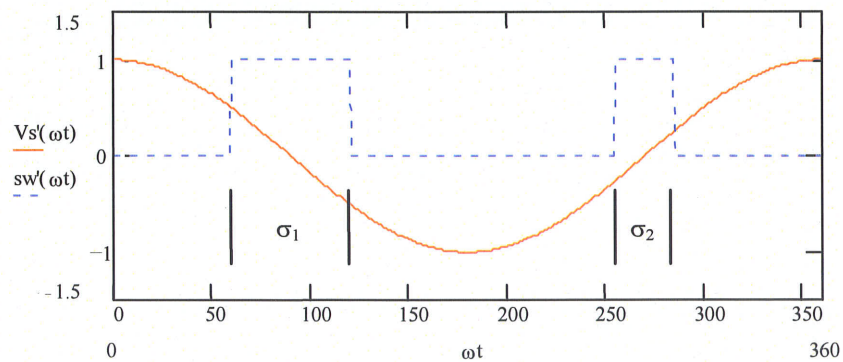


Figure 5-16 Thyristor Controlled Reactor Conduction Interval for Switching Function Demonstration

The switching function can be defined mathematically in the time domain [13] using the following algorithm, where ωt is in degrees and the conduction intervals 'σ' are in radians:

$$s'(\omega t, \sigma_1, \sigma_2) = \begin{cases} \omega t - \omega t - \text{deg} \\ S = 1 \\ S = 0 \text{ if } \left(\omega t < \frac{\pi}{2} - \frac{\sigma_1}{2} \right) \\ S = 0 \text{ if } \left(\omega t > \frac{3 \cdot \pi}{2} + \frac{\sigma_2}{2} \right) \\ (S = 0) \text{ if } \left(\omega t > \frac{\pi}{2} + \frac{\sigma_1}{2} \right) \cdot \left(\omega t < \frac{3 \cdot \pi}{2} - \frac{\sigma_2}{2} \right) \end{cases}$$

Algorithm 5-1

This switching function does not take into account the effect of phase shift or harmonics present in the source voltage. The author has modified this algorithm towards a more general switching function and is used herein. It takes into account overall phase shift as well as a relative shift in firing of each thyristor by introducing the actual thyristor firing angle.

$$s'(\omega t, \alpha_1, \sigma_1, \alpha_2, \sigma_2) = \begin{cases} \omega t - \omega t - \text{deg} \\ S = 1 \\ S = 0 \text{ if } (\omega t < \alpha_1) \\ S = 0 \text{ if } [\omega t > (\alpha_2 + \sigma_2)] \\ S = 0 \text{ if } [\omega t > (\alpha_1 + \sigma_1)] \cdot [\omega t < (\alpha_2)] \end{cases}$$

Algorithm 5-2

The Fourier coefficients of the switching function can be determined using the following algorithm where 'n_{max}' represents the maximum number of harmonics to be assumed in the approximation:

$$S(n_{\max}, \alpha_1, \sigma_1, \alpha_2, \sigma_2) := S_0 \frac{\sigma_1 + \sigma_2}{2}$$

for $i \in 1..n_{\max}$ if $n_{\max} > 0$

$$S_{2i-1} = \frac{1}{i} \left[-\sin(i\alpha_1) + \sin[i(\alpha_1 + \sigma_1)] \right] \dots$$

$$+ \frac{1}{i} \left[-\sin(i\alpha_2) + \sin[i(\alpha_2 + \sigma_2)] \right]$$

$$S_{2i} = \frac{1}{i} \left[\cos(i\alpha_1) - \cos[i(\alpha_1 + \sigma_1)] \right] \dots$$

$$+ \frac{1}{i} \left[\cos(i\alpha_2) - \cos[i(\alpha_2 + \sigma_2)] \right]$$

$$\frac{S}{\pi}$$

Algorithm 5-3

During conduction, the voltage across the thyristors is zero; hence, the voltage across the reactor and resistor is equal to the applied voltage. At other times, the current through the reactor-resistor is constant at a value of zero; hence, the voltage across the reactor-resistor is zero. The voltage (V_a) across the reactor-resistor at any point in time is therefore equal to the product of the switching function at that time and the source voltage at the corresponding point in time.

In the harmonic domain:

$$\vec{V}_a = T(\vec{S}) \cdot \vec{V}_s \tag{5-29}$$

Here, $T(\vec{S})$ is the matrix representation of the switching function described by Algorithm 5-1 earlier in this section.

This equation is used in this analysis in partitioned (dc and harmonics) form. I.e.:

$$\begin{bmatrix} \vec{V}_{a0} \\ \vec{V}_{ah} \end{bmatrix} = \begin{bmatrix} \bar{T}_{0,0} & \bar{T}_{0,h} \\ \bar{T}_{h,0} & \bar{T}_{h,h} \end{bmatrix} \begin{bmatrix} \vec{V}_{s0} \\ \vec{V}_{sh} \end{bmatrix} \tag{5-30}$$

The reactor current $I_r(\omega t)$ as given in the time domain is related to applied voltage by the first order differential equation:

$$2 \cdot \pi \cdot f_o \cdot L \cdot \frac{d}{d\omega t} I_r(\omega t) + R \cdot I_r(\omega t) = V_a(\omega t) \quad \{ 5-31 \}$$

The corresponding relationship in the harmonic domain (see Chapters 2 and 3) is given by:

$$(R \cdot \bar{I} + 2 \cdot \pi \cdot f_o \cdot L \cdot \bar{D}) \cdot \bar{I}_r = \bar{V}_a \quad \{ 5-32 \}$$

where the ' \bar{I} ' is an identity matrix of order $(2 \cdot n_{\max} + 1)$ and ' \bar{D} ' houses the harmonic domain derivative matrix. Equation 5-32 can be rewritten as:

$$\bar{Z} \cdot \bar{I}_r = \bar{V}_a \quad \{ 5-33 \}$$

where:

$$\bar{Z} = R \cdot \bar{I} + 2 \cdot \pi \cdot f_o \cdot L \cdot \bar{D} \quad \{ 5-34 \}$$

The direct solution of \bar{I}_r (in Equation 5-33) in terms of \bar{V}_a is not possible if the resistance is zero since the first row and column of \bar{Z} become zero, as forced by the harmonic domain derivative operator. This is not a limitation to the HDA methodology as will be explained herein.

The matrix Equation (5-33) can be partitioned as follows:

$$\begin{bmatrix} R & \bar{0}_h^T \\ \bar{0}_h & \bar{Z}_h \end{bmatrix} \cdot \begin{bmatrix} \bar{I}_{r0} \\ \bar{I}_{rh} \end{bmatrix} = \begin{bmatrix} \bar{V}_{a0} \\ \bar{V}_{ah} \end{bmatrix} \quad \{ 5-35 \}$$

In this equation, the subscript 'h' denotes the harmonic component of the matrix or array.

The harmonic component of \bar{I}_r can be determined from:

$$\bar{I}_{rh} = \bar{Z}_h^{-1} \cdot \bar{V}_{ah} \quad \{ 5-36 \}$$

As current can only flow through the reactor during conduction, then the relationship between the dc component and the harmonic component of the current can be determined directly from the switching matrix:

$$\begin{bmatrix} \bar{I}_{r0} \\ \bar{I}_{rh} \end{bmatrix} = \begin{bmatrix} \bar{T}_{0,0} & \bar{T}_{0,h} \\ \bar{T}_{h,0} & \bar{T}_{h,h} \end{bmatrix} \begin{bmatrix} \bar{I}_{r0} \\ \bar{I}_{rh} \end{bmatrix} \quad \{ 5-37 \}$$

from which:

$$\bar{I}_{r0} \cdot (1 - \bar{T}_{0,0}) = \bar{T}_{0,h} \cdot \bar{I}_{rh} \quad \{ 5-38 \}$$

or since ' $\bar{T}_{0,0}$ ' is a scalar:

$$\bar{I}_{r0} = \frac{1}{(1 - \bar{T}_{0,0})} \cdot \bar{T}_{0,h} \cdot \bar{I}_{rh} \quad \{ 5-39 \}$$

Substituting in the earlier relationship for the harmonic component \bar{I}_{rh} (from Equation 5-36), and ' \bar{V}_{ah} ' (from Equation 5-30):

$$\bar{I}_{r0} = \frac{1}{(1 - \bar{T}_{0,0})} \cdot \bar{T}_{0,h} \cdot \bar{Z}_h^{-1} \cdot \bar{T}_h \bar{V}_s \quad \{ 5-40 \}$$

where ' \bar{T}_h ' is a matrix housing all but the first row of the matrix $\bar{T}(\bar{S})$, i.e.:

$$\bar{T}_h = \begin{bmatrix} \bar{T}_{h,0} & \bar{T}_{h,h} \end{bmatrix} \quad \{ 5-41 \}$$

The dc component can therefore be defined to be:

$$\bar{I}_{r0} = \bar{Y}_0^T \cdot \bar{V}_s \quad \{ 5-42 \}$$

where:

$$\bar{Y}_0 = \frac{1}{(1 - \bar{T}_{0,0})} \cdot \bar{T}_{0,h} \cdot \bar{Z}_h^{-1} \cdot \bar{T}_h \quad \{ 5-43 \}$$

which is a row array including both dc and harmonic elements.

In a similar fashion, the expression for \bar{I}_{rh} can be expanded:

$$\bar{I}_{rh} = \bar{Z}_h^{-1} \cdot \bar{V}_{ah} \quad \{ 5-44 \}$$

Substituting for \bar{V}_{ah} from (Equation 5-30):

$$\bar{I}_{th} = \bar{Z}_h^{-1} \cdot \bar{T}_h \bar{V}_s \quad \{ 5-45 \}$$

or:

$$\bar{I}_{th} = \bar{Y}_h \bar{V}_s \quad \{ 5-46 \}$$

where:

$$\bar{Y}_h = \bar{Z}_h^{-1} \cdot \bar{T}_h \quad \{ 5-47 \}$$

The equations can be combined to give the harmonic domain admittance matrix representation of the circuit:

$$\bar{I}_r = \bar{Y} \cdot \bar{V}_s \quad \{ 5-48 \}$$

where:

$$\bar{Y} = \begin{pmatrix} \bar{Y}_0 \\ \bar{Y}_h \end{pmatrix} \quad \{ 5-49 \}$$

The following algorithm can be used to generate the elements of the admittance matrix:

$Y(n, \alpha_1, \sigma_1, \alpha_2, \sigma_2, f_0, L, R) =$	$T_s = T(S(n, \alpha_1, \sigma_1, \alpha_2, \sigma_2))$
	$\text{dim} = 2 \cdot n$
	$T_{0n} = \text{submatrix}(T_s, 0, 0, 1, \text{dim})$
	$T_n = \text{submatrix}(T_s, 1, \text{dim}, 0, \text{dim})$
	$Z_n = \text{submatrix}(2 \cdot \pi \cdot f_0 \cdot L \cdot D(n) + \text{identity}(2 \cdot n + 1) \cdot R, 1, \text{dim}, 1, \text{dim})$
	$Y_0 = \frac{1}{(1 - T_{s_{0,0}})} \cdot T_{0n} \cdot (Z_n)^{-1} \cdot T_n$
	$Y_n = Z_n^{-1} \cdot T_n$
	$Y = \text{stack}(Y_0, Y_n)$

Algorithm 5-4

The following section will show numerical solutions of the circuit considered in this section.

5.3.3 Sample Applications of the Harmonic Domain Model

Knowing the equivalent admittance, the circuit can be solved directly using basic analysis techniques. A Mathcad® calculation sheet was used to solve the circuit for the condition with a purely sinusoidal applied voltage and no series resistance. The solution method is as follows:

```

Test Case 1 Fundamental Frequency Only, No Resistance
fo := 50 L := .01 R := 0.0 nmax := 50
α1 := 60-deg σ1 := 60-deg α2 := 255-deg σ2 := 30-deg
φ1 := 0-deg Vs1 := 1.0 Vs1 := Vs1·cos(φ1) Vs2 := -Vs1·sin(φ1) ii := 3..2·nmax Vsii := 0
Equivalent Admittance Matrix of the Circuit
Yeq := Y(nmax, α1, σ1, α2, σ2, fo, L, R)
Circuit Current
Id := Yeq·Vs
Voltage across Switch
Vd := Vs - (identity(2·nmax+1)·R + 2·π·fo·L·D(nmax))·Id
Voltage across Inductor
Vl := 2·π·fo·L·D(nmax)·Id
Voltage across Resistor
Vr := identity(2·nmax+1)·R·Id
    
```

The first non-zero harmonic coefficients of the calculated currents and voltages are shown in Table 5-5.

Table 5-5 Harmonic Content of Waveforms for TCR Case 1

Harmonic Content of Waveforms								
Circuit Current (kA)			Thyristor Switch Voltage (kV)			Inductor Voltage (kV)		
n	series	I _d	n	series	V _d	n	series	V _l
0	a	0.00411	1	a	0.96741	1	a	0.03259
1	a	0.01037	2	b	-0.04569	2	b	0.04569
2	b	-0.00727	3	a	0.07958	3	a	-0.07958
3	a	-0.00844	4	b	0.06074	4	b	-0.06074
4	b	0.00483	5	a	-0.08478	5	a	0.08478
5	a	0.00540	6	b	-0.03700	6	b	0.03700
6	b	-0.00196	7	a	0.05305	7	a	-0.05305
7	a	-0.00241	8	b	-0.00628	8	b	0.00628
8	b	-0.00025	9	a	-0.01165	9	a	0.01165
9	a	0.00041	10	b	0.03842	10	b	-0.03842
10	b	0.00122	11	a	-0.01165	11	a	0.01165
11	a	0.00034	12	b	-0.04054	12	b	0.04054
12	b	-0.00108	13	a	0.00832	13	a	-0.00832
13	a	-0.00020	14	b	0.01765	14	b	-0.01765
14	b	0.00040	15	a	0.00832	15	a	-0.00832

Time domain waveforms can be generated from the harmonic content. The following Mathcad® function calculates the value of the waveform at time 'ωT' where the waveform is defined by the Fourier coefficients housed in the array 'v'.

```

f(v, ωT) :=
    dim ← rows(v) - 1
    (f ← v) if dim < 0
    otherwise
        f ← v0
        for i ∈ 1..dim
            n ← floor((i + 1) / 2)
            (f ← f + vi · cos(n · ωT · deg)) if mod(i, 2) ≠ 0
            (f ← f + vi · sin(n · ωT · deg)) otherwise
    f
    
```

Algorithm 5-5

The circuit current waveform is computed as follows:

$$\omega t := 0..360$$

$$I_{d'_{\omega t}} := f(I_d, \omega t)$$

and is shown in Figure 5-17.

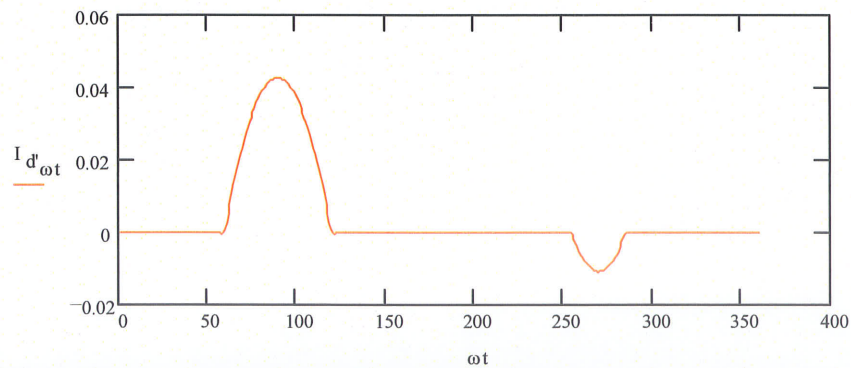


Figure 5-17 Thyristor Controlled Reactor Circuit Current for Case 1

The voltage waveforms are computed as follows:

$$\begin{aligned} V_{s'\omega t} &:= f(V_s, \omega t) \\ V_{d'\omega t} &:= f(V_d, \omega t) \\ V_{l'\omega t} &:= f(V_l, \omega t) \\ V_{r'\omega t} &:= f(V_r, \omega t) \\ V_{r'\omega t} &:= f(V_r, \omega t) \end{aligned}$$

and their time domain response is given in Figure 5-18.

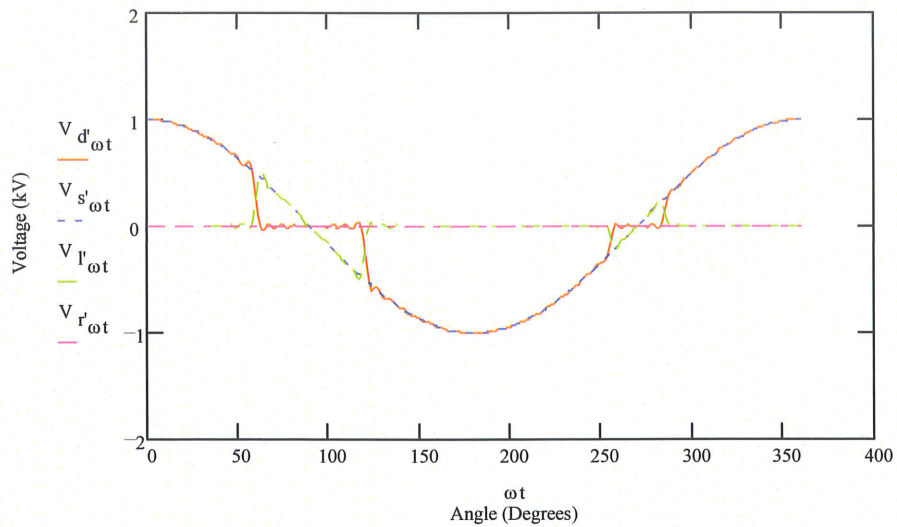


Figure 5-18 Thyristor Controller Reactor Voltage Waveforms for Case 1

Both the voltage and current waveforms are as expected and have been visually validated using a time domain simulation. The same model was implemented in PSCAD/EMTDC™ and the EMTDC™ waveforms were of the same shape and magnitude as the waveforms shown in Figure 5-17 and Figure 5-18.

The methodology can be applied to the condition where there is harmonic content in the applied voltage waveform, as follows, where a third harmonic with a magnitude equal to 20% of the fundamental component is applied.

The harmonic content of the waveforms, calculated in the same manner, is shown in Table 5-6 and the circuit current and voltage waveforms, regenerated from the calculated

harmonic content are shown in Figure 5-19 and Figure 5-20. Again, both the voltage and current waveforms are as expected and have been visually validated using a PSCAD/EMTDC™ simulation with the same large 3rd harmonic component in the source waveform.

Table 5-6 Harmonic Content of Waveforms for TCR Case 2

Source Voltage (kV)		
n	series	V _s
1	a	1.00000
3	a	0.20000

Circuit Current (kA)			Thyristor Switch Voltage (kV)			Inductor Voltage (kV)		
n	series	I _d	n	series	V _d	n	series	V _l
0	a	0.00220	1	a	0.98333	1	a	0.01667
1	b	0.00531	2	b	-0.02441	2	b	0.02441
2	a	-0.00388	3	a	0.24019	3	a	-0.04019
3	b	-0.00426	4	b	0.03205	4	b	-0.03205
4	a	0.00255	5	a	-0.04130	5	a	0.04130
5	b	0.00263	6	b	-0.01871	6	b	0.01871
6	a	-0.00099	7	a	0.02316	7	a	-0.02316
7	b	-0.00105	8	b	-0.00474	8	b	0.00474
8	a	-0.00019	9	a	-0.00104	9	a	0.00104
9	b	0.00004	10	b	0.02137	10	b	-0.02137
10	a	0.00068	11	a	-0.00999	11	a	0.00999
11	b	0.00029	12	b	-0.02122	12	b	0.02122
12	a	-0.00056	13	a	0.00599	13	a	-0.00599
13	b	-0.00015	14	b	0.00776	14	b	-0.00776
14	a	0.00018	15	a	0.00479	15	a	-0.00479

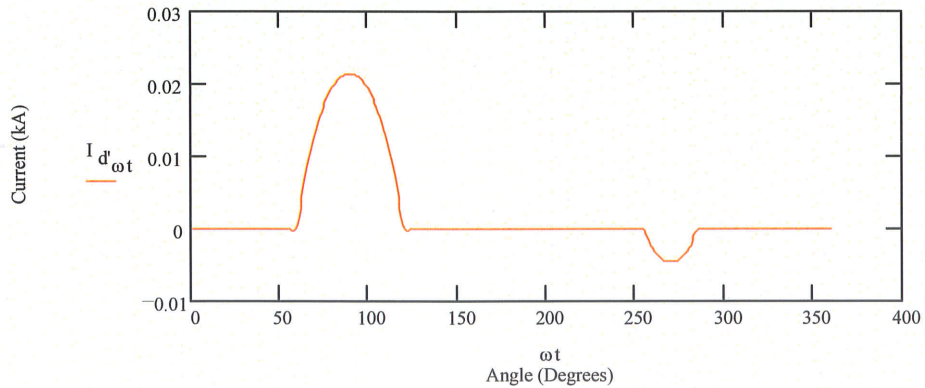


Figure 5-19 Thyristor Controlled Reactor Circuit Current for Case 2

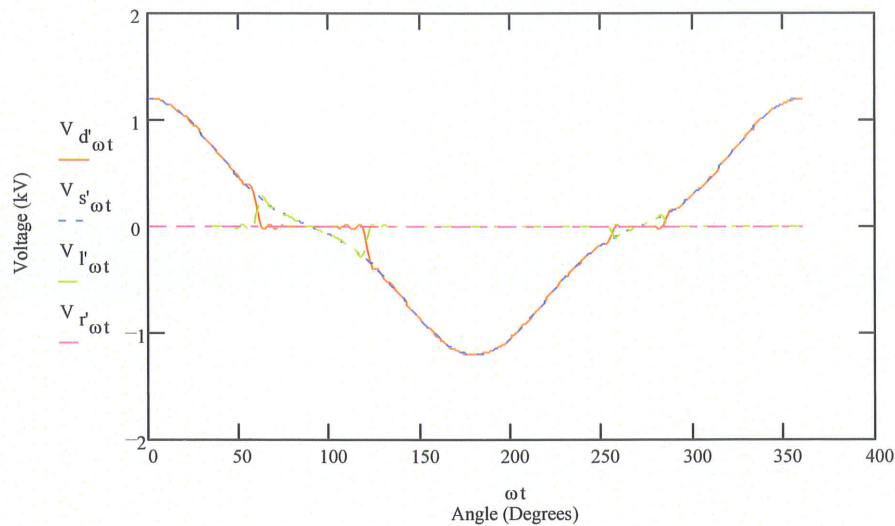


Figure 5-20 Thyristor Controller Reactor Voltage Waveforms for Case 2

At this stage of development of the Harmonic Domain model for the thyristor controlled reactor, it is represented as a fixed harmonic domain admittance that is as function of essentially only its conduction angles. The fixed admittance model is certainly useful for obtaining a picture of the impact of variations in fundamental frequency voltage and 3rd harmonic voltage magnitude on the harmonics in the network.

The first two cases above indicate that unbalanced conduction intervals introduce a dc component into the TCR current along with both odd and even harmonics. Also, a third harmonic in the source voltage waveform significantly reduces the fundamental component of the TCR current, hence its output for any given set of conduction angles. A third harmonic distortion of 20% will reduce the TCR output by almost 50%.

While all of this information could be extracted from time domain simulations, followed by Fourier analysis, they are immediately available in the harmonic domain with a single calculation. For example, the reduction in output can be quantified by comparing the fundamental frequency component of the circuit current in Example 1 (0.01 kA from Table 5-5) to the corresponding current in Example 2 (.005 kA from Table 5-6). The dc component of the network current, which is extremely important in the design of power systems, can be extracted directly from the solutions in the two tables as 4 A and 2 A

(4.11 A from first column, first row of Table 5-5, 2.2 A from first column, first row of Table 5-6) respectively.

However, the switching function as defined by Rico et al [13], without adjustment to the firing angles, is only valid for the conditions where there is:

- no phase shift in applied fundamental frequency voltage,
- no even order harmonic voltages, and
- no phase shift in odd order harmonics.

Although not indicated in the reference [13], the switching function must be locked to the phase of the source voltage, or incorrect results will be obtained. This is a problem with Rico's algorithm as presented in his paper. In order to overcome this, the proposed HDA algorithm implementation adds a phase shift into the switching function.

The phase shift can also compensate for the effects of odd order harmonics if the positive and negative conduction intervals are the same²⁵. The switching function, without adjustment to the firing angles, will provide incorrect harmonic content if the above conditions are not satisfied, possibly indicating a weakness in the model proposed by Rico et al [13] if it is used in conjunction with operating conditions outside of the norm.

Any TCR control system that uses conduction angle for closed-loop feedback control will automatically adjust the firing angle until the target conduction angle(s) is(are) achieved. This includes automatically (in the time domain) compensating for harmonics and phase shift in the source voltage waveform.

In the following case (Case'3'), the voltage source is assumed to include significant 2nd and 3rd harmonic components (not in phase with the fundamental frequency). The circuit

²⁵ In a 'normal' mode of operation, conduction angles would indeed be similar, but to be general, the model should be able to handle serious distortion in the firing angle circuit resulting in unequal conduction angles.

is also assumed to display some resistance²⁶. The following Mathcad[®] calculation sheet summarises the test case.

Test Case 3 Fundamental Frequency 2nd & 3rd Harmonic, with Resistance			
$f_o := 50$ $L := .01$ $R := 0.5$ $n_{max} := 50$			
$\sigma_1 := 60\text{-deg}$	$\alpha_1 := 95.78\text{deg} - \frac{\sigma_1}{2}$	$\alpha_1 = 65.78\text{-deg}$	α_1 and α_2 selected based
$\sigma_2 := 30\text{-deg}$	$\alpha_2 := 261.6\text{deg} - \frac{\sigma_2}{2}$	$\alpha_2 = 246.6\text{-deg}$	on trial and error
$ii := 0..2 \cdot n_{max}$			
$V_{s_{ii}} := 0$			
$V_{s_1} := 1.0$	$\phi_1 := 0\text{-deg}$	$V_{s_1} := V_{s_1} \cdot \cos(\phi_1)$	$V_{s_2} := -V_{s_1} \cdot \sin(\phi_1)$
$V_{s_2} := .2$	$\phi_2 := -125\text{-deg}$	$V_{s_3} := V_{s_2} \cdot \cos(\phi_2)$	$V_{s_4} := -V_{s_2} \cdot \sin(\phi_2)$
$V_{s_3} := .1$	$\phi_3 := 30\text{-deg}$	$V_{s_5} := V_{s_3} \cdot \cos(\phi_3)$	$V_{s_6} := -V_{s_3} \cdot \sin(\phi_3)$
Equivalent Admittance Matrix of the Circuit			
$Y_{eq} := Y(n_{max}, \alpha_1, \sigma_1, \alpha_2, \sigma_2, f_o, L, R)$			
Circuit Current			
$I_d := Y_{eq} \cdot V_s$			
Voltage across Switch			
$V_d := V_s - (\text{identity}(2 \cdot n_{max} + 1) \cdot R + 2 \cdot \pi \cdot f_o \cdot L \cdot D(n_{max})) \cdot I_d$			
Voltage across Inductor			
$V_l := 2 \cdot \pi \cdot f_o \cdot L \cdot D(n_{max}) \cdot I_d$			
Voltage across Resistor			
$V_r := \text{identity}(2 \cdot n_{max} + 1) \cdot R \cdot I_d$			

The choice of α_1 and α_2 involved a 'trial and error' process. The circuit was first solved for a single thyristor switch and an assumed value of α_1 . Waveforms were generated from the harmonic content and examined. The firing angle was adjusted until the thyristor voltage at the start, end and during conduction was zero on average. At the same time the circuit current was monitored to ensure that the current remained at approximately zero from end of conduction until start of conduction. Turning on the second thyristor at an 'incorrect' firing angle again introduced errors into the voltage and current waveforms. The 'incorrect' harmonic current waveform generated with $\alpha_2 = 250$ degrees is shown in Figure 5-21. However, after adjustment to only the second firing angle, reasonable

²⁶ This is not a requirement of the proposed HDA. In fact inclusion of resistance creates a more onerous test condition.

waveforms were restored. After adjustment to the firing angle ($\alpha_2 = 261.6$ degrees), the harmonic content of the current waveform is as shown in Figure 5-22. The corresponding voltage waveforms are given in Figure 5-23.

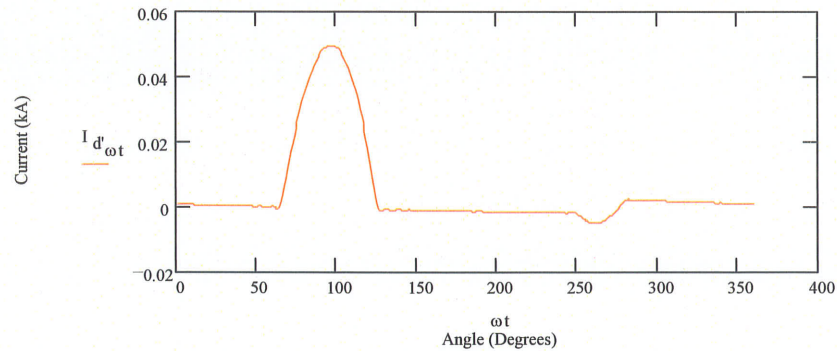


Figure 5-21 Incorrect TCR Current Waveform

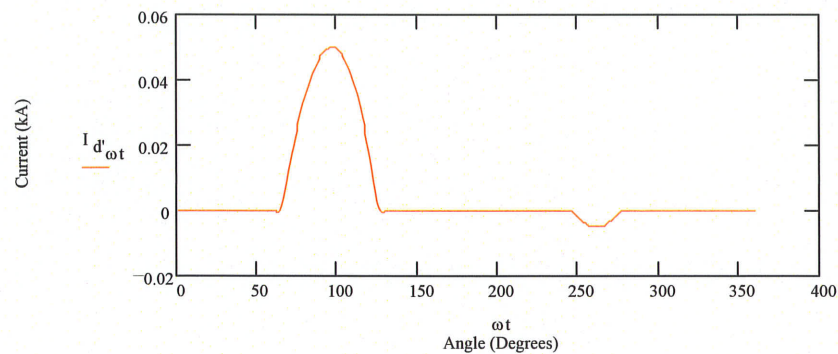


Figure 5-22 TCR Current Waveform after Adjustment to Second Firing Angle

The harmonic content used to generate the waveforms is given in Table 5-7 below.

This demonstration shows that the proposed HDA methodology can be applied to conditions outside of its current implementation. In theory, with a more robust harmonic domain square root function, the HDA treatment of the thyristor controlled reactor would be completely flexible.

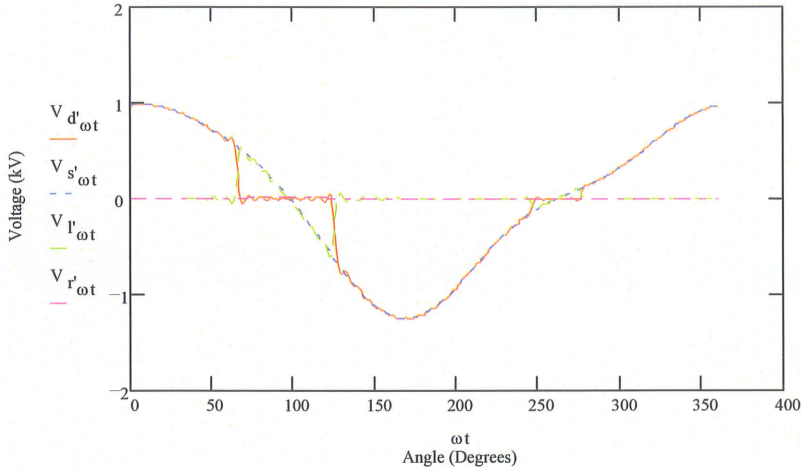


Figure 5-23 TCR Voltage Waveforms after Adjustment to Second Firing Angle

Table 5-7 Harmonic Content of Waveforms after Adjustment to Firing Angle

Source Voltage (kV)			Circuit Current (kA)		
n	series	I_d	n	series	I_d
1	a	1.00000	0	a	0.00525
2	a	-0.11472	1	a	-0.00109
2	b	0.16383	1	b	0.01125
3	a	0.08660	2	a	-0.00914
3	b	-0.05000	2	b	-0.00232
			3	a	0.00256
			3	b	-0.00858
			4	a	0.00584
			4	b	0.00327
			5	a	-0.00243
			5	b	0.00469
			6	a	-0.00236
			6	b	-0.00250
			7	a	0.00103
			7	b	-0.00142

Thyristor Switch Voltage (kV)			Inductor Voltage (kV)			Resistor Voltage (kV)		
n	series	V_d	n	series	V_l	n	series	V_r
0	a	-0.00262	1	a	0.03533	0	a	0.00100
1	a	0.96522	1	b	0.00343	1	a	0.00100
1	b	-0.00905	2	a	-0.01455	1	b	0.00200
2	a	-0.09559	2	b	0.05743	2	a	0.00100
2	b	0.10756	3	a	-0.08085	2	b	0.00200
3	a	0.16617	3	b	-0.02417	3	a	0.00100
3	b	-0.02155	4	a	0.04106	3	b	0.00200
4	a	-0.04399	4	b	-0.07342	4	a	0.00100
4	b	0.07178	5	a	0.07370	4	b	0.00200
5	a	-0.07249	5	b	0.03810	5	a	0.00100
5	b	-0.04044	6	a	-0.04710	5	b	0.00200
6	a	0.04828	6	b	0.04443	6	a	0.00100
6	b	-0.04318	7	a	-0.03133	6	b	0.00200
7	a	0.03082	7	b	-0.02262	7	a	0.00100
7	b	0.02334	8	a	0.02193	7	b	0.00200

5.3.4 Summary

The switching function methodology provides a method for preliminary harmonic calculations. It is not a 'purely' frequency domain method. It carries time domain information indirectly through the harmonic content of the switching waveform, i.e., the characteristics of the switching function are dependent on the firing angles and conduction angles which are in fact time domain quantities.

The admittance matrix methodology described in Section 5.3.3 above could be used for small signal analysis. It provides a convenient means to quickly determine the dependence of harmonics in the circuit current on harmonics in the source voltage.

Its primary weakness is that it requires a reasonably accurate estimate of firing angles and conduction angles to give correct results for operating conditions outside the norm. These

angles could come from time domain analysis. Alternatively, an algorithm could be developed to emulate the trial and error process described for test case 3 above, possibly based on a neural net solution. Again, with a more robust harmonic domain square root function the HDA treatment of the thyristor controlled reactor would be completely flexible.

In the form described above, and when used with circuits where commutation is involved, the harmonic domain switching function would have only limited application in the overall HDA methodology as proposed by the author. It could be used, though, for small signal harmonic analysis of most power electronic switching devices.

When the harmonic domain switching function is used to model the switching of non-commutating circuits, it is very compatible with the author's methodology. Its use together with HDA simulation of controls is shown in the next section where it is applied to the modelling of a voltage chopping circuit.

5.4 APPLICATION TO VOLTAGE CHOPPING CIRCUIT WITH CONTROLS

A 50 Hz voltage chopping circuit (VCC) was developed to demonstrate that the proposed harmonic domain solution methodology can be applied to the analysis of circuits involving a combination of power system linear elements, electronic switching elements and controls with non-linear elements. The VCC is a fundamental element of most three-phase voltage sourced converter (VSC) circuits. The VCC assumed is a single pulse (per cycle) 50 Hz device, operating off a 1 kV ideal dc voltage bus. It is represented as shown in Figure 5-24 as an ideal voltage source that generates no output for ' α ' degrees of the power frequency cycle and a constant output for the remaining portion of the cycle. The VCC supplies a resistive load ' R_{load} ' through a 2nd harmonic lossless series blocking filter as shown in Figure 5-24(a). The load current is monitored and a signal representing the dc component is generated from the measured current by passing the absolute value of the measured current through a first order lag control circuit filter to reduce the harmonic content as indicated in Figure 5-24(b). The equivalent dc component is

compared to a signal proportional to the reference current. A proportional-integral (PI) controller is used to establish the reference angle ' α ' that minimizes the error between the reference current and measured signal.

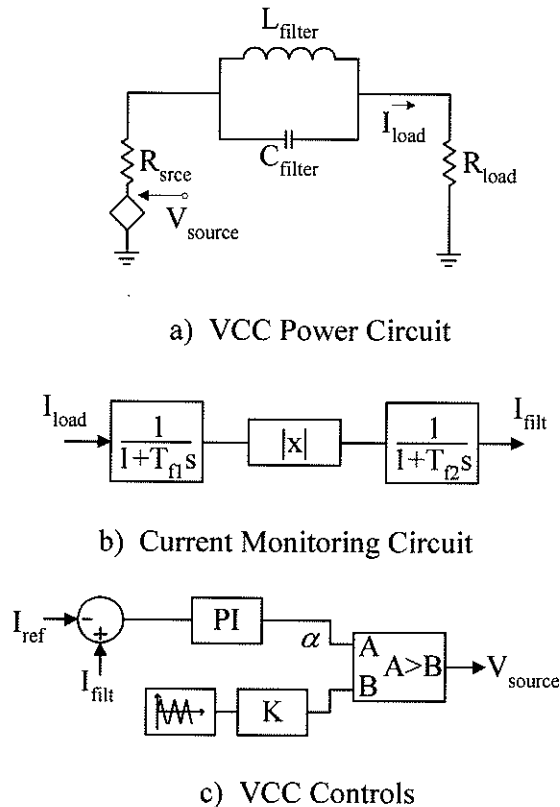


Figure 5-24 Circuit Diagram of Test VCC and Controls

The simulation of the VCC itself and its low level firing angle controls is based on its equivalent behaviour in the time domain. In the time domain, the reference angle ' α ' is compared to a ramp with a period of 1 cycle and a magnitude of 360 degrees. If the ramp has a greater magnitude than the reference angle ' α ', the VCC is turned on, creating a 1 kV voltage at the output. When the ramp is less than ' α ', the output of the VCC is set to zero.

The parallel L-C circuit forming the blocking filter in practice has a net impedance of zero for the dc component, due to the presence of the inductor. Standard admittance

matrix definition of the network for the complete harmonic domain is therefore precluded due to the resultant singularity in the dc component of the admittance.

The blocking filter also creates a very high impedance and corresponding low admittance at the second harmonic. This exposes the solution of the network to potential numerical issues.

The PI controller also creates a numerical anomaly in the dc component as the effective gain of the integral component of the controller is infinite. The dc component of the input to the controller must be set to zero numerically, affecting the output of downstream calculations and at the same time the dc component of the output becomes independent of the input vector making it a function of upstream calculations. It is not possible to define a single matrix that represents the harmonic relation between the input and the output of the PI controller. Therefore, the harmonic and dc components must be treated differently.

The relationship between the harmonic voltage produced by the voltage chopping circuit itself to the firing angle ' α ' can be defined by a switching function matrix. For this demonstration, a fixed dc voltage input to the converter has been assumed, i.e., with no superimposed harmonics on the converter supply voltage. The product of the switching function matrix and the dc voltage source supply vector (with no harmonic components) becomes a simple harmonic voltage vector that is a function of ' α '. If the firing angle contains a harmonic component (i.e. it is time varying, which is the case in this demonstration), the switching function matrix concept has to be adjusted to take into account the harmonic content of ' α '.

The controller to the hypothetical VCC contains the control block function ' $|x|$ '. In the time domain, this function would simply invert the input signal if it became negative. The harmonic domain equivalent of this function as described in Section 2.7 is nonlinear, with the characteristics of the transfer function dependent on the characteristics of the input. The use of this element was included to demonstrate how the HDA methodology proposed can readily handle this type of non-linearity.

While many of the mathematical techniques to model the electrical network linear components and the linear control system components are similar, the relative magnitudes of the data in the resultant matrices could vary by orders of magnitude introducing numerical problems when the matrix-matrix and matrix-vector numerical operations are carried out. In a conventional power flow analysis, use of the per unit system normalizes the data such that the admittance matrix or Jacobian matrix contain numerical entries of similar orders of magnitude. For this demonstration, no scaling has been introduced and as a result introduces numerical issues in the iterative solution of the network.

The harmonic domain equations defining the power circuit (determined from the representation of basic electrical components given in Chapter 3) can be shown to be:

$$\bar{I}_{load} = \bar{Z}_{equiv}^{-1} \cdot \bar{V}_{srce} \quad \{ 5-50 \}$$

where:

$$\bar{Z}_{equiv} = \begin{bmatrix} (R_{srce} + R_{load}) & \bar{0}_h^T \\ \bar{0}_h & (R_{srce} + R_{load}) \cdot \bar{I}_h + \left((2\pi f_o \cdot L_{filter} \cdot \bar{D}_h)^{-1} + 2\pi f_o \cdot C_{filter} \cdot \bar{D}_h \right)^{-1} \end{bmatrix} \quad \dots\{ 5-51 \}$$

and 'f_o' is the nominal system frequency.

In the above partitioned expression for ' \bar{Z}_{equiv} ', the subscripts 'h' denote the harmonic components only of the identity ' \bar{I} ' and derivative ' \bar{D} ' operator matrices and the zero vector $\bar{0}$. The limitations introduced by the zero net dc impedance of the 2nd harmonic filter are eliminated by combining the filter with the resistance of the source and load.

The harmonic domain equations describing the transfer characteristics of the measuring circuit are:

$$\bar{I}_{meas} = \bar{K}_{\tau 1} \cdot \bar{I}_{load} \quad \{ 5-52 \}$$

where $\bar{K}_{\tau 1}$ is a sparse harmonic domain matrix representing the characteristics of a first order lag function. It is determined using the HDA function FOL as described in Chapter 4. I.e.:

$$\bar{K}_{\tau 1} = \text{FOL}(2\pi f_0 \cdot \tau_{f1}) \quad \{ 5-53 \}$$

Similarly, the filtered current is:

$$\begin{aligned} \bar{I}_{\text{abs}} &= \text{Abs}(\bar{I}_{\text{meas}}) \\ \bar{I}_{\text{filt}} &= \bar{K}_{\tau 2} \cdot \bar{I}_{\text{abs}} \end{aligned} \quad \{ 5-54 \}$$

where:

$$\bar{K}_{\tau 2} = \text{FOL}(2\pi f_0 \cdot \tau_{f2}) \quad \{ 5-55 \}$$

The Abs function returns a harmonic vector housing the harmonics included in the absolute value of the measured current ' \bar{I}_{meas} '

In the control block diagram, the harmonic response of the control angle α is given by:

$$\begin{aligned} \bar{I}_{\text{err}} &= \bar{I}_{\text{filt}} - \bar{I}_{\text{ref}} \\ \bar{\alpha} &= \bar{K}_{\tau 3} \cdot \bar{I}_{\text{err}} \end{aligned} \quad \{ 5-56 \}$$

where:

$$\bar{K}_{\tau 3} = \text{PID}(G_{\text{pi}}, 2\pi f_0 \cdot \tau_{\text{pi}}, 0) \quad \{ 5-57 \}$$

and G_{pi} and τ_{pi} are the proportional gain and integral time constant of the PI controller.

The function PID generates a sparse harmonic domain matrix representing the characteristics of a proportional, integral, derivative control circuit. For this application, the derivative time constant is zero. Because of the integral term, the net dc transfer characteristic of the PID function, although infinite, is set to zero. As the output of the integrator is finite, the dc component of the error signal must be zero, i.e.:

$$\bar{I}_{\text{err}0} = 0.0 \quad \{ 5-58 \}$$

The reference voltage is derived using the integrated harmonic domain function CompRamp that returns a vector housing the harmonics of a pulse waveform depending on the harmonic content of vector ' $\vec{\alpha}$ '. I.e.,

$$\vec{V}_{ref} = \text{CompRamp}(\vec{\alpha}, f_o) \quad \{ 5-59 \}$$

The source voltage is assumed equal to the reference voltage, i.e.:

$$\vec{V}_{srce} = \vec{V}_{ref} \quad \{ 5-60 \}$$

The equations can be combined into three simultaneous harmonic expressions:

$$\left. \begin{aligned} \vec{V}_{srce} - \text{CompRamp}(\vec{\alpha}) &= \vec{0} \\ \vec{I}_{err} + \vec{I}_{ref} - \bar{K}_{\tau 2} \cdot \text{Abs}(\bar{K}_{\tau 1} \cdot \bar{Z}_{equiv}^{-1} \cdot \vec{V}_{srce}) &= \vec{0} \\ \vec{I}_{err0} &= 0 \\ \vec{\alpha}_h - \bar{K}_{\tau 3h} \cdot \vec{I}_{errh} &= \vec{0}_h \end{aligned} \right\} \{ 5-61 \}$$

Initial attempts to solve the above set of simultaneous equations entirely in the frequency domain were unsuccessful. As discussed in Chapter 4, Gibb's-like oscillations associated with the ramp function created multiple intersections of the fixed ramp and the reference signal. This translates into multiple solutions in the frequency domain creating numerical stability issues.

Even after slipping into the time domain to solve these problems, numerical issues were still present associated with forcing the dc component of the current error vector ' \vec{I}_{err0} ' to zero.

The author believed that it was essential to demonstrate that the model could be applied to combined electrical and non-linear control systems, to add credibility to the proposed HDA model. To this end, an alternative algorithm was developed to solve the above set of equations, { 5-61 }, that does involve a slight digression into the time domain.

The solution for this example was divided into two separate components.

The HDA method was used to establish the scalar or time domain value of ' α ' that would be required to force the dc component of the current error vector to zero. This required a modification to the CompRamp function to accept a scalar value as an input.

The modified Mathcad[®] implementation of the algorithm is as follows:

$$\text{CompRamp}(\beta, n_{\max}) = \begin{cases} f_0 - 1 - \frac{\beta}{2\pi} \\ \text{for } i \in 1..n_{\max} \\ \left| \begin{array}{l} f_{2i-1} - \frac{\sin(i\beta)}{i\pi} \\ f_{2i} - \frac{\cos(i\beta) - 1}{i\pi} \end{array} \right. \\ f \end{cases}$$

Algorithm 5-6

The resultant algorithm is a very minor calculation and is the same as the algorithm that would be used to define the harmonic content of a switching function with the same characteristics.

The harmonic domain equations can be re-arranged to define the relationship between the dc component of the current error and the scalar ' α ' as follows:

$$\left[(K_{\tau 2} \cdot \text{abs}(K1Y \cdot \text{CompRamp}(\alpha_0, n_{\max})))_0 \cdot 1000 - I_{\text{ref}0} \right] = 0$$

K1Y above is a sparse matrix defined to be:

$$K1Y = K_{\tau 1} \cdot Z_{\text{equiv}}^{-1}$$

The derivative of the modified CompRamp function with respect to 'α' in Mathcad® implementation format can be shown to be:

$$\begin{aligned}
 \text{dbyd } \alpha(\alpha, n_{\text{max}}) &:= \frac{f_0}{2} \\
 &\text{for } i \in 1..n_{\text{max}} \\
 &\quad \left\{ \begin{array}{l} f_{2,i-1} := \cos(i \cdot \alpha) \\ f_{2,i} := \sin(i \cdot \alpha) \end{array} \right. \\
 &\quad - \frac{f}{\pi}
 \end{aligned}$$

Algorithm 5-7

This permits a Newton-Raphson solution algorithm as follows:

$$\begin{aligned}
 \text{iter} &:= 0 & \alpha_0 &:= 0 \cdot \text{deg} \\
 \text{iter} &:= \text{iter} + 1 & \text{iter} &= 1.000 \\
 \text{Jac} &:= \left(K_{\tau 2} \cdot T_p \left(\text{sign} \left(K1Y \cdot \text{CompRamp}(\alpha_0, n_{\text{max}}) \right) \right) \cdot K1Y \cdot \text{dbyd } \alpha(\alpha_0, n_{\text{max}}) \right)_0 \cdot 1000 \\
 \Delta\alpha &:= - \frac{1}{\text{Jac}} \cdot \left[\left(K_{\tau 2} \cdot \text{abs} \left(K1Y \cdot \text{CompRamp}(\alpha_0, n_{\text{max}}) \right) \right)_0 \cdot 1000 - I_{\text{ref}0} \right] \\
 \alpha_0 &:= \alpha_0 + \Delta\alpha
 \end{aligned}$$

Algorithm 5-8

Note that the Jacobian and firing angle are both scalar quantities in the above expressions.

Having solved the dc component of the current error, the harmonic content can also be directly calculated. I.e.:

$$\begin{aligned}
 V_{\text{srce}} &:= \text{CompRamp}(\alpha_0, n_{\text{max}}) \\
 KYV &:= K1Y \cdot V_{\text{srce}} \\
 \text{AbsKYV} &:= \text{abs}(KYV) \\
 I_{\text{eq}} &:= K_{\tau 2} \cdot \text{AbsKYV} \cdot 1000 \\
 I_{\text{err}} &:= (I_{\text{eq}} - I_{\text{ref}})
 \end{aligned}$$

Algorithm 5-9

The product of the matrix $\bar{K}_{\tau 3}$ (defining the characteristics of the PI controller) and the current error vector contains only harmonic content since the dc component of $\bar{K}_{\tau 3}$ was originally set to zero. Here we will introduce a new variable θ equal to the product:

$$\theta := K_{\tau 3} \cdot I_{err} \cdot \text{deg}$$

The dc component of θ must be defined such that the time domain evaluation at ' $\omega t = \alpha_0$ ' is correct, i.e.:

$$\theta_0 := \sum_{i \in 1..n_{max}} \theta_{2,i-1} \cdot \cos(i \cdot \alpha_0) - \theta_{2,i} \cdot \sin(i \cdot \alpha_0)$$

Algorithm 5-10

The circuit was solved using the data shown in Figure 5-25

The harmonic content of the individual voltages, currents and the reference angle ' $\bar{\alpha}$ ' were calculated as follows:

$$\begin{aligned} V_{srce} &:= \text{CompRamp}(\alpha_0, n_{max}) \\ I_{load} &:= Z_{equiv}^{-1} \cdot V_{srce} \cdot 1000 \\ I_{filt} &:= K_{\tau 1} \cdot I_{load} \\ I_{abs} &:= \text{abs}(I_{filt}) \\ I_{meas} &:= K_{\tau 2} \cdot I_{abs} \\ I_{err} &:= I_{meas} - I_{ref} \\ \theta_0 &:= \theta_0 \quad \theta := K_{\tau 3} \cdot I_{err} \cdot \text{deg} \quad \theta_0 := \theta_0 \quad \alpha := \theta \\ V_{load} &:= \frac{R_{load} \cdot I_{load}}{1000} \\ V_{load} &:= \frac{V_{load}}{\Omega} \end{aligned}$$

Algorithm 5-11

The solution algorithm solved in less than 6 iterations. The correction to the firing angle at the end of the 6th iteration was in the order of 10^{-6} degrees. With the modified algorithm, there was no evidence of numerical instability for the adverse conditions selected. The magnitude of the harmonic content of the voltage and currents is shown in Figure 5-26. The lack of 2nd harmonic in the load voltage and current confirms that the 2nd harmonic blocking filter is performing correctly. The absolute function results in the generation of 2nd harmonic in the control signal \bar{i}_{abs} but is again reduced in the control signal \bar{i}_{filt} by the first-order lag circuit.

$f_o := 50\text{-Hz}$	$n_{max} := 1$	$\omega := 2 \cdot \pi \cdot f_o$	$toler := .00000001$	$it_{max} := 20$
$R_{srce} := .01 \cdot \Omega$	$L_{filter} := 100\text{-mH}$	$C_{filter} := 25 \cdot \mu\text{F}$	$R_{load} := 99.99 \Omega$	
$\tau_{f1} := .001\text{-sec}$	$\tau_{f2} := .2\text{-sec}$	$G_{pi} := 200$	$\tau_{pi} := .0001\text{-sec}$	
$I_{ref_0} := 4$	$I_{ref_{2:n_{max}}} := 0$			

Figure 5-25 Data used in HDA Analysis of VCC

The potential singularity introduced by the zero impedance dc component of the blocking filter was avoided in the example by combining the impedance of the filter in series with the source and load resistance. This allowed the use of the standard admittance matrix definition for the equivalent circuit of the network. The equivalent sparse matrix \bar{Z}_{equiv} used is poorly conditioned as a result of the high impedance at the second harmonic, but it is non-singular for the condition studied and did not result in numerical problems where its inverse was used in the calculation of system currents.

The numerical anomaly introduced by the dc component of the PI controller was solved by solving the dc and frequency dependent components of the network separately.

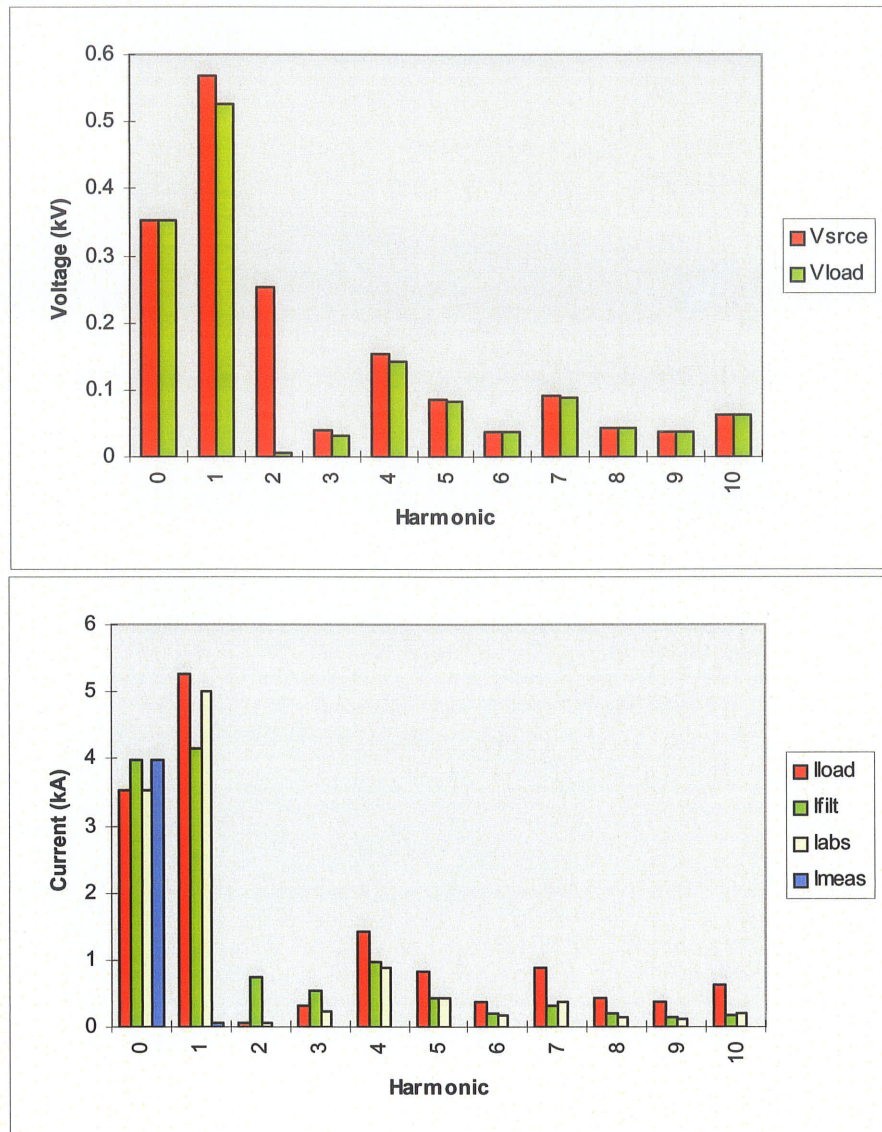


Figure 5-26 Harmonic Content of Voltages and Currents

The example shows that non-linear functions such as the 'Abs' harmonic domain function can be readily included in a network solution. As the function and for this example its input is continuous, its harmonic derivative (the sign function) is available which allows for its symbolic inclusion in the Jacobian for the Newton-Raphson solution.

Although no magnitude scaling was used in the development of the equivalent matrices for this example, there were no numerical issues evident.

Waveforms for each of the major currents and voltages were re-generated from the harmonic content and are shown in Figure 5-27 for time domain validation of results. The circuit was analyzed in the time domain using PSCAD/EMTDC™ (Version 2) to validate the harmonic domain analysis. The EMTDC™ waveforms shown in Figure 5-28 are virtually identical to the harmonic domain analysis waveforms, validating the HDA methodology used for this application. The letter labelling on the PSCAD/EMTDC™ waveforms (Figure 5-28) is to compare with the reconstructed HDA time domain waveforms of Figure 5-27.

With the proposed HDA methodology, it is relatively straight forward to include harmonics on the dc bus of the voltage chopping circuit. In Algorithm 5-9 the voltage V_{src} , when harmonics are included, simply becomes the convolution of the harmonics from the CompRamp function and the harmonic content of the voltage on the dc bus. The result when 20% 3rd harmonic is present is shown in Figure 5-29

With satisfactory validation, it is concluded that the HDA method can be applied to combined electrical/control circuits with nonlinear and switching elements. For this demonstration, time domain concepts were used to establish the instant at which the VCC would start to conduct. The author believes however that it should be possible to carry out the analysis entirely the harmonic domain, given the appropriate algorithm. This is one area where additional research would benefit the 'pure' HDA approach, as discussed further in Chapter 7.

Proposed

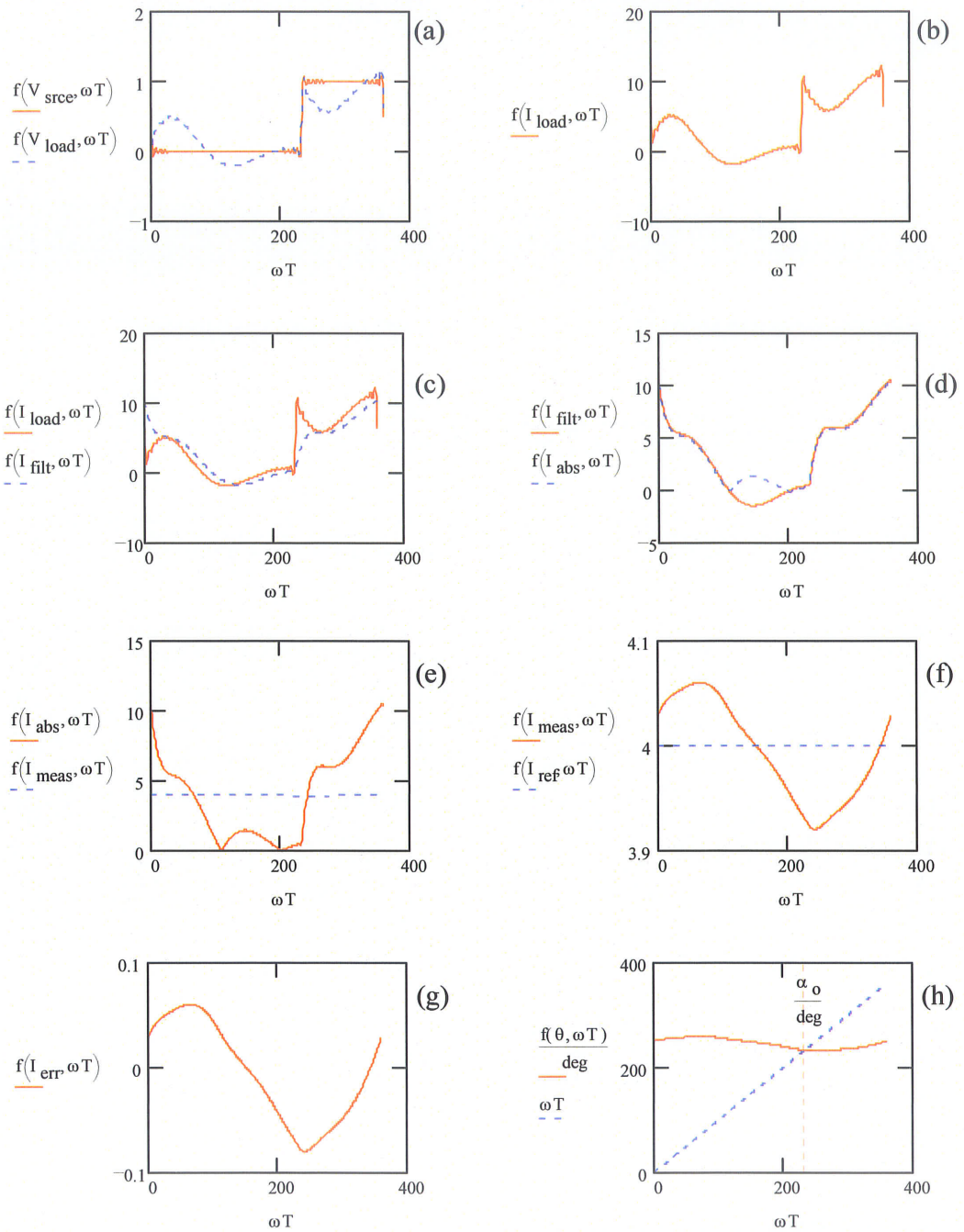


Figure 5-27 Re-generated from Harmonic Content of HDA Results

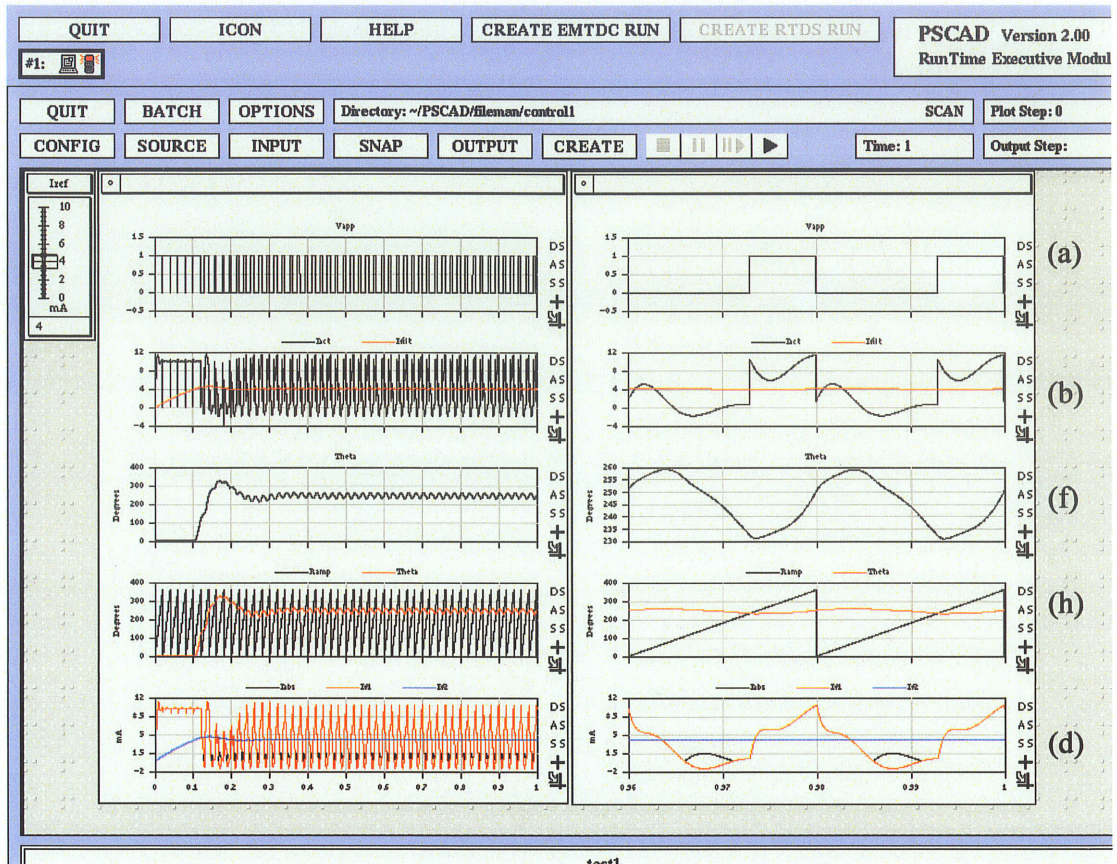


Figure 5-28 PSCAD/EMTDC™ Time Domain Simulation of the VCC

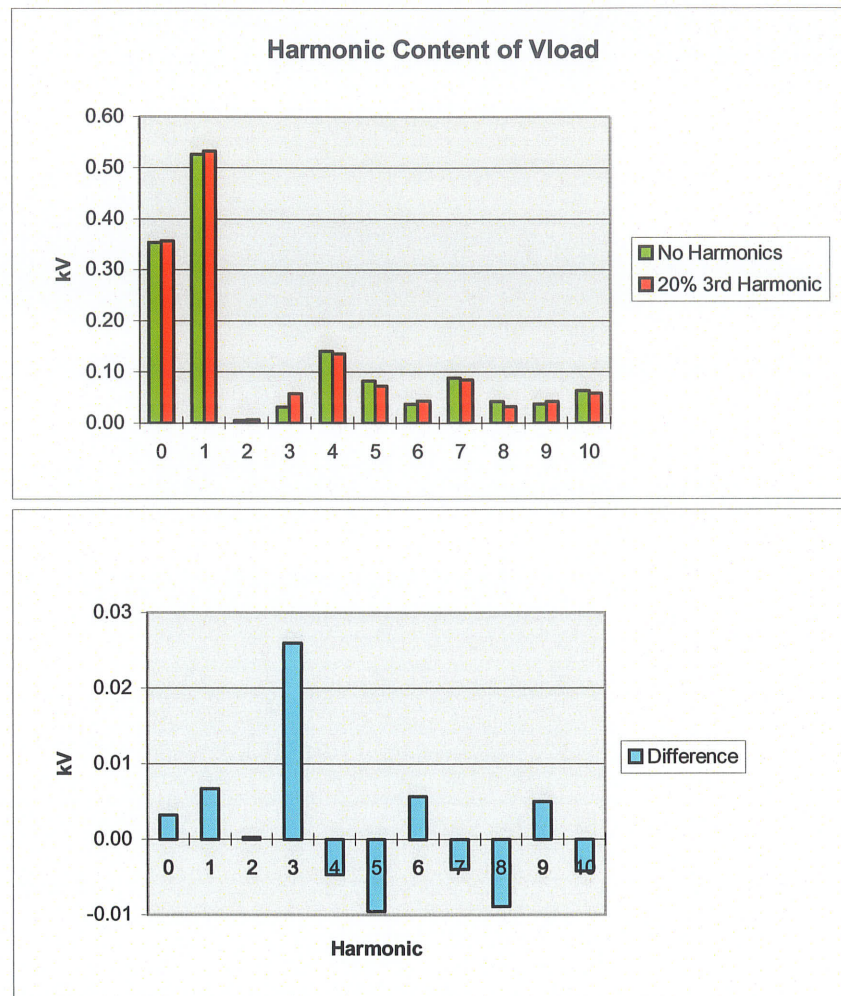


Figure 5-29 Influence of the Presence of 3rd Harmonic on the DC Bus

5.5 LIMITATIONS OF HDA

In order to see if circuits with capacitive elements could be handled, the simple circuit shown in Figure 5-30 was studied. The basic iterative algorithms described for the resistance and resistance-inductor networks when used with the resistor-capacitor circuit frequently failed to converge.

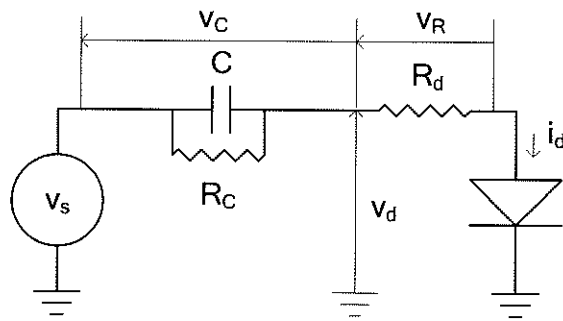


Figure 5-30 Simple Diode Resistor Capacitor Test Circuit

The failure to converge is attributed to the incorporation of the capacitor directly into the admittance matrix formulation of the network equations, i.e.: ' $\bar{I} = \bar{Y} \cdot \bar{E}$ ' and its direct inclusion in the Jacobian. In the admittance matrix formulation, the capacitor creates large admittance matrix entries at high frequencies. Any numerical corrections to the diode bus voltage will make large numerical corrections to the current through the capacitor. The large numerical corrections to the current cause large corrections to the diode voltage at the next iteration; and, the solution diverges.

In a passive network, the Jacobian consists of only the admittance matrix, and the inclusion of a capacitor introduces only numerical concerns at high frequencies. The admittance matrix equation is solvable. However, the large off-diagonal elements in the admittance matrix at high frequencies reduce the condition of the matrix, increasing the likelihood of numerical errors in the solution.

The author believes, but has not shown that there is an entirely harmonic domain solution to the divergence problem. This is discussed further in Chapter 7.

5.6 OVERVIEW

The proposed HDA is a useful approach for solving power electronic circuits consisting of diodes, thyristors and IGBT's. Generally, the implementation worked well for the cases examined. Some weaknesses were identified in the numerical solution, particularly for the R-C diode circuit described in Section 5.5. In principle, the approach is self contained and does not need recourse to the time domain. However, the author has been so far only

able to improve the accuracy of the HDA square root function to a certain limit, which proved to be insufficient for some of the problems discussed here. Hence a small but elementary time domain solution was required for the solution of the TCR circuit.

This Page is Intentionally Blank

CHAPTER 6

APPLICATION TO TRANSFORMER SATURATION

6.1 INTRODUCTION

Much work has been carried out modelling transformer saturation in the harmonic domain. All of the reviewed published effort has involved some excursion into the time domain to establish the magnetizing current waveform. Harmonic components of the flux are used to generate a time domain representation of the flux. The magnetizing current is determined at each point in time using some defined relationship between flux and magnetizing current. The harmonic components of the waveform are then determined and brought back into the harmonic domain in the form of pure harmonic current injections, Norton equivalent, or equivalent switching functions. This approach, while successful, still involves the time domain to establish harmonic domain quantities.

In the harmonic domain approach proposed by the author, this is not necessary. Transformer saturation can be modelled entirely in the harmonic domain with a one-to-one correspondence between the equations used in the time domain and the equations used in the harmonic domain.

6.2 HARMONIC DOMAIN MODEL OF TRANSFORMER SATURATION

The time domain analysis package PSCAD/EMTDC™ uses a continuous function to describe the direct relationship between transformer magnetizing current and flux as shown in Figure 6-1. The equation results in a curve which is asymptotic to two straight lines on the flux-current diagram. One line passes through the origin and is proportional to the transformer magnetizing impedance. The second line intercepts the flux axis at a

'cut-off' flux level and at a slope that is proportional to the saturated impedance of the transformer.

The parameters used to define the saturation characteristics of Figure 6-1 are:

$m_1 = .2$
$m_2 = 50$
$b_0 = 1.2$

where:

m_1 is the saturated reactance(p.u.)

m_2 is the magnetizing reactance (p.u.)

b_0 is the 'cut-off' flux

The scalar algorithms defining the relationship between transformer flux and magnetizing current²⁷ can be expressed two ways.

1) Flux expressed as a function of magnetizing current is:

$\Psi_{sat}(i_{sat}, m_1, m_2, b_0) :=$	$B \frac{1}{m_1}$
	$D \frac{b_0}{m_1}$
	$E \frac{-b_0}{m_1 \cdot m_2}$
	$\Psi_{sat} \leftarrow -i_{sat} \frac{ i_{sat} + D}{B i_{sat} + E}$

Algorithm 6-1²⁸

²⁷ The equations presented here are a slightly more mathematically rigorous model of the saturation curve used in PSCAD™ in that no simplifying approximations are made.

²⁸ B, D, and E are constants used to simplify the ultimate expression for flux 'ψ'

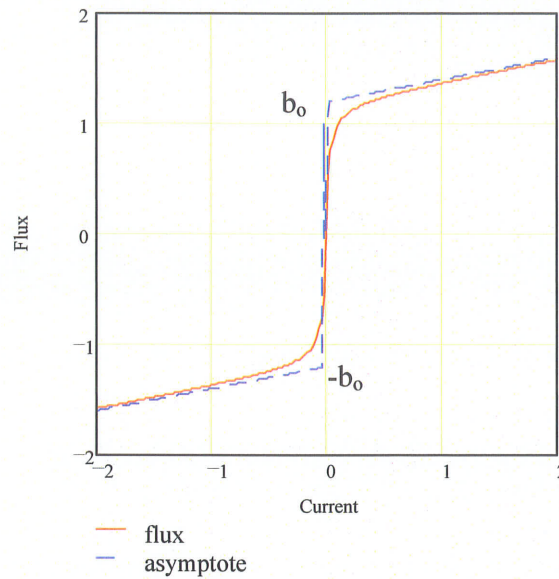


Figure 6-1 PSCAD/EMTDC™ Model of Transformer Saturation Characteristic

- 2) The magnetizing current can also be expressed as a continuous function of flux. This is the more 'useful' presentation. In most mathematical analyses, the flux is established by external sources and the saturated current is an unknown quantity.

$$i_{\text{sat}}(\psi, m_1, m_2, b_0) := \begin{cases} B \leftarrow \frac{1}{m_1} \\ D \leftarrow \frac{b_0}{m_1} \\ E \leftarrow \frac{-b_0}{m_1 \cdot m_2} \\ i_{\text{sat}} \leftarrow \frac{-(D + |\psi| \cdot B) + \sqrt{(D + |\psi| \cdot B)^2 - 4 \cdot |\psi| \cdot E \cdot \text{sign}(\psi)}}{2} \end{cases}$$

Algorithm 6-2

The real power of the proposed harmonic domain analysis technique is demonstrated with modelling of the same transformer saturation characteristic but in the harmonic domain. All of the functions and operators used in the scalar algorithm have direct equivalents in the proposed HDA methodology. These include the absolute value, square root and sign functions. Each of the mathematical operations was described in Chapter 2.

As a result, the calculation of the magnetizing current harmonic spectrum given the fundamental frequency and harmonic components of the applied flux can be carried out entirely in the harmonic domain. The algorithm for the harmonic domain analysis is essentially the same as the scalar algorithm, except that it uses the corresponding harmonic domain functions and operators. The flux ' ψ ' is now an array housing the fundamental frequency and harmonic components of the flux. The current ' i_{sat} ' is also an array housing the fundamental frequency and harmonic components of the magnetizing current.

The harmonic domain algorithm is:

$$i_{sat}(\psi, m_1, m_2, b_0) := \begin{array}{l} B \frac{1}{m_1} \\ D \frac{b_0}{m_1} \\ E \frac{-b_0}{m_1 \cdot m_2} \\ j \leftarrow \text{rows}(\psi) - 1 \\ \text{One}_0 \leftarrow 1.0 \\ \text{One}_j \leftarrow 0 \\ \text{Ab}\psi \leftarrow \text{abs}(\psi) \\ F \leftarrow D \cdot \text{One} + B \cdot \text{Ab}\psi \\ \text{root} \leftarrow T(F) \cdot F - 4 \cdot E \cdot \text{Ab}\psi \\ i_{sat} \leftarrow T\left(\frac{-F + \text{sqrt}(\text{root})}{2}\right) \cdot \text{sign}(\psi) \end{array}$$

Algorithm 6-3

The use of the harmonic domain analysis method for calculating harmonics due to transformer saturation is demonstrated in the following examples.

Consider first the case of a non-linear inductor connected across a sinusoidal voltage source of magnitude 1.2 p.u. The saturation characteristic is shown in Figure 6-1. This applied voltage results in a purely sinusoidal flux of peak magnitude 1.2 p.u. (equal to the cut off flux). A Mathcad[®] calculation sheet was used to calculate the harmonic content for

this condition. In the example, flux is represented by the array 'E_{test}' magnetizing current is represented by the array 'I_{sat}'.

Test Case 1 Fundamental Frequency Only

$$m_1 = 0.2 \quad m_2 = 50 \quad b_o = 1.2$$

$$E_{test_1} = 0.849 \quad E_{test_2} = -0.849$$

$$I_s := i_{sat}(E_{test}, m_1, m_2, b_o)$$

The harmonic content of the applied flux and resultant magnetizing current is shown in Table 6-1

Table 6-1 Transformer Magnetizing Harmonics for Sinusoidal Flux, Determined using Direct HDA

Flux (p.u.)			Magnetizing Current (p.u.)		
n	series	I _d	n	series	I _d
1	a	0.849	1	a	0.149
1	b	-0.849	1	b	-0.149
			3	a	-0.076
			3	b	-0.076
			5	a	-0.030
			5	b	0.030
			7	a	0.011
			7	b	0.011
			9	a	0.003
			9	b	-0.003

The current and flux waveforms were generated from the harmonic content to visually validate the harmonic calculations. The current waveform was also calculated in the time domain from the flux waveform using the algebraic flux current relationship. The waveforms are shown in Figure 6-2. The current calculated using harmonic domain analysis is virtually identical to the time domain analysis results.

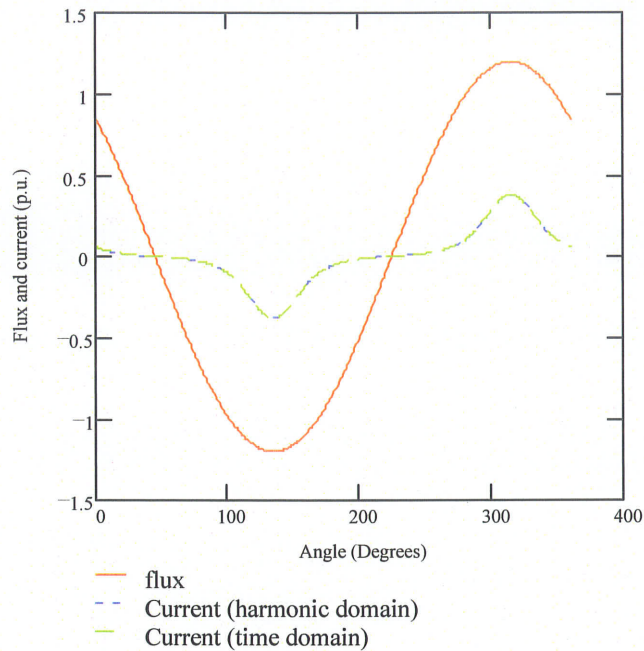


Figure 6-2 Transformer Magnetizing Current Waveforms for Sinusoidal Flux

In test case 2, the effect of single-sided saturation effects can be easily demonstrated by simply adding a dc component to the flux, to represent the remnance in a magnetic circuit. I.e.:

Test Case 2 Fundamental Frequency Plus dc Component
 $m_1 = 0.2 \quad m_2 = 50 \quad b_o = 1.2$
 $E_{test_0} := 0.5 \quad E_{test_1} = 0.849 \quad E_{test_2} = -0.849$
 $I_s := i_{sat}(E_{test}, m_1, m_2, b_o)$

The harmonic content of the two waveforms is shown in Table 6-2.

Table 6-2 Transformer Magnetizing Harmonics for Sinusoidal Flux with DC Offset, Determined using Direct HDA

Flux (p.u.)			Magnetizing Current (p.u.)		
n	series	I_d	n	series	I_d
0	a	0.500	0	a	0.547
1	a	0.849	1	a	0.704
1	b	-0.849	1	b	-0.704
			2	b	-0.673
			3	a	-0.251
			3	b	-0.251
			4	a	-0.101
			5	a	0.018
			5	b	-0.018
			6	b	-0.056
			7	a	-0.022
			7	b	-0.022
			9	a	0.011
			9	b	-0.011
			10	b	-0.012

The visual validation of the harmonic content for this condition is shown in Figure 6-3. Again, the complete agreement with time domain should be noted.

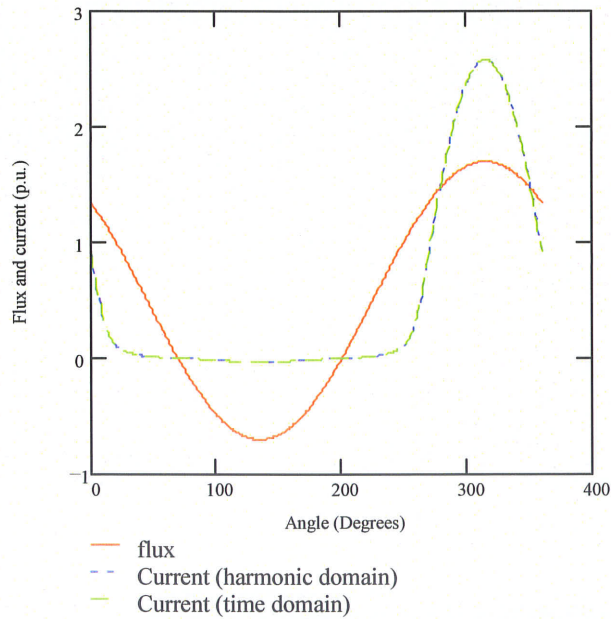


Figure 6-3 Transformer Magnetizing Current Waveforms for Sinusoidal Flux with DC Offset

In test case 3, the effect of flux distortion on magnetizing current is demonstrated. The applied flux contains a dc component along with significant 2nd and 3rd harmonic

components. The harmonic content of the flux and magnetizing current is shown in Table 6-3.

Table 6-3 Transformer Magnetizing Harmonics for Flux with DC Offset and Harmonics, Determined using Direct HDA

Flux (p.u.)			Magnetizing Current (p.u.)		
n	series	I_d	n	series	I_d
0	a	-0.200	0	a	0.092
1	a	1.182	1	a	0.693
1	b	-0.208	1	b	-0.069
2	a	0.283	2	a	0.177
2	b	-0.283	2	b	-0.191
3	a	0.295	3	a	0.477
3	b	-0.052	3	b	-0.146
			4	a	0.088
			4	b	-0.245
			5	a	0.232
			5	b	-0.150
			6	a	0.015
			6	b	-0.185
			7	a	0.072
			7	b	-0.089

The waveforms are shown in Figure 6-4.

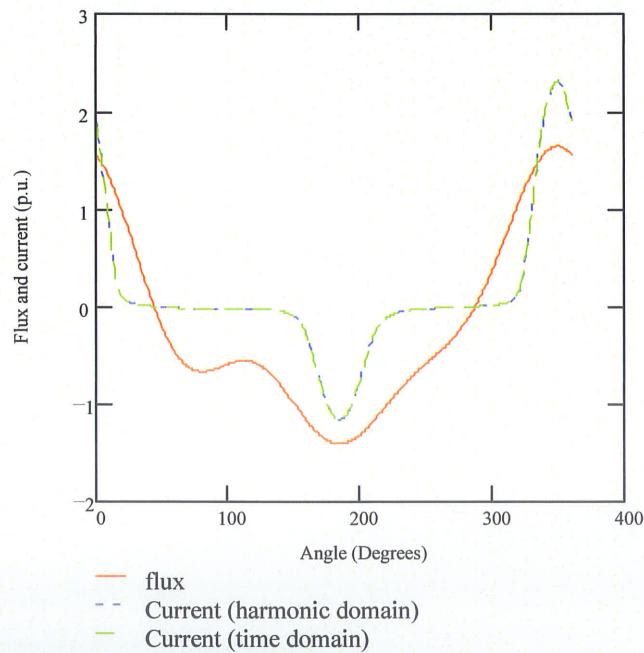


Figure 6-4 Transformer Magnetizing Current Waveforms for Flux with DC Offset and Harmonics

For each of the above three cases, the HDA results can be supported by time domain simulations, validating the proposed HDA saturation algorithm. This result is extremely satisfying, given the ultimate objective of developing a harmonic domain analysis tool that would be one-to-one compatible with time domain modelling applications such as PSCAD/EMTDC™.

After preliminary validation using the simple test cases, the developed model is used in the following example to solve an actual industrial filter problem.

6.3 HARMONIC DOMAIN ANALYSIS OF INDUSTRIAL FILTER COMMISSIONING PROBLEMS

This section provides a practical example of the application of HDA to ac filter analysis. During the course of validating the HDA transformer saturation model, the author was also involved in the replacement of an ac filter bank at an industrial plant where the major load consists of four six-pulse star-connected rectifiers with interphase transformers. Each six-pulse group produces 5th, 7th, 11th, 13th, etc. harmonics. Two of the rectifier transformers are equipped with ungrounded star-star transformers and the other two have ungrounded star-delta connections. The rectifier transformers are supplied from the main 63 kV switchyard over two 63 kV feeders. A star connected and a delta connected transformer are normally paired on each of the feeders to provide effective 12-pulse operation of each feeder (i.e. with approximate cancellation of the 5th and 7th harmonics). Each rectifier however is operated independently so 6-pulse operation can occur, particularly during start-up and shut down of the process.

The single filter bank that was originally in service consisted of two single-tuned filters (5th harmonic and 7th harmonic) and two high-pass filters (12th and 24th harmonic). The filter has been redesigned into two smaller but identical filter banks. Each filter consists of two single-tuned filters and one 12th harmonic high pass filter arm. Each filter is rated for the condition with one complete filter out of service to provide operating flexibility in terms of system voltage and reactive power control. Each bank is designed for full load operation of the plant in either one by six-pulse, or up to two times twelve-pulse modes.

The plant was originally supplied by an extensive 63 kV network. In parallel with the replacement of the ac filters, the supply to the system was upgraded. A simplified single-line diagram of the final network is shown in Figure 6-5.

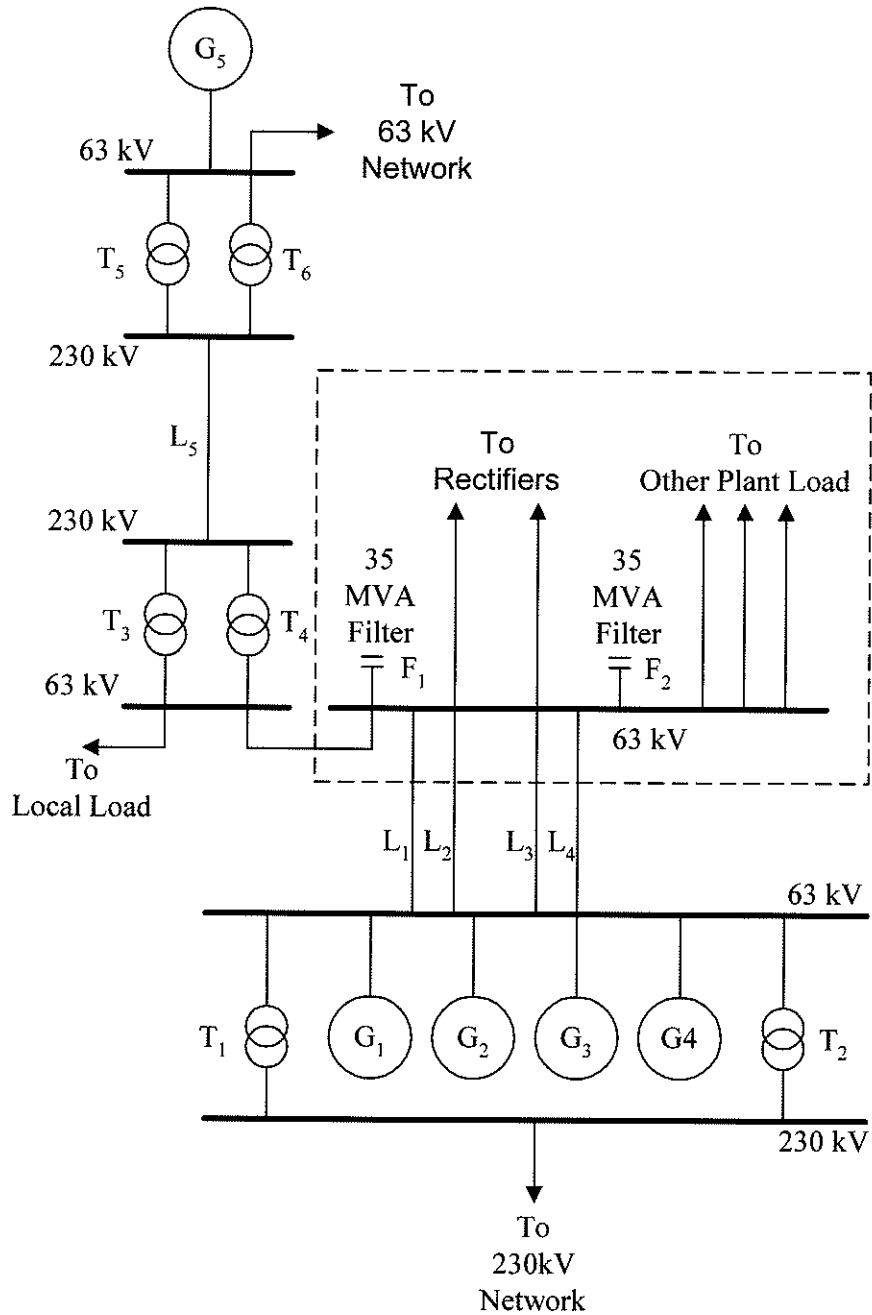


Figure 6-5 Single Line Diagram of Supply to Industrial Plant

During commissioning of the new filters, problems were encountered from the moment the filters were first energized. Modifications were required to the filter protection to energize the filter banks even without the rectifiers in service. Once the filters were in service, almost all switching events close to the station would result in loss of both filters. Tripping of the second filter would occur within cycles of the loss of the first bank. As changes to the ac system were being made at the same time as the replacement of the filters, there were many switching operations including switching of transformers (63/230 kV, rectifiers, station service and local load) and transmission lines (63 kV and 230 kV). The filters even tripped as load was ramped-up on the rectifiers.

An urgent solution was required. The cost of lost production at the plant as a result of filter outages was a major concern.

To gather as much information as possible on the cause of the filter trips, all of the relays at the 63 kV filter and switching station were reconfigured to record a time slice of about 500 ms of the waveforms as used by the protection, for any activity by the relay, not just the trip signal to the breaker. Depending on the event, the recorded waveform available could be total current into the filter or current into any one of the three individual branches.

While a complete set of waveforms was not available for any given event, it was apparent that there were very high levels of 4th and 6th harmonics flowing into the filters and that the magnitude of the harmonics in the waveforms were approaching continuous design values for the filter components. This was not a good situation as both filters were in service, but the filters were originally designed for single filter operation.

Design conditions for the filters took into account resonances between the filters and the ac system at these harmonics, but only considering the rectifier to be the major source of these harmonics, typically in the range of a few amperes. Harmonic currents in the filter branches were as high as 50 to 60 amperes at the 4th or the 6th harmonics. Some conditions indicated lower levels with both harmonics present. The amount of harmonic

content was dependent on the filter branch monitored and the nature of the initiating disturbance.

Energizing one of the 63/230 kV transformers ('T₃' or 'T₄') close to the plant almost always resulted in a trip of the filters. One event was captured when the plant was being supplied by only the four 63 kV circuits to the nearby generating station (generators 'G₁' to 'G₄') of Figure 6-5. One of the transformers was in the process of being energized from the 63 kV bus as the first stage of connecting to additional generation via the new single 230 kV circuit identified as 'L₅' in the figure. The rectifiers were not operating at the time. The 7th harmonic filter arm protection resulted in many of the resulting trips, including the energization case. In almost all conditions, there was evidence of extremely high levels of 6th harmonic current in the 7th harmonic filter branch.

The author's HDA toolbox was used to assist in determining the nature of the problem, which in turn led to a method for solving it. The high levels of 4th and 6th harmonics in the filters could result from

- 1) Magnitudes of harmonic current sources in the system being much larger than design values.
- 2) Amplification of current in the AC filters due to resonance with the rest of the system being greater than design conditions.

The network was simplified to the equivalent circuit shown in Figure 6-6, and an equivalent HDA model of the circuit was developed. Appendix B gives the Mathcad[®] implementation of the set-up and initialisation of the HDA model. Filters are represented explicitly, the ac system is modeled as an equivalent, and, the transformer is modeled as an impedance in series with non-linear saturation characteristics. The HDA model permitted the direct analysis of harmonic current in the voltages (to ground) at any location as well as the harmonic current in any of the branches.

Selection of models and parameters was, in general, made to minimise the damping exhibited by the modelled network and hence amplify any resonances that may occur. The selection of conservative parameters is based on two objectives, namely:

- to provide an indication of the minimum level of harmonic current sources required to excite the levels of current observed in the field
- to provide a severe test for the proposed HDA method

The filters were represented by fixed inductors, resistors and capacitors. The parameters for the capacitors and the inductors and the resistor of the high-pass filter were based on design specifications for each of the components. The resistors modelled in each of the 5th and 7th harmonic single-tuned filters were selected to provide a filter 'Q' of 100 at the tuned frequency. The net impedance-frequency characteristics of both banks are shown in Figure 6-7(a). The impedance of each individual filter branch was validated against field measurements. The validation showed that the total calculated impedance of each filter is likely within several percent of actual impedance at all but a narrow range of frequencies between the 5th and 6th harmonics. The net impedance of the filter at the 6th harmonic is heavily influenced by the sharply tuned parallel resonance that occurs between the 5th and 7th harmonic filters. Slight variations in the filter component parameters will affect the exact frequency at which the resonance occurs. Variations in damping from the 'Q' values assumed will also have an impact. Both effects introduce uncertainties into the total filter impedance at the 6th harmonic.

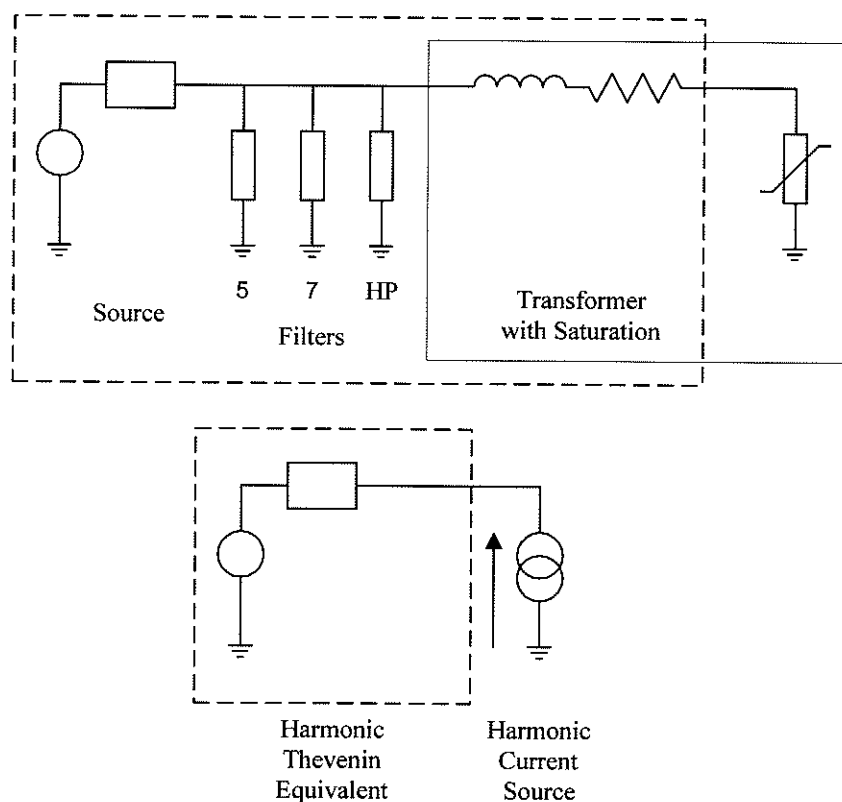


Figure 6-6 Energization Circuit and Equivalent Circuit

The ac system is modelled as a resistor and inductor in series and represents the variable with the largest possible range of values in the analysis. The impedance of the ac system at any given frequency will vary significantly with time as a result of changes to system operating conditions and changes in network configuration. Short circuit studies of the network carried out by others estimated the range of short circuit levels to be within 1600 to 2000 MVA. The inductance of the system was arbitrarily selected for this analysis to create a resonance between the ac filters and the ac system at exactly the 6th harmonic. The inductance corresponds roughly to a short circuit level of about 2200 MVA at 60 Hz. This is slightly outside the estimated range but the author was more interested in the harmonic analysis than the behaviour at fundamental frequency. The ac system resistance was selected to provide an X to R damping ratio of 15 at 60 Hz. This is consistent with the damping ratio of 15 used in the design of the ac filters.

The impedance of the ac system is compared to the impedance of the ac filter in Figure 6-7(b). Intersections of the system impedance characteristic (primarily inductive) with the negatively sloped (primarily capacitive) characteristics of the filter indicate potential resonance conditions (about $n = 4.2, 6,$ and 7.8).

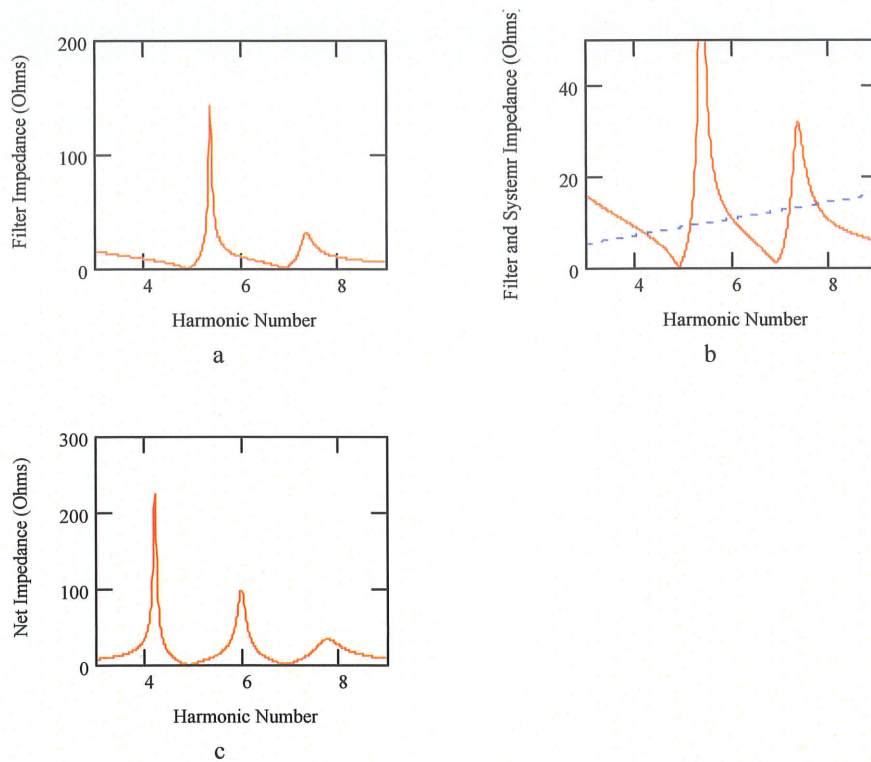


Figure 6-7 Variation of AC Filter, System and Net Harmonic Impedance

An initial analysis of the network reveals the following potential interaction.

The net filter and ac system impedance is shown in Figure 6-7. This figure shows that the filter and system are in resonance at the 6th harmonic. It also shows that there is a severe resonance very close to the 4th harmonic and a resonance of lesser severity close to the 8th harmonic.

The leakage path of the transformer is also modelled as a series resistor inductor circuit. The transformer saturation characteristic and impedances used are based on 60 Hz test

results for an identical unit. The non-linear magnetizing circuit is represented by the Harmonic Domain Saturation characteristic described in Section 6.2.

In the HDA model, the harmonic impedance for the ac system is calculated only once and stored in the sparse impedance matrix \bar{Z}_{sys} . Although a constant resistance - constant inductance system model is used in this analysis to facilitate the set-up of the impedance matrix, the matrix could have been based on full system network reduction analysis with no increase in complexity. It could have also been set-up arbitrarily to create simultaneous resonances at more than one harmonic.

In a similar manner the harmonic impedance of each filter branch and the total harmonic impedance of both filters is calculated only once based on the filter parameters, configuration and harmonic number and stored in sparse matrices for each of the components. The total admittance of both filters is stored in a matrix \bar{Y}_f . The harmonic impedance of the transformer leakage reactance and resistance is stored in the matrix \bar{Z}_x .

While both the ac system and transformer were modelled as constant resistance devices, factors such as skin effect and transformer eddy currents will tend to increase the resistance with frequency. The more conservative approach adopted (i.e. less damping at harmonic frequencies) is consistent with the two stated objectives of this demonstration.

A harmonic Thévenin equivalent of the ac network was developed that included the ac system, the ac filters and the series impedance of the energized transformer. The harmonic equivalent is determined using the same numerical algorithm that would be used for the formation of a single frequency equivalent except matrix operations are involved rather than scalar operations. The Mathcad[®] implementation of the Thévenin equivalent impedance calculation is:

$$\boxed{Z_{\text{th}} := (Y_f + Y_{\text{sys}})^{-1} + Z_x} \quad \{ 6-1 \}$$

where:

$$\boxed{Y_{\text{sys}} := Z_{\text{sys}}^{-1}} \quad \{ 6-2 \}$$

and the Thévenin equivalent voltage is given by:

$$V_{th} = V_{fact} \cdot V_{src} \cdot V_o \cdot \sqrt{\frac{2}{3}} \quad \{ 6-3 \}$$

where:

$$V_{fact} := (Y_f + Y_{sys})^{-1} \cdot Y_{sys} \quad \{ 6-4 \}$$

$$V_o = 63 \quad \{ 6-5 \}$$

and:

$$V_{src} := \begin{matrix} V_0 = 0 \\ V_1 = 1.0 \\ V_{2:n_{max}} = 0 \\ V \end{matrix} \quad \{ 6-6 \}$$

For this example, the source voltage \vec{v}_{src} was assumed to consist of only a fundamental frequency component ($V_1 = 1$). Peak voltage quantities were used in the analysis for compatibility with the saturation characteristics. These were adjusted to RMS quantities for output of individual harmonic content.

The only source for harmonic excitation of the system-filter configuration shown in Figure 6-6 is the harmonic content of the magnetizing current of the open-circuit but energized transformer.

In linear single frequency HDA models, flux at 60 Hz with a dc offset would be applied to the transformer saturation characteristic in the time domain. The waveform of the magnetizing current would be analysed and the harmonic content determined. The fixed impedance network would be analysed with harmonic current injections to determine the harmonic flow in the filters. This process, however, does not take into account the impact that the magnetizing current will have on the flux.

Later HDA models as described by Semlyen [18] and Dommel [17] calculate the harmonics of the excitation voltage based on the fundamental frequency and harmonic

response of the initial current calculations. The time domain waveform of the flux is re-generated by summing the Fourier coefficients at each time step. The waveform is applied to the saturation characteristics to obtain a new magnetizing current waveform and the new currents, based on a Fourier analysis of the waveform, are injected into the network. The process is repeated until there is no refinement to the magnitudes of the currents.

Although the HDA saturation model developed by the author lends itself to other iterative network solution techniques such as Newton-Raphson, the author has for this example used a Gauss-Seidel iterative process similar to the repetitive methodology described above. The most significant difference is that in the author's methodology, the harmonic currents in the magnetizing current are determined directly from the harmonic content of the flux. No flux and current waveforms are required.

The Mathcad® implementation of the algorithm used is shown in Figure 6-8. It is simply a Gauss-Seidel iterative solution with an acceleration factor of 0.2. New values of voltage ' \bar{V}_{sat} ' across the saturated element are computed at the start of each iteration based on the differences between the harmonic voltages at the previous iteration and the new voltages ' $\bar{V}_{sat,new}$ ' calculated based on the previous set of harmonic current injections. The change to the voltage is limited by the acceleration factor 'accel'. Flux is set equal to the integral of the voltage ' \bar{V}_{sat} ' by the operator 'OneByD'. This matrix is simply the inverse of the harmonic component of the derivative operator matrix with the dc component arbitrarily set to zero. The calculation of Z_{th} is not visible in Figure 6-8, but it is readily calculable per equations 6-1, 6-2, and is shown in Appendix B.

Here, a Gauss-Seidel iterative approach (popular in load flow programs) is used as the engine instead of the Newton-Raphson solution that was used in earlier chapters. The solution converges within about 20 iterations to an acceptable level of correction. For this application, a maximum change of 1% of the 6th current harmonic injection was used as a guide. The iterations were increased to over 50 to insure numerical stability of the solution.

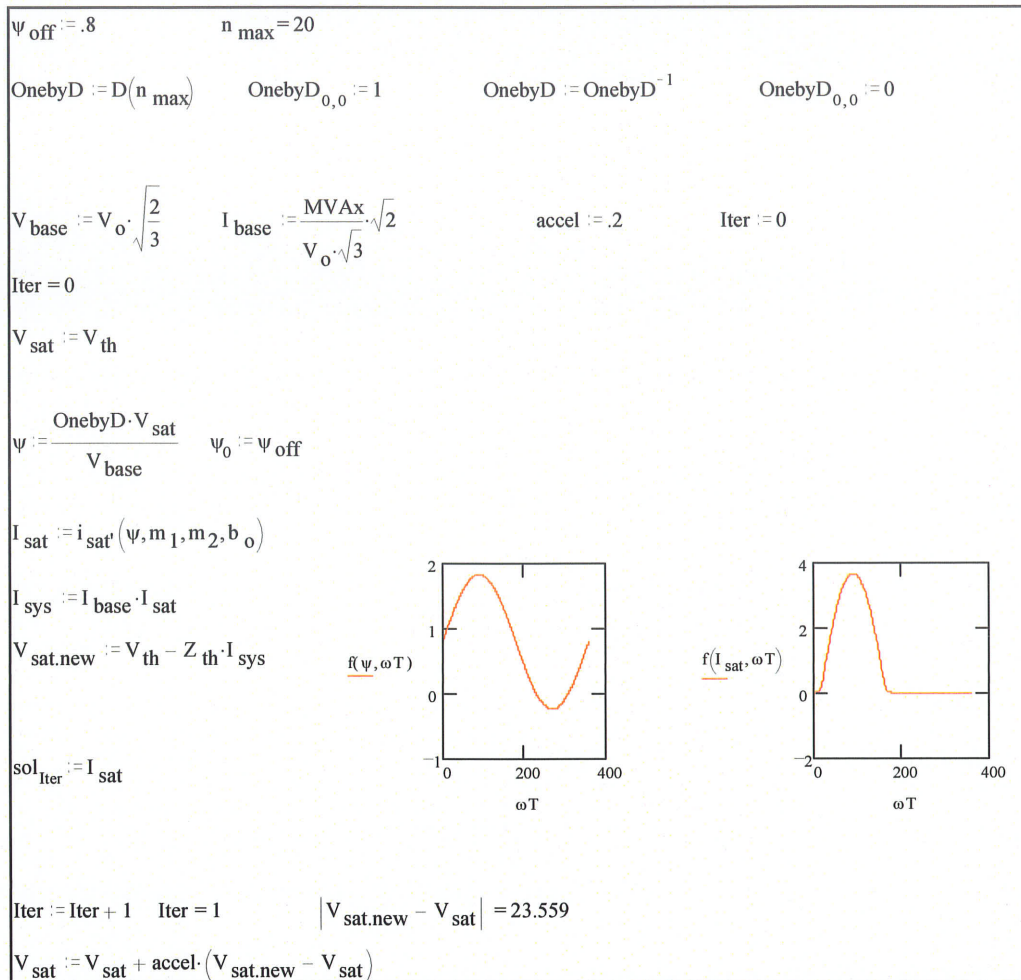


Figure 6-8 Segment of Mathcad® Implementation of HDA Gauss-Seidel Solution

The calculated magnitude of the harmonic content of the magnetizing current is plotted for each harmonic in Figure 6-9 as a function of iteration count. The author was particularly interested in the convergence characteristics at the 6th harmonic, given the known resonance condition and the lack of damping in the system. The figure indicates that each harmonic converges at approximately the same rate, including the 6th harmonic. The magnitude of the harmonics produced by the transformer at convergence is in excess of 1 A peak for all but the 17th and 19th harmonics.

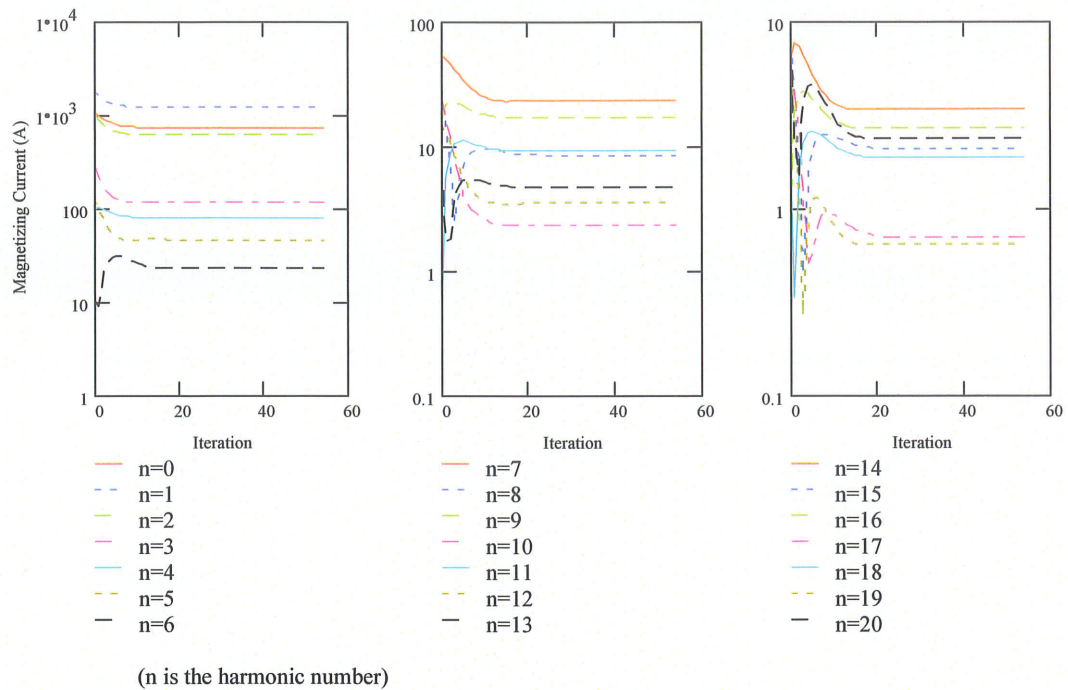


Figure 6-9 Convergence of HDA Solution of Transformer Filter Interaction Investigation

Bar charts depicting the harmonic components of the solution for flux and magnetizing current are shown in Figure 6-10 and Figure 6-11 respectively. The current and flux is dominated by dc, 60 Hz and low order harmonic component. The harmonic content reduces rapidly with harmonic number. The harmonic content of the magnetizing current has reduced by several orders of magnitude by the 20th harmonic. The harmonic content of the flux is reduced by three to four orders of magnitude.

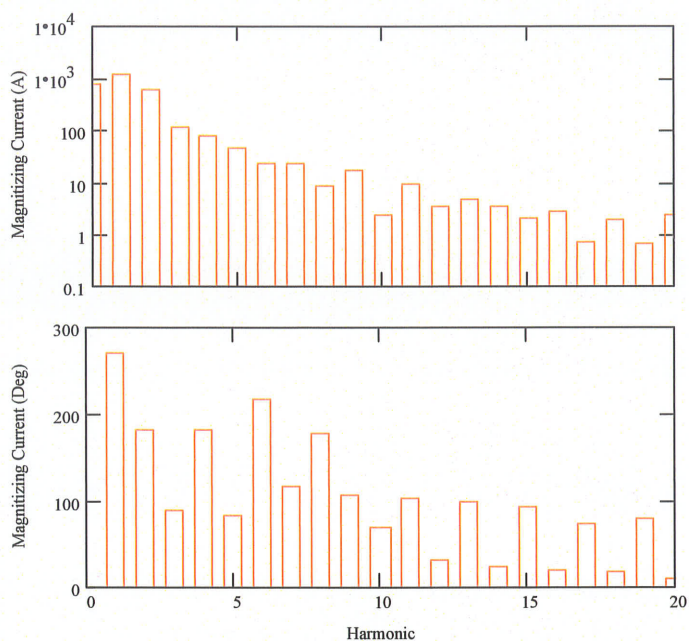


Figure 6-10 Harmonic Component of the Transformer Magnetizing Current

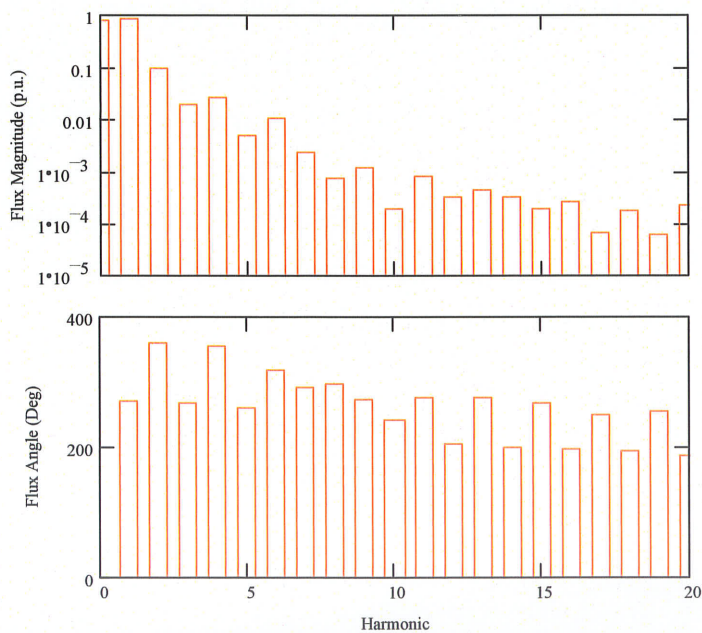


Figure 6-11 Harmonic Component of the Transformer Flux

The harmonic content of the voltage at the 63 kV filter bus is shown in Figure 6-12. The harmonic content at frequencies greater than the 10th harmonic are all less than 1% of the

nominal bus voltage. Harmonic voltage at the 2nd, 3rd, 4th, and 6th harmonics are very high.

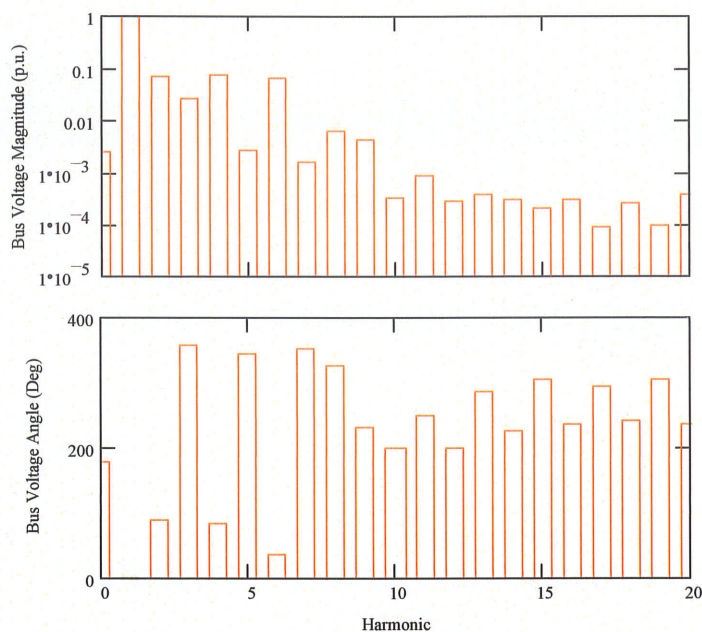


Figure 6-12 Harmonic Component of the AC Filter 63 kV Bus Voltage

Figure 6-13 shows the ultimate distribution of the magnetizing current between the ac system and the ac filters. Most of the low order harmonic current (2nd and 3rd) flow into the ac system.

Although the ac system 60 Hz voltage source is the driving force behind the magnetizing current, the fundamental current from the system is less than the magnetizing current. At 60 Hz the transformer magnetizing circuit behaves like a large shunt reactor whose effects are reduced by the ac filters that are effectively in parallel. This is a well known phenomena but this does demonstrate that the HDA model proposed can reproduce this type of interaction.

The resonances expected at the 4th and 6th harmonics are evident in Figure 6-13. The harmonic current in both the ac system and ac filter at the 4th and 6th harmonics are

considerably greater than the harmonics produced by the sole harmonic source in the system, (i.e. transformer magnetizing current).

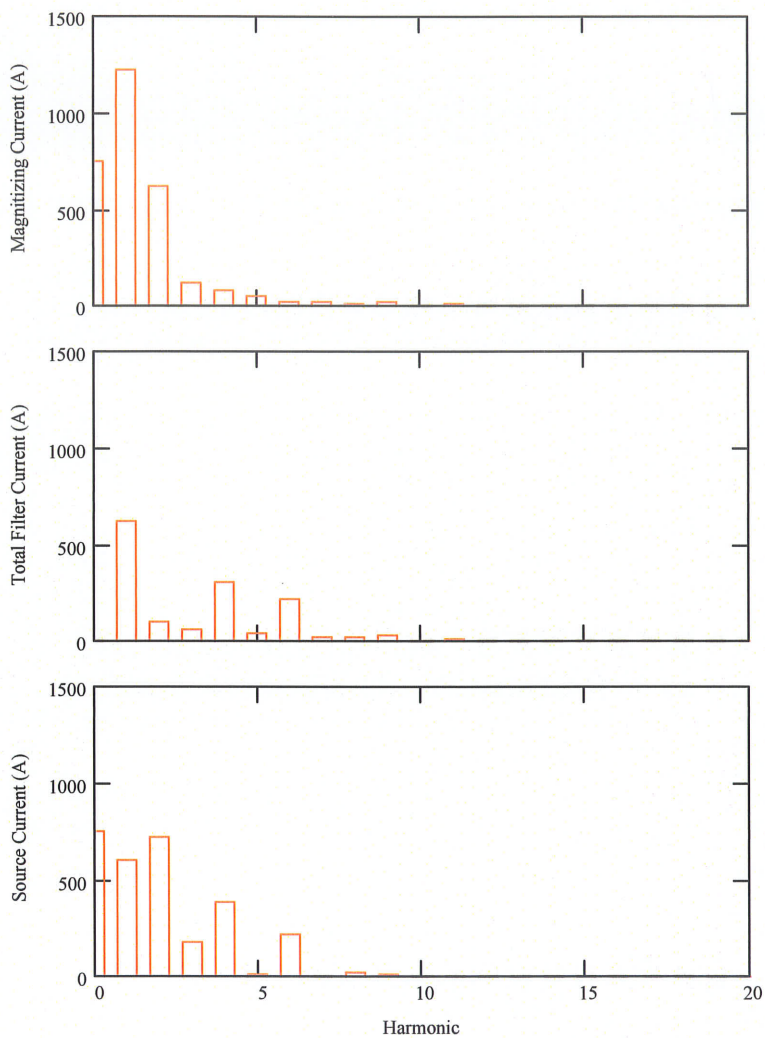


Figure 6-13 Distribution of Transformer Magnetizing Current

Figure 6-14 shows the harmonic current flow in each of the filter branches. The harmonic content of the currents in all three branches are dominated by the 4th and 6th harmonics. The harmonic content in the high-pass filter is much less than the 60 Hz component and is therefore not of immediate concern.

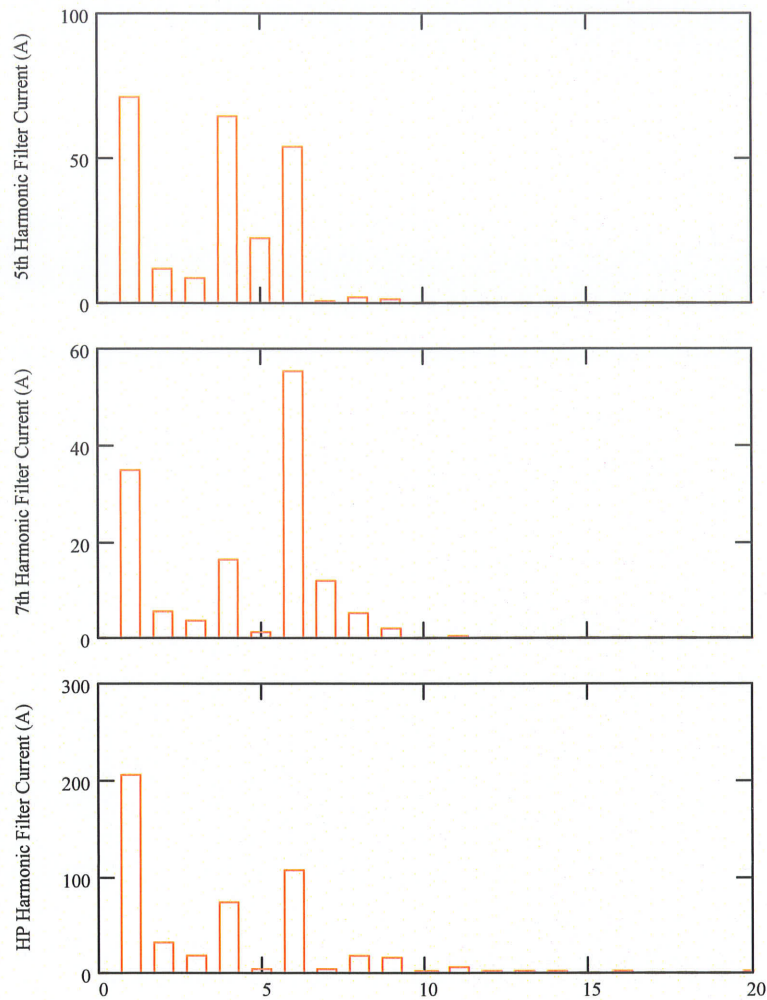


Figure 6-14 AC Filter Branch Harmonic Current

The 4th and 6th harmonic currents into the 5th and 7th filters however exceed the fundamental frequency component, and in fact, the magnitudes are comparable to the design values of the filters for the 5th and 7th harmonics respectively. The high levels of 4th and 6th harmonic current in the filter determined using the HDA analysis is consistent with the field observations.

A comparison of the HDA calculated magnetizing current to the currents in the 5th and 7th filters is as follows:

	Current (A RMS)	
	4 th harmonic	6 th harmonic
Magnetizing Circuit	80	24
5 th Harmonic Filter	65	54
7 th Harmonic Filter	16	55

These currents are in agreement with the 50-60 A filter currents at the 4th and 6th harmonics observed in the field!

Based on the table it can be seen that even with a very sharply tuned resonance at the 6th harmonic, the amplification from source (magnetizing circuit) to the 7th harmonic filter is only about a factor of about two. The amplification factors are less at the 4th harmonic. The amplification at the 4th harmonic would have been larger if the filter and system were also tuned to a 4th harmonic resonance.

The fact that the amplification at the 6th harmonic, as established by HDA, was only a factor of two was a key factor leading to the ultimate solution to the problem. (i.e.: simply an adjustment to the protection.) A change was made initially to the time dial setting on the basis that transformer saturation inrush currents are temporary (possibly lasting up to 20 seconds). The manufacturer adjusted the protection to be closer to the short time capability of the equipment.

Had the amplification factor as determined by HDA been larger, the consequences could have been much more serious. It may have been necessary to redesign the filter. Lower values of 4th and 6th harmonic currents in the system (possibly from other sources) could have also caused the filters to trip.

The conclusions that can be drawn from the above demonstration are that:

- The HDA methodology proposed by the author has been tested and used in the analysis and was instrumental in establishing a solution of an actual system problem. The methodology was able to reproduce levels of harmonic currents similar to those obtained by system measurement.

- The HDA methodology has worked well in an environment that appeared to pose difficulty from a numerical viewpoint.

The author's proposed HDA in general provides a very powerful tool for the design and analysis of systems where ac filtering is an integral component. HDA provides answers directly in a form that can be used in design or compared to design parameters of equipment.

The HDA methodology proposed by the author provides additional flexibility in that the HDA model is extremely simple, can be setup quickly and provides the type of immediate answers that are required in the practical solution of field problems.

6.4 USE OF HDA FOR TIME DOMAIN ANALYSIS

In this section it is shown how the proposed HDA methodology can be quickly used to solve a problem that traditionally would have been dealt with only in the time domain.

In this example, HDA is used to confirm the likely cause of bursts of severe current distortion from the same rectifier system described in Section 6.3 of this chapter. During one of the filter tripping incidents, protection on one of the 63 kV feeders to the plant also picked-up but reset and did not trip the rectifier feeder. The plant advised that no switching operations occurred at the time, ruling out rectifier transformer energization as a cause of the filter trip.

Because the feeder protection picked-up, waveforms of the feeder three phase currents were automatically recorded by the relay at the time of the incident. These were downloaded for analysis. It was apparent that the waveform included a rectifier load component both prior to and during the burst of distortion. This component was removed from the waveforms by simply subtracting the waveforms prior to the burst from the waveforms during the burst. The resultant waveforms are shown in Figure 6-15.

As two of the resultant waveforms exhibit a sustained zero component over a portion of each cycle, it was deduced that subtracting the rectifier load component from the waveform was reasonable, and that the disturbance originated from the second rectifier where the transformer had been energized but the valves were not initially conducting.

Several possible explanations of the phenomena were proposed, all related to some form of disturbance on the dc side of the rectifier transformer. The waveforms are similar to those that might be expected as a result of transformer saturation.

To demonstrate that rectifier transformer saturation could be the source of the problems, the author's HDA saturation routine was used to calculate the harmonics in the magnetizing current of a three phase ungrounded star-delta transformer energized at 63 kV, but with varying levels of dc flux offset in each winding. The results are shown in Figure 6-16.

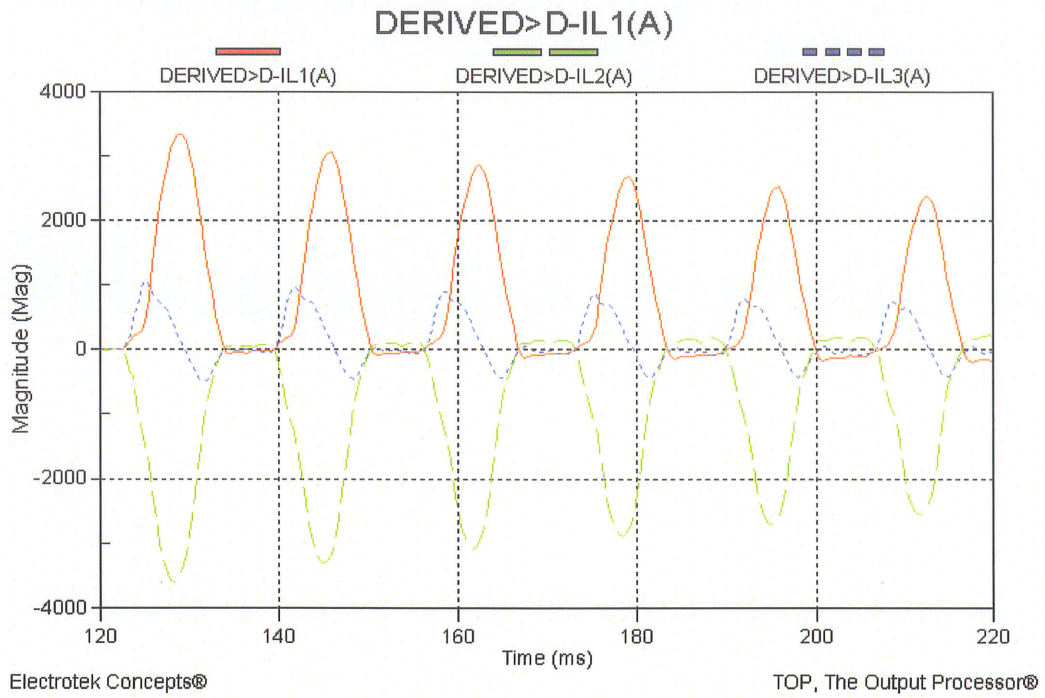


Figure 6-15 Measured Burst of Distorted Current in Rectifier 63 kV Feeder

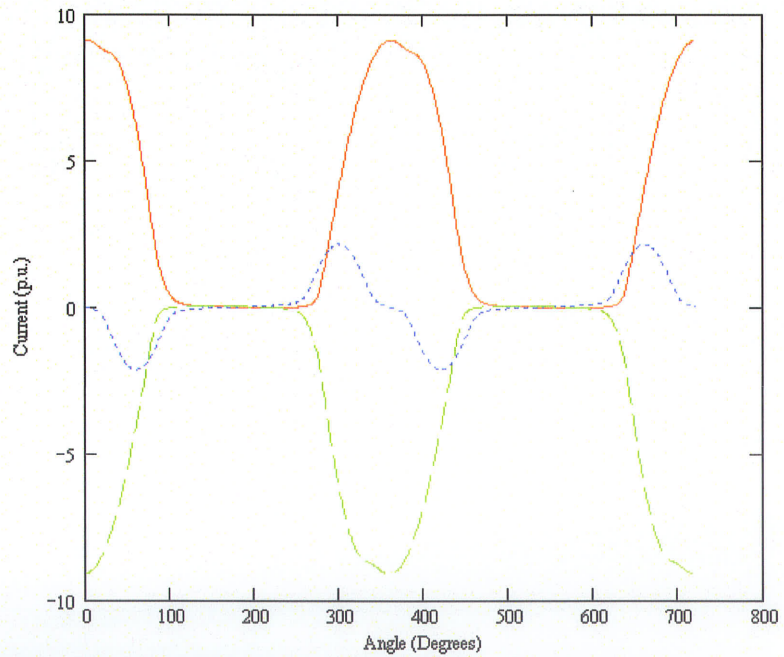


Figure 6-16 HDA Analysis of Three Phase Transformer Saturation

The waveforms shown in Figure 6-16 were generated from the harmonic content in the three current vectors \bar{i}_a , \bar{i}_b and \bar{i}_c . The process involved a 'trial and error' approach, adjusting the dc component of the flux (AB_0 , BC_0 and CA_0) in each of the delta windings until the HDA waveforms were similar to the adjusted field measurement waveforms. The Mathcad[®] implementation of the HDA calculations is shown in Figure 6-17. The current vectors \bar{i}_a , \bar{i}_b and \bar{i}_c house the harmonics of the magnetizing currents supplied by each phase of the 63 kV bus.

Comparing Figure 6-16 to Figure 6-15, the waveforms show a remarkable similarity to the modified field measurements. The HDA analysis indicates that the burst of current distortion could occur as a result of single sided saturation of the rectifier transformer. It is suspected that during start-up of the second rectifier, a control system malfunction can occur that results in unequal current pulses through the valve windings of the rectifier transformer. Unequal current pulses result in dc components of the currents also flowing through the valve windings of the rectifier transformers resulting in saturation type currents flowing in the primary windings.

This type of analysis is a traditional time domain problem. The author's HDA methodology, however, does offer an alternate, simple and convenient mechanism for carrying out the same analysis.

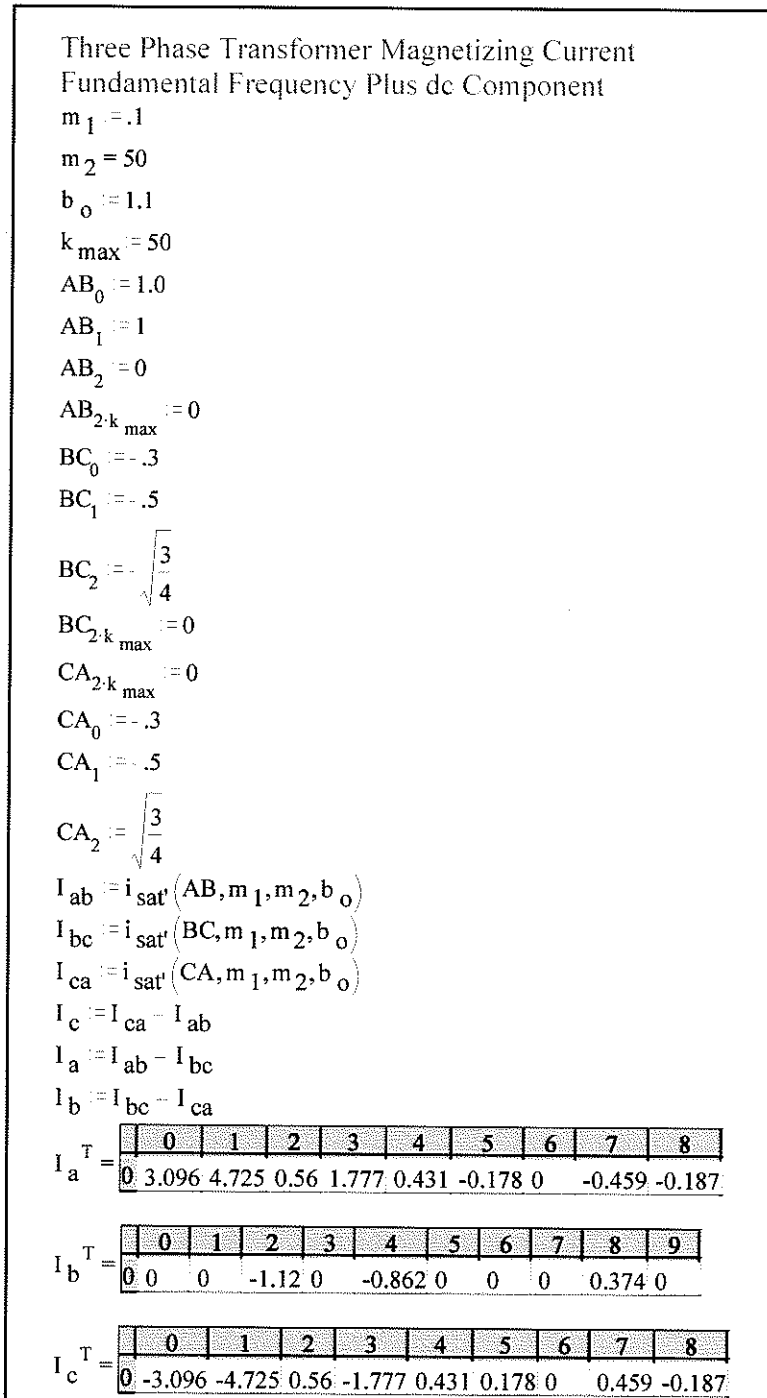


Figure 6-17 Mathcad® Implementation of HDA of Transformer Saturation

CHAPTER 7

CONCLUDING REMARKS

7.1 GENERAL

The harmonic domain approach developed in this thesis is useful to the electrical engineering community. The rigorous mathematical treatment extends the art of network solution theory. The direct calculation of harmonics is an independent check for time domain solutions followed by Fourier analysis. Computationally, the HDA method could be more efficient than the time domain, particularly for systems with low damping and systems excited with a large range of harmonics (e.g. dc and up to 1 MHz) or with a large difference in their natural time constants. If the development of the proposed Harmonic Domain Analysis methodologies continues, it could eventually be used to define initial conditions for time domain transients solutions.

Chapter 1 of this thesis has provided background to harmonic domain analysis, provided the motivation for this work and explained why the author believed that the HDA methodology could be developed. Chapter 2 has described the development of the basic harmonic domain mathematical tools (harmonic domain addition, subtraction, multiplication, division, square root, absolute value and sign functions). Their use in the development of harmonic domain models for basic electrical and control system components has been described in Chapters 3 and 4.

Chapter 5 has shown that the HDA methodology can be directly applied to the modelling of basic power electronic switching elements, while Chapter 6 has shown that the proposed HDA methodology can be applied to the solution of electrical networks with

non-linear elements such as transformer saturation, and has successfully demonstrated the methodology by its application to the solution of a real harmonic domain problem.

7.2 CONCLUSIONS

The prime objective of this research was to develop a Harmonic Domain Analysis (HDA) methodology given the hypothesis that the harmonic analysis can be done entirely in the harmonic domain. The HDA methodology presented in the thesis achieves this objective and includes:

- 1) development and demonstration of algorithms for the direct evaluation of advanced mathematical functions,
- 2) application of the mathematical algorithms to typical sources of harmonic interactions such as non-linear elements and power electronic devices,
- 3) an indication of how the algorithms can be incorporated into methodologies for other types of power system analyses.

Based on these objectives, it was concluded that the hypothesis given in Chapter 1, i.e.:

That given three basic harmonic domain operators, i.e. add, subtract, and multiply can be carried out entirely in the harmonic domain, it should be possible, also, to directly divide two waveforms in the harmonic domain. With these four harmonic domain tools it should be possible, similar to the time domain, to develop more complex mathematical functions such as the square root absolute value and sign functions.

Given the availability of robust mathematical functions, it should be possible to model nonlinear elements such as power electronic switching equipment and transformer saturation directly in the harmonic domain.

Given basic mathematical tools and the ability to model non-linear elements directly in the harmonic domain, it should be possible to develop a methodology where these non-linear elements can be incorporated into existing data structures

and algorithms to permit the solution of large electrical power networks entirely in the harmonic domain.

has been verified and that it is indeed possible to apply the Harmonic Domain Analysis methodology to practical problems.

7.3 PRINCIPAL ORIGINAL CONTRIBUTIONS

The principle original contributions made in this thesis include:

- 1) development of mathematical tools to do a number of time domain operations (multiply, divide, square root, absolute value and sign) directly in the harmonic domain. These tools allow the direct computation of the harmonic content (frequencies, magnitudes and angles) of a waveform without recourse to Fourier series transformations of the corresponding time domain values. The original contribution to the multiplication operator is its treatment as a transformation matrix.
- 2) development of derivatives of the advanced harmonic domain functions, permitting the use of these functions in the Newton-Raphson or other predictive type solution of non-linear harmonic domain simultaneous equations.
- 3) combining the above tools into a circuit analysis algorithm that uses admittance matrix solutions. This allows for the direct harmonic domain calculation of arbitrarily large circuits with non-linear elements.
- 4) inclusion of basic power electronic circuits, and non-linear control function blocks in the above HDA procedure.
- 5) development of a composite environment that permits mixing controls, circuit elements and switching functions for direct use in the harmonic domain.
- 6) validation of the approach taken with detailed time domain simulation.
- 7) development of a harmonic domain model for non-linear magnetising branches.
- 8) application of the saturation model to an actual filter-transformer interaction example, including validation with measured waveforms and current values. This shows that the approach is a valid design tool in real applications.

- 9) demonstration that the proposed HDA methodology is compatible with both Newton-Raphson and Gauss-Seidel algorithms for the solution of non-linear equations, and as such would be compatible with the large network solution algorithms developed for load flow fundamental frequency analysis.

7.4 LIMITATIONS OF HDA AND FURTHER WORK

The approach developed so far is very effective and clearly establishes the feasibility of the methodology. Angles of attack for some remaining limitations and suggestions for potential improvements are now outlined below. These issues could be addressed by future researchers in this field.

The Square Root Function

The HDA square root function described in Section 2.6 could be improved to allow a better approximation for the harmonic content of waveforms that have time domain step function equivalents with a significant length of time where the waveform is close to a value of zero.

Much work has been done in the transformation from frequency domain (entire spectrum, not just harmonics) to time domain and the author understands that a Lanczos filter is often used in these transformations to reduce the Gibb's-like oscillation effect as a result of frequency truncation. Application of a Lanczos filter in the harmonic domain to the waveform prior to using the 'best fit' square root algorithms may reduce the dc offset effect and could be examined as part of further development of the authors proposed methodology.

In algebraic evaluations of the square root, the argument can be scaled by a factor with a known root²⁹ into a range where the product of a large and small number does not occur during the square root calculations. The author believes that it may be possible to divide the time slice (in the harmonic domain) into periods where

²⁹ For example a scaling factor 100 could be used as the known root is 10.

the argument lies within a given range, apply a scaling factor to this range and evaluate the square root in the harmonic domain only over the range. Superposition of harmonics should apply to evaluate the harmonic content of the complete waveform. Again this could be investigated as part of further research in this area to improve the HDA square root function.

Ongoing development of HDA mathematical operators and functions

The author has developed the appropriate mathematical tools as was required to achieve the objectives of the research. Additional mathematical tools can be developed as required by future HDA developers. An example of this is to expand the HDA mathematical tool box to include logical functions. The sign function discussed in Section 2.8 of Chapter 2 can be adapted to a primitive analogue-to-digital converter.

As a first step the sign function can be used to develop an HDA equivalent of a time domain comparison function that compares two harmonic domain inputs, say \bar{A} and \bar{B} returning one level of output if \bar{A} is greater than \bar{B} (in the time domain) and a second level if \bar{A} is less than \bar{B} . In this case the argument to the sign function would be $\bar{A} - \bar{B}$.

The magnitude of the swing in the output of the resultant sign function (either +1 or -1) can be scaled by scalar multiplication, and shifted by increasing or decreasing the dc component of the output to correspond to the desired output levels. If the output levels are selected to be say 1 and 0 for the positive and negative inputs respectively, the sign function is the first step in the modelling of logical functions in the harmonic domain.

The ability to model logical functions in the harmonic domain would create many more possible avenues for future investigations, entirely in the harmonic domain.

The square root function provided satisfactory results for many of the applications tested but as noted earlier, there is room for improvement. Even with the somewhat limited functionality of the square root function, however, other mathematical models dependent on the square root function were developed and successfully demonstrated.

The author believes that with additional research and development, a complete library of 'robust' mathematical and logical harmonic domain operators and functions could be developed. These higher level functions would be required if complete compatibility with time domain system modelling tools such as PSCAD™ is to be achieved.

HDA models of Thyristors

Sections 5.2 and 5.4 of Chapter 5 demonstrate that circuits including diodes and gate turnoff devices (IGBT, MOSFET, GTO etc.) as used in several modern topologies such as voltage sourced converter circuits can be readily modelled in the harmonic domain. As a thyristor is simply a diode with conduction intervals determined by logic, the author believes that it should be possible to also model a thyristor circuit directly in the harmonic domain. This could be subject of ongoing research into direct harmonic domain modelling of components.

HDA Modelling of Ideal Inductors and Capacitors

The treatment of capacitors and inductors in the proposed HDA could be improved. The HDA admittance matrix representing an inductor and the HDA impedance matrix representing a capacitor are both singular. The singularity associated with the inductor is eliminated if a small resistance is inserted in series with the inductor.

An ideal capacitor can be introduced into the HDA admittance matrix representing the network, but it de-couples the two connected nodes for dc

phenomena. Successful solution of the network is dependent on the presence of a resistive type connection to ground at each of the terminating nodes, (which could be sufficiently large so as to not influence the results)

The author's proposed HDA methodology is based on an admittance matrix formulation with both the dc and harmonic components integrated into the same matrix. A refinement to this methodology to treat the dc differently from the harmonic component may eliminate the limitations imposed on the modelling of ideal inductors and capacitors.

HDA Modelling of Ideal Derivative and Integrator Control Functions

Modelling ideal derivative and integrator functions in the HDA have the same limitations as ideal inductors and capacitors. Derivative functions can be incorporated provided there is a proportional term as well. Integrators can be incorporated provided there is some additional means to define the dc conditions of the input (must be zero) and output, (completely independent of input, dependent only on output of other control system functions).

Similar to the ideal inductor and capacitor, a refinement to the HDA methodology to treat the dc differently from the harmonic component may eliminate the limitations imposed on the modelling of these components.

Derivative of the CompRamp Function

The derivative of the non-linear CompRamp function is a matrix that is easy to define and can be readily incorporated into a Newton-Raphson iterative solution of its non-linear effects. The demonstration of its use in Section 5.4 of Chapter 5 is based on a full matrix model. Its implementation in production software would likely take advantage of the fact that the two single dimension arrays that define the contents of the matrix are almost identical.

The Time Domain Ramp Function

The time domain ramp function is a common mathematical and control system modelling function. It is not only just used in conjunction with a comparator function (as demonstrated in Section 5.4). It could be used in conjunction with many other types of circuits such as input to sweep circuits, harmonic generator circuits, etc. In some applications, for example, if the output of the ramp was used as input to an integrator or first order lag filter, it may be possible to neglect the Gibb's-like oscillation effects. In other applications, however, the oscillations could cause solution difficulties similar to those experienced with the development of the 'CompRamp' function as described above.

The Gibb's-like oscillation effects could also introduce numerical issues associated with the output of the sign function or with other discontinuous functions. To provide the greatest flexibility for future development of HDA models, it would be very beneficial to be able to model any function, independent of its ultimate use in the control circuit.

The author believes that there should be a solution to the Gibb's-like oscillation effects. The Lanczos filter appears to offer some direction for the solution, and additional research and development along this path would improve the flexibility of the proposed HDA methodology.

Other control Block Functions

Chapter 4 described the modelling of first order lag and PID type of controllers in the proposed HDA. It is suggested that with additional research and development, the same procedures described in that Chapter can be applied to the development of other control function block diagrams such as lead lag functions and 2nd order filtering functions.

Methodologies similar to that used in the development of the HDA CompRamp function could be used to develop more complex non-linear models and their analytical derivatives.

Capacitor Diode Circuits

Although the author has explored (unsuccessfully) other treatments of the capacitor-diode configuration discussed in Section 5.6, it is still believed that there is an entirely harmonic domain solution to the divergence problem. This may involve restructuring the Jacobian to include an impedance model of capacitor elements, solving for voltages instead of currents associated with capacitor elements. This should improve the condition of the Jacobian.

The solution of the diode-capacitor combination would make a very interesting topic for future research.

Norton Equivalents

As the algebraic saturation function described in Section 6.2 of Chapter 2 is continuous, it is possible to symbolically differentiate the flux-current expression with respect to flux, establishing an equivalent small signal admittance at any operating point on the waveform. In a similar fashion, it should also be possible to differentiate the harmonic domain expression with respect to each component of the flux, building up a small signal admittance matrix for each set of harmonic operating conditions. The small signal admittance matrix would aid in the development of a harmonic Norton equivalent of the saturation characteristics. As well it would assist in the direct incorporation of saturation characteristics into the Jacobian of a Newton-Raphson solution. Both would be useful for the iterative analysis required for the harmonic domain analysis of very large systems. This could be a subject for future research and development into proposed HDA methodology.

With resolution of the above limitations, the author's proposed HDA methodology could be integrated into an admittance based harmonic domain analysis tool with graphic interface (GHDA), capable of examining harmonic impacts between devices across an entire power system network. The tool would be able to link with conventional power flow and stability data (such as PSS/E™ or PSLF®) to define the fundamental frequency component of the network admittance matrix and generator dynamic data, link with frequency domain programs (such as NIMSCAN®) to establish the harmonic effect in the electrical network and with compatibility in network configuration and data with time domain software such as PSCAD/EMTDC™ for cross-validation of harmonic domain and time domain analysis results and for defining the initial conditions for the transients solution, avoiding time domain initialization.

REFERENCES

- [1] CIGRE Working Group 14.30, *Guide to the Specification and Design Evaluation of AC Filters for HVDC Systems*, Publication 139, April 1999.
- [2] IEEE, *Guide for Analysis and Definition of DC Side Harmonic Performance of HVDC Transmission Systems*, IEEE Std 1124, September 2003.
- [3] D.J. Melvold, F.J. Hormozi, 'AC Filter Specifications and Performance on Various HVDC Projects of the Los Angeles Department of Water and Power', *Proceedings of the Third International Conference on Harmonics in Power Systems*, 1988, pp 85-93.
- [4] IEEE PES Task Force on Harmonics Modelling and Simulation, *Tutorial on Harmonics Modeling and Simulation*, TP-125-0, 1998.
- [5] C. Adamson, N.G. Hingorani, *High Voltage Direct Current Power Transmission*, Garraway Limited, 1960.
- [6] E.W. Kimbark, *Direct Current Transmission*, Vol. 1, John Wiley & Sons Inc, 1971.
- [7] J. Reeve, P. C.S. Krishnayya, 'Unusal Current Harmonics Arising from High-Voltage DC Transimission', *IEEE Transactions on Power Apparatus and Systems*, Vol. PAS-87, No. 3, March 1968, pp 883-893.
- [8] J. Reeve, J.A. Baron, P.C.S. Krishnayya, 'A General Approach to Harmonic Current Generation by HVDC Convertors', *IEEE Transactions on Power Apparatus and Systems*, Vol. PAS-88, No. 7, July 1969, pp 989-995.
- [9] A.G. Phadke, 'Generation of Abnormal Harmonics in High-Voltage AC-DC Power Systems', *IEEE Transactions on Power Apparatus and Systems*, Vol. PAS-87, No. 3, March 1968, pp 873-883.

References

- [10] B.C. Smith, 'A Harmonic Domain Model for the Interaction of the HVDC Converter with AC and DC Systems.', A Thesis presented for the degree of Doctor of Philosophy in Electrical and Electronic Engineering at the University of Canterbury, Christchurch, New Zealand, 23 May, 1996.
- [11] J. Arrillaga, L. Juhlin, M. Lahtinen, P. Ribeiro, A.R.Saavedra, 'AC System Modelling for AC Filter Design - An overview of Impedance Modelling', CIGRE Joint Task Force 36.06.02/14.03.03 Publication, Electra No 164 February, 1996.
- [12] B.C. Smith, N.R. Watson, A.R. Wood, J. Arrillaga, 'A Newton Solution for the Harmonic Phasor Analysis of AC/DC Converters', IEEE paper 95 SM 379-8 PWRD, presented at 1995 IEEE/PES Summer Meeting, July 23-27, 1995, Portland, Or.
- [13] J.J. Rico, E. Acha, T.J.E. Miller, 'Harmonic Domain Modelling of Three Phase Thyristor-Controlled Reactors by Means of Switching Vectors and Discrete Convolutions', IEEE paper 96 WM 093-5 PWRD, presented at 1996 IEEE/PES Winter Meeting, January 21-23, 1996, Baltimore, MD.
- [14] P.M. DeRusso, R.J. Roy, C.M. Close, *State Variables for Engineers*, John Wiley & Sons, Inc. 1967.
- [15] K. Ogata, *State Space Analysis of Control Systems*, Prentice Hall, Inc, 1967.
- [16] B.C. Smith, J. Arrillaga, 'Power Flow Constrained Harmonic Analysis in AC-DC Power Systems', IEEE Transactions on Power Systems, Vol 14, No. 4, November 1999, pp 1251-1261.
- [17] H. Dommel, A. Yan, W. Shi, 'Harmonics from Transformer Saturation', IEEE Transactions on Power Delivery, Vol. 1, No. 2, 1986.
- [18] A. Semlyen, E. Acha, J. Arrillaga, 'Newton-Type Algorithms for the Harmonic Phasor Analysis of Non-Linear Power Circuits in Periodical Steady State with Special Reference to Magnetic Non-Linearities', IEEE Transactions on Power Delivery, Vol. 3, No. 3, July 1988, pp 1090-1097.
- [19] R.S. Burton, 'Modelling of Transformer Saturation in Stability Studies', CEA No. 288 T 586, Prepared by Manitoba HVDC Research Centre, April, 1989.

References

- [20] R.S. Burton, C.F. Fuchshuber, D.A. Woodford, A.M. Gole, 'Prediction of Core Saturation Instability at and HVDC Converter', Paper 96-WM 117-2 PWRD, accepted for publication, IEEE Transmission and Distribution Committee of the IEEE Power Engineering Society, presented at PES Winter Meeting, Baltimore, January 21-25, 1996.
- [21] E.V. Larson, D.H. Baker, J.C. McIver, 'Low Order Harmonic Interaction on AC/DC Systems', IEEE Transactions on Power Delivery, Vol. 4, No. 1, January 1989, pp 493-501.
- [22] A.R. Wood, J. Arrillaga, 'HVDC Converter Waveform Distortion: a Frequency-Domain Analysis', IEE paper 1501c(P7) , IEE Proceedings Generation, Transmission, Distribution, Vol. 142, No. 1, January 1995.
- [23] A.R. Wood, B.C. Smith, J. Arrillaga, 'The Harmonic Impedance of an HVDC Converter', EPE Conference, Sevilla, September 1995.
- [24] A.R. Wood, J. Arrillaga, 'The Frequency Dependent Impedance of an HVDC Converter', IEEE Transactions Power Delivery, Vol 10 No. 3. pp1635-1647.
- [25] R.S. Burton, 'Main Report on Harmonic Effects on HVDC Control and Performance', CEA No. 337 T 750, Prepared by Manitoba HVDC Research Centre, February, 1994.
- [26] R.S. Burton, 'Study Guide on Harmonic Effects on HVDC Control and Performance', CEA No. 337 T 750, Prepared by Manitoba HVDC Research Centre, February, 1994.
- [27] R.S. Burton, 'Modelling AC/DC Systems for the Analysis of AC/DC Interactions', IEEE Wescanex 95 Communications Power and Computing, Conference Proceedings, pp. 264-269.
- [28] L. Bohmann, R.H. Lasseter, 'Harmonic Interactions in Thyristor Controlled Reactor Circuits', IEEE Transactions on Power Delivery, Vol. 4, No3, July 1989.
- [29] E. Acha, J.J. Rico, S. Acha, M. Madrigal, 'Harmonic Modelling in Hartley's Domain with Particular Reference to Three Phase Thyristor-Controlled Reactors', Unpublished.

- [30] A.M. Gole M. Mohaddes, S. Elez, 'Frequency Dependence of STATCOM Admittances', Submitted for review to the IEEE Power Engineering Society Transactions, October, 1997.
- [31] I. Papic, A.M. Gole, 'Frequency Response Characteristics of the Unified Power Flow Controller', Submitted (Oct 2001) for review to IEEE Transactions on Power Delivery.
- [32] A. Daneshpooy, A.M. Gole, 'Frequency Response of the Thyristor Controlled Series Capacitor', IEEE Transactions on Power Delivery, Vol. 16, No. 1, January 2001.
- [33] Erik V. Persson, 'Calculation of Transfer functions in Grid-controlled Converter Systems With Special Reference to H.V.D.C.. Transmissions, Paper 6117 P, Proc. IEE, Vol. 117, No. 5, May 1970, pp 989-997.
- [34] L. Hu, R. Yacamini, ' Harmonic Transfer through Converters and HVDC Links', IEEE Transactions on Power Electronics', Vol. 7, No.3,Jul 1992, pp514-525.
- [35] H.W. Dommel, 'Digital Computer Simulation of Electromagnetic Transients in Single and Multiphase Networks', IEEE Transactions on Power Apparatus and Systems, Vol. PAS-88, No. 4, April 1969, pp. 388-399.
- [36] I.S. Duff, A.M. Erisman, J.K. Reid, *Direct Methods for Sparse Matrices*, Oxford University Press, 1986.
- [37] S.M. Selby (editor), *CRC Standard Mathematical Tables*, 16th ed., The Chemical Rubber Co., 1964
- [38] Edith Clarke, *Circuit Analysis of A-C Power Systems*, Volume II, John Wiley and Sons, New York, 1950.
- [39] M.R. Spiegel, *Theory and Problems of Laplace Transforms*, Shauam Publishing Company, 1965.
- [40] N.G. Hingorani, P. Chadwick, 'A New Constant Extinction Angle Control for AC/DC/AC Static Convertors', IEEE Transactions on Power Apparatus and Systems, Vol. PAS-87, No. 3, March 1968, pp 866-872.

APPENDICES

This Page is Intentionally Blank

**APPENDIX A MATHCAD® IMPLEMENTATION OF THE HDA
COMPRAMP FUNCTION**

```

CompRamp( $\theta, it_{max}, toler$ ) :=  $\beta - \theta_0$ 
n := floor( $\frac{length(\theta)}{2}$ )
iter := 0
 $\epsilon := 10^{25}$ 
while (iter  $\leq$  itmax) · ( $\epsilon \geq$  toler)
    num :=  $\beta + \theta_0$ 
    den := 1
    for i ∈ 1..n
        k := 2·i
        j := k - 1
        num := num + ( $\theta_j \cdot \cos(i \cdot \beta) + \theta_k \cdot \sin(i \cdot \beta)$ )
        den := den + i · ( $-\theta_j \cdot \sin(i \cdot \beta) + \theta_k \cdot \cos(i \cdot \beta)$ )
     $\Delta\beta := \frac{num}{den}$ 
     $\epsilon := |\Delta\beta|$ 
     $\beta := \beta + \Delta\beta$ 
    ansiter :=  $\Delta\beta$ 
    iter := iter + 1
 $f_0 := 1 - \frac{\beta}{2 \cdot \pi}$ 
    for i ∈ 1..n
         $f_{2 \cdot i - 1} := \frac{-\sin(i \cdot \beta)}{i \cdot \pi}$ 
         $f_{2 \cdot i} := \frac{\cos(i \cdot \beta) - 1}{i \cdot \pi}$ 
    f

```

Mathcad® Solution Algorithm - HDA CompRamp Function

Appendix A - Mathcad® implementation of the HDA CompRamp function

```

n_max := 50      ωT := 0..360      toler := .00000001      it_max := 20
θ_0 := 192      θ_{2:n_max} := 0      θ_1 := 20      θ_2 := -5      θ_3 := 25      θ := θ·deg
V_ref := CompRamp(θ, it_max, toler)

Disp(V) := | n ← length(V)
           | for ωT ∈ 0..360
           |   Disp_{ωT} ← V_0
           |   for i ∈ 1..floor(n/2)
           |     Disp_{ωT} ← Disp_{ωT} + V_{(2·i-1)}·cos(i·ωT·deg) + V_{2·i}·sin(i·ωT·deg)
           | Disp

θ_{ωT} := Disp(θ) / deg
Ramp_{ωT} := ωT / 360
P := Disp(V_ref)
β := Disp(θ) / (360·deg)

```

Normalized Response

V_ref T =	0	1	2	3	4	5	6	7	8	
	0	0.457	0.085	-0.625	-0.082	-0.023	0.077	-0.179	-0.07	-0.042

Testing of the CompRamp Function:

APPENDIX B MATHCAD® DATA AND SET-UP FOR SAMPLE SYSTEM DESCRIBED IN CHAPTER 6

Parameters

$$\begin{aligned}
 f_0 &:= 60 \text{ Hz} & \omega_0 &:= 2 \cdot \pi \cdot f_0 & n_{\max} &:= 20 & n &:= 0..n_{\max} & I &:= \text{identity}(2 \cdot n_{\max} + 1) \\
 V_0 &:= 63 & \text{MVAsys} &:= 2193 & \text{Qsys} &:= 15 \\
 \text{MVAX} &:= 120 & z_x &:= .1 & b_0 &:= 1.1 & m_1 &:= .200 & m_2 &:= 200 & \text{Qx} &:= 60 \\
 R_5 &:= .5287 \Omega & L_5 &:= 57.24 \text{ mH} & C_5 &:= 5.12 \mu\text{F} \\
 R_7 &:= 2.5028 \Omega & L_7 &:= 57.73 \text{ mH} & C_7 &:= 2.56 \mu\text{F} \\
 R_{\text{hp}} &:= 36 \cdot \Omega & L_{\text{hp}} &:= 3.18 \text{ mH} & C_{\text{hp}} &:= 15.36 \mu\text{F}
 \end{aligned}$$

Calculation of Filter Admittance and Impedance

$$\begin{aligned}
 Y_{c5} &:= \omega_0 \cdot C_5 \cdot D(n_{\max}) & Y_{c5_{0,0}} &:= \frac{1}{\Omega} & Z_{c5} &:= Y_{c5}^{-1} & Z_{c5_{0,0}} &:= 0 \cdot \Omega \\
 Z_5 &:= \frac{R_5 \cdot I + \omega_0 \cdot L_5 \cdot D(n_{\max}) + Z_{c5}}{\Omega} & Z_{5_{0,0}} &:= 1 & Y_5 &:= Z_5^{-1} & Y_{5_{0,0}} &:= 0 \\
 Y_{c7} &:= \omega_0 \cdot C_7 \cdot D(n_{\max}) & Y_{c7_{0,0}} &:= \frac{1}{\Omega} & Z_{c7} &:= Y_{c7}^{-1} & Z_{c7_{0,0}} &:= 0 \cdot \Omega \\
 Z_7 &:= \frac{R_7 \cdot I + \omega_0 \cdot L_7 \cdot D(n_{\max}) + Z_{c7}}{\Omega} & Z_{7_{0,0}} &:= 1 & Y_7 &:= Z_7^{-1} & Y_{7_{0,0}} &:= 0 \\
 Z_{\text{Lhp}} &:= \omega_0 \cdot L_{\text{hp}} \cdot D(n_{\max}) & Z_{\text{Lhp}_{0,0}} &:= 1 \cdot \Omega & Y_{\text{Lhp}} &:= Z_{\text{Lhp}}^{-1} & Y_{\text{Lhp}_{0,0}} &:= \frac{0}{\Omega} & Z_{\text{Lhp}_{0,0}} &:= 0 \cdot \Omega \\
 Y_{\text{Chp}} &:= \omega_0 \cdot C_{\text{hp}} \cdot D(n_{\max}) & Y_{\text{Chp}_{0,0}} &:= \frac{1}{\Omega} & Z_{\text{Chp}} &:= Y_{\text{Chp}}^{-1} & Z_{\text{Chp}_{0,0}} &:= 0 \cdot \Omega & Y_{\text{Chp}_{0,0}} &:= \frac{0}{\Omega} \\
 Z_{\text{hp}} &:= \frac{Z_{\text{Chp}} + \left(\frac{1}{R_{\text{hp}}} \cdot I + Y_{\text{Lhp}} \right)^{-1}}{\Omega} & Z_{\text{hp}_{0,0}} &:= 1 & Y_{\text{hp}} &:= Z_{\text{hp}}^{-1} & Y_{\text{hp}_{0,0}} &:= 0 \\
 Y_f &:= 2 \cdot (Y_5 + Y_7 + Y_{\text{hp}}) & Y_{f_{0,0}} &:= 1 & Z_f &:= Y_f^{-1} & Z_{f_{0,0}} &:= 0 & Y_{f_{0,0}} &:= 0
 \end{aligned}$$

System Impedance

$$Z_{\text{sys}} := \frac{V_o^2}{\text{MVA}_{\text{sys}}} \cdot \left(D(n_{\text{max}}) + \frac{1}{Q_{\text{sys}}} \cdot \text{Identity}(n_{\text{max}}) \right)$$

$$Y_{\text{sys}} := Z_{\text{sys}}^{-1} \quad \text{Constant system R}$$

Transformer Impedance

$$Z_x := \frac{V_o^2}{\text{MVA}_x} \cdot \left(D(n_{\text{max}}) + \frac{1}{Q_x} \cdot \text{Identity}(n_{\text{max}}) \right) \cdot z_x$$

$$Y_x := Z_x^{-1}$$

$$Z_{\text{th}} := (Y_f + Y_{\text{sys}})^{-1} + Z_x$$

$$V_{\text{fact}} := (Y_f + Y_{\text{sys}})^{-1} \cdot Y_{\text{sys}}$$

Source Voltage

$$V_{\text{src}} := \begin{cases} V_0 \leftarrow 0 \\ V_1 \leftarrow 1.0 \\ V_{2:n_{\text{max}}} \leftarrow 0 \\ V \end{cases} \quad V_{\text{th}} := V_{\text{fact}} \cdot V_{\text{src}} \cdot V_o \cdot \sqrt{\frac{2}{3}}$$

<----Note: Vth is a peak voltage

Mathcad® Data and Set-up for Sample System Described in Section 6.4 of Chapter 6